แผ่นดินไหวโบราณตามเขตรอยเลื่อนไซยบุรีทางตะวันตกของประเทศสาธารณรัฐประชาธิปไตยประชาชนลาว

นางสาวพัชชาวี นวลขาว

วิทยานิพนธ์นี้เป็นส่วนหนึ่งของการศึกษาตามหลักสูตรปริญญาวิทยาศาสตรมหาบัณฑิต
สาขาวิชาธรณีวิทยา ภาควิชาธรณีวิทยา
คณะวิทยาศาสตร์ จุฬาลงกรณ์มหาวิทยาลัย
ปีการศึกษา 2557

PALEOEARTHQUAKE ALONG XAIGNABOULI FAULT ZONE IN WESTERN LAO PDR

Miss Patchawee Nualkhao

A Thesis Submitted in Partial Fulfillment of the Requirements

for the Degree of Master of Science Program in Geology

Department of Geology

Faculty of Science

Chulalongkorn University

Academic Year 2014

Thesis Title	PALEOEARTHQUAKE ALONG XAIGNABOULI FAULT ZONE IN WESTERN LAO PDR
By	Miss Patchawee Nualkhao
Field of Study	Geology
Thesis Advisor	Associate Professor Punya Charusiri
Thesis Co-Advisor	Dr. Chinda Sutiwanich

Accepted by the Faculty of Science, Chulalongkorn University in Partial Fulfillment of the Requirements for the Master's Degree

.....Dean of the Faculty of Science

(Professor Supot Hannongbua)

THESIS COMMITTEE

.....Chairman

(Professor Montri Choowong)

.....Thesis Advisor

(Associate Professor Punya Charusiri)

.....Thesis Co-Advisor

(Dr. Chinda Sutiwanich)

.....Examiner

(Assistant Professor Santi Pailoplee)

.....External Examiner

(Suwit Kosuwan)

พัชชาวี นวลขาว : แผ่นดินไหวโบราณตามเขตรอยเลื่อนไซยบุรีทางตะวันตกของประเทศสาธารณรัฐประชาธิปไตยประชาชนลาว (PALEOEARTHQUAKE ALONG XAIGNABOULI FAULT ZONE IN WESTERN LAO PDR) อ.ที่ปรึกษาวิทยานิพนธ์หลัก: รศ. ดร. ปัญญา จารุศิริ, อ.ที่ปรึกษาวิทยานิพนธ์ร่วม: ดร. จินดา สุทธิวานิช, 134 หน้า.

การศึกษาธรณีวิทยาแผ่นดินไหวโบราณบริเวณแนวรอยเลื่อนในพื้นที่ไซยบุรี ทางด้านตะวันตกของประเทศสาธารณรัฐประชาธิปไตยประชาชนลาว จากเหตุการณ์แผ่นดินไหวเมื่อเดือนมีนาคม 2556 เกิดแผ่นดินไหวขนาด 5.4 M_L และ 3.9 M_L ลักษณะของการเลื่อนตัวของรอยเลื่อนมีความสอดคล้องกับผลลูกบอลชายหาดวิเคราะห์กลไกการเกิดแผ่นดินไหว วัตถุประสงค์ของการศึกษาเพื่อบ่งชี้อายุการเลื่อนตัวครั้งล่าสุดของรอยเลื่อน ทายพฤติกรรมการเลื่อนตัวของรอยเลื่อน และระบุคาบอุบัติซ้ำของการเกิดแผ่นดินไหวโบราณ ตลอดจนอธิบายธรณีวิทยาแปรสัณฐานของรอยเลื่อนดังกล่าว

ผลการศึกษาบริเวณแอ่งไซยบุรีและแอ่งเพียงพบลักษณะธรณีสัณฐานที่สัมพันธ์กับรอยเลื่อน ได้แก่ธารเหลื่อม หุบเขาเส้นตรง สันเขาเหลื่อม หนองหล่ม และผารอยเลื่อน กลุ่มรอยเลื่อนไซยบุรี วางตัวในแนวเหนือค่อนตะวันออกเฉียงเหนือ-ใต้ค่อนตะวันตกเฉียงใต้ แสดงลักษณะการเลื่อนตัวของรอยเลื่อนแบบซ้ายเข้าประกอบกับรอยเลื่อนปกติ โดยรอยเลื่อนกลุ่มแรกพาดผ่านทางด้านตะวันตกของขอบแอ่งไซยบุรี มีความยาวรวมทั้งสิ้นประมาณ 250 กิโลเมตร ประกอบด้วยรอยเลื่อนย่อยจำนวน 20 รอยเลื่อนย่อย มีความยาวตั้งแต่ 10 ถึง 100 กิโลเมตร รอยเลื่อนกลุ่มที่สองซึ่งแสดงลักษณะธรณีสัณฐานที่เด่นชัดกว่า ประกอบด้วยรอยเลื่อนย่อย 3 รอยเลื่อนย่อย มีความยาวตั้งแต่ 18 ถึง 35 กิโลเมตร พาดผ่านทางด้านตะวันออกของแอ่งเพียง

จากค่าความยาวรอยแตกปรากฏบนพื้นผิว สามารถเกิดแผ่นดินไหวขนาดสูงสุดระหว่างแมกนิจูด 5.6 และ 7.3 ผลการหาอายุโดยวิธีเรืองแสงด้วยความร้อนของชั้นตะกอนในร่องสำรวจที่สัมพันธ์กับรอยเลื่อน บ่งชี้ว่าเคยเกิดแผ่นดินไหวมาแล้ว 3 ครั้ง เมื่อประมาณ 3,000, 2,000 และ 1,000 ปี และมีคาบอุบัติซ้ำประมาณ 1,000 ปี นอกจากนั้นผลการศึกษาบ่งชี้ถึงการเคลื่อนตัวในแนวระดับและในแนวดิ่งของรอยเลื่อนในพื้นที่ศึกษามีความสัมพันธ์กับการพัฒนาของแอ่งเพียงและแอ่งไซยบุรี และต่อเนื่องไปทางตอนเหนือเชื่อมกับรอยเลื่อนเดียนเบียนฟูในตอนเหนือของเวียดนาม และต่อเนื่องไปทางใต้เชื่อมกับรอยเลื่อนอุตรดิตถ์ในตอนเหนือของประเทศไทย

ภาควิชา ธรณีวิทยา ลายมือชื่อนิสิต .....

สาขาวิชา ธรณีวิทยา ลายมือชื่อ อ.ที่ปรึกษาหลัก .....

ปีการศึกษา 2557 ลายมือชื่อ อ.ที่ปรึกษาร่วม .....

5572059823 : MAJOR GEOLOGY

KEYWORDS: ACTIVE FAULT / LAO PDR / OSL DATING / PALEOEARTHQUAKE / PALEOSEISMOLOGY / XAIGNABOULI

PATCHAWEE NUALKHAO: PALEOEARTHQUAKE ALONG XAIGNABOULI FAULT ZONE IN WESTERN LAO PDR. ADVISOR: ASSOC. PROF. PUNYA CHARUSIRI, CO-ADVISOR: DR. CHINDA SUTIWANICH, 134 pp.

Paleoseismological investigation has been carried out to determine the fault evidence in the Xaignabouli (XYB) province, western Lao PDR, prompted by two recent earthquakes (5.4 and 3.9 M_L in 2011) with similar sense of movement as the focal mechanism determined from recent events in the area. The main objectives are to determine the age of the most recent movement, the sense of movement and estimate the paleoearthquake recurrence interval. Major techniques include remote-sensing, field investigation, and paleoseismic excavation together with optical stimulated luminescence (OSL) dating. Several morphotectonic features, particularly offset streams, linear valleys, facet spurs, sag pond, and scarplets, have been recognized along the fault within the two basins, Phiang and Xaignabouli, in the XYB province. Two major strike-slip fault zones have been recognized with an approximate trend in NNE-SSW direction, displaying not only sinistral but also normal movement faults. The sinistral movement along the studied fault, for the first zone passes the western edge of the Xaignabouli basin with a total length of 250 km, consisting of 20 segments ranging from 10 to 110 km. The second zone, showing better tectonic geomorphology, consists of 3 segments varying from 18 to 35 km and passes the eastern edge of the Phiang basin. The surface rupture length from the investigated faults indicate maximum credible earthquake magnitudes between 5.6 and 7.3 M. Results from OSL dating show 3 earthquake events, ca. 3,000, 2,000 and 1,000 years ago, suggesting a recurrence interval of 1,000 years. Results also indicate that vertical and horizontal slip-rate along two studied faults control the development of the Phiang and Xaignabouli basins, and that they extend further and connect northward to the Dien Bien Phu Faults in northern Vietnam and southward to the Uttaradit Fault in north Thailand.

Department:	Geology	Student's Signature	.....
Field of Study:	Geology	Advisor's Signature	.....
Academic Year:	2014	Co-Advisor's Signature	.....

ACKNOWLEDGEMENTS

The author wishes to express her profound and sincere appreciation to her advisor, Associate Professor Punya Charusiri and Dr. Chinda Suttivanich for his enthusiastic support, continuous and invaluable guidance throughout the period of this study.

Thanks are also extended to CH. Karnchang (Lao) Company Limited, for facilitating my visit and collection to Lao PDR and Dr. Santi Pailoplee, for invaluable guidance and providing valuable input and materials in my graduate studies.

I would like to thank the Meteorological Department of Thailand for the seismograph data, the CGIAR Consortium for Spatial Information (CGIAR-CS) for SRTM DEM.

A special thanks to the Geophysics Research Group, Mahidol University, especially for Mr. Sutthipong Noisagool for his help with focal mechanism. I also would like to express my sincerely gratitude to Associate Professor Weerachai Siripunvaraporn for his support in my education and career.

Special thanks extend to Mr. Peerasit Surakiatchai for their helping manage all sample analyses. I would like to thank staff of the Department of geology, Chulalongkorn University for all their help and support.

This research was supported by the 90th Chulalongkorn University Fund from Graduate School Chulalongkorn University.

Finally, a very special thanks to my family, my parents for emotional support throughout the program. No amount of gratitude to would be sufficient. Last, but not least, my husband, Mr. Henrik Erkkonen, thank you for your continuous support.

CONTENTS

Page

Page

LIST OF FIGURES

LIST OF TABLES

CHAPTER I
INTRODUCTION

1.1 Background

There have been earthquakes with the intermediate magnitudes 5.4 M_L and 3.9 M_L in February and March 2011 respectively, in the study area have reported by Thailand Meteorological Department (TMD) in 2011. These earthquakes have affected people in the northern part of Thailand as well as people living near the border of Thai-Lao PDR and the vibration were felt in Lao PDR. In contrast to northern Thailand where there have been numerous earthquake studies no detailed investigation has been done so far for the geology and neotectonic studies within and around the area of Xaignabouli basin and Phiang basin in Lao PDR. In general the study area is located in the so called Loei–Paklay fold belt (Stokes, Lovatt Smith, & Soumphonphakdy, 1996). Earthquakes that may occur in Lao PDR can directly affect people in Thailand and for life and building safety, research should be done in the Xaignabouli fault zone in Xaignabouli basin and Phiang basin as the studied by P. Tapponnier, Peltzer, Le Dain, Armijo, and Cobbold (1982); Hutchison (1989); Polachan et al. (1991) who said that the present-day tectonic activities indicate that the Xaignabouli basin and Phiang basin are located in the area which is seismotectonically active.

The instrumental earthquake records reveal that the area was continuously impacted posed by earthquakes. At least six earthquake events with magnitude <6 Richter were recorded in a radius of 100 km from the location of study area (Figure 1.1), in particular, the M_L 5.4 earthquake (TMD) in A.D. 2011 was less than 50 km away from the study area and the most recent M_w 7.0 earthquake (USGS) in Thailand-Myanmar border (200 km from epicenter to study area). This evidence strongly assures that the Xaignabouli basin and Phiang basin may be affected by an upcoming earthquake hazard in the future. The seismic issues (i.e., earthquake) are, therefore, recognized for this study.

However, as reported very recently by P. Warnitchai (2011), the Xaignabouli basin and Phiang basin area under this survey may have been subject to earthquakes related to the northeast-southwest trending active faults which commences in the north from Dien Bien Phu in northern Vietnam through the Xaignabouli study area and to the eastern part of northern Thailand, particularly in the Nan and Uttaradit areas. The locations and orientation of faults are mainly from Pailoplee, Sugiyama, and Charusiri (2009).

1.2 Objective

The main purpose of this thesis is to study the characteristics of the fault in Xaignabouli basin and Phiang basin area in detail and to clarify the paleoearthquakes along the fault zone. The techniques used for paleoearthquake investigation in this study include remote-sensing interpretation in addition to investigations on morphotectonic analyses, geomorphic indices, image processing and optical stimulated luminescence-dating results. The results of this thesis fulfill the following three purposes:

1. To determine the age of the most recent movement of the Xaignabouli fault;
2. To document the sense of movement of the Xaignabouli fault; and
3. To estimate the paleoearthquake recurrence interval and document the geotectonic associated with the Xaignabouli fault

1.3 Study Area

The Xaignabouli basin and Phiang basain (Figure 1.1) is on the lower Mae Khong River in western Lao PDR. The area under investigation is bounded by latitude 16°N to 22°N and longitude 99°E to 105°E covered western part of Lao PDR.

1.4 Previous Active Fault Study in Southeast Asia

No detailed investigations have been done relating to the precise age of the last movement of the Xaignabouli fault. However, a few researchers have reported on subjected, more or less concerned with the structural geology and seismicity of the Xaignabouli and adjacent areas.

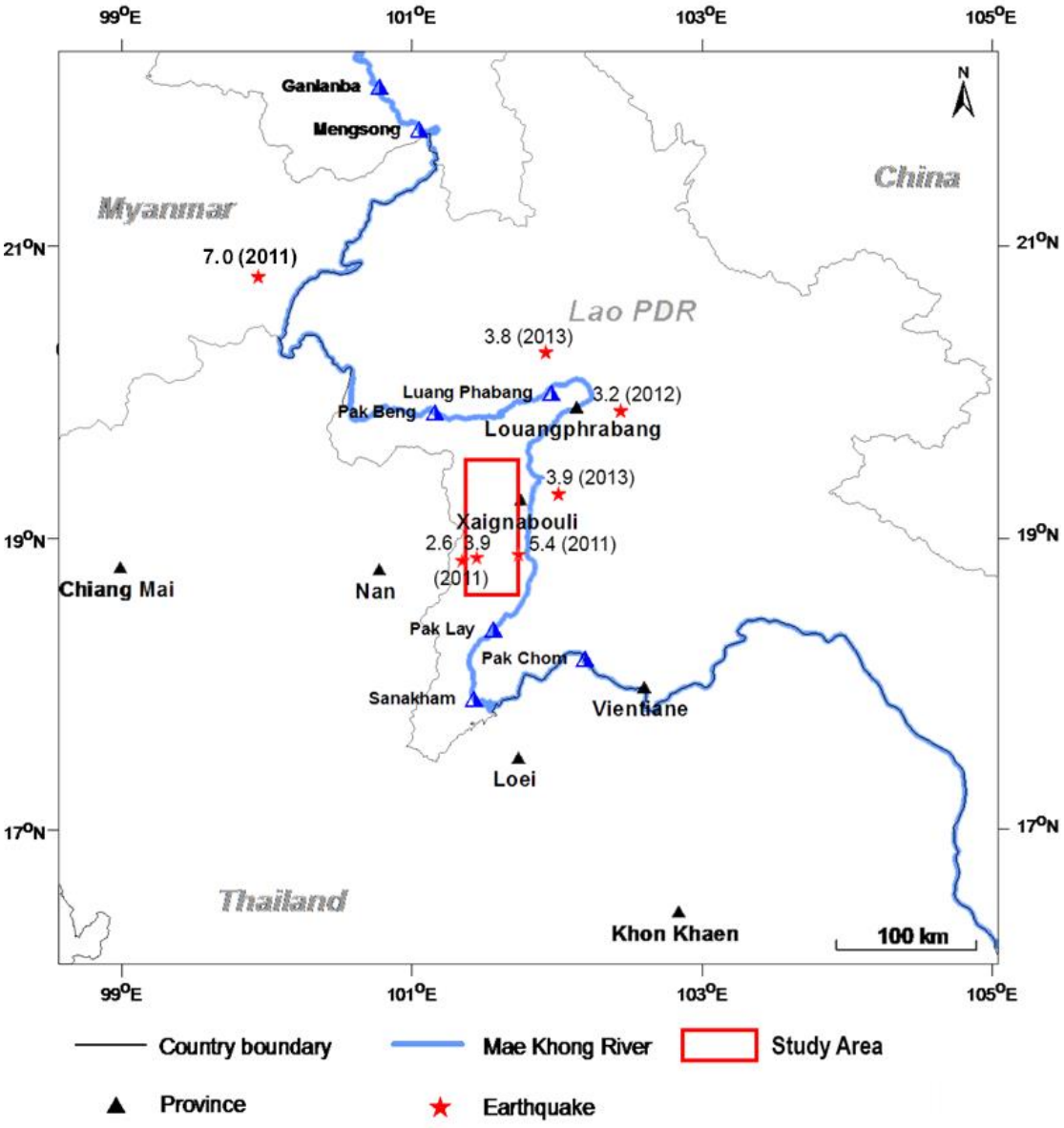

Figure 1.1 Map of northern and central Lao PDR and adjacent areas showing the location of the study area and past earthquake events in adjacent area.

Nutalaya, Sodsri, and Arnold (1985) separated the seismic source zone in mainland Southeast Asia into twelve zone. The Xaignabouli fault zone is located in zone H – North Indochina (Figure 1.2). This area lies to the south and west of the Red River and falls in the territories of China, Vietnam and Lao PDR. In N-W Lao PDR, seismicity seems to line up along a N-S trending Xayabouli Fault on the west side of the Mekong River since it passed through the town of Xayabouli. The movement of this fault is probably the source

of the earthquake along it, and might well relate to the one that occurred on 12-17 Feb, 1933. Reports received from Ngoen Province of Lao PDR stated that there were cracks in the ground, water in the river dried up, walls cracked, loud noise similar to a rock-burst was heard from the mountain east of town.

Fenton, Charusiri, and Wood (2003) conducted an investigation of recent paleoseismic events and identified several active faults in the north and west of Thailand. In northern Thailand, six major faults show sense of movement in normal-oblique fault with slip-rates between 0.5-2.0 mm/yr with earthquake damages around M7.0 on the Richter scale (Figure 1.3).

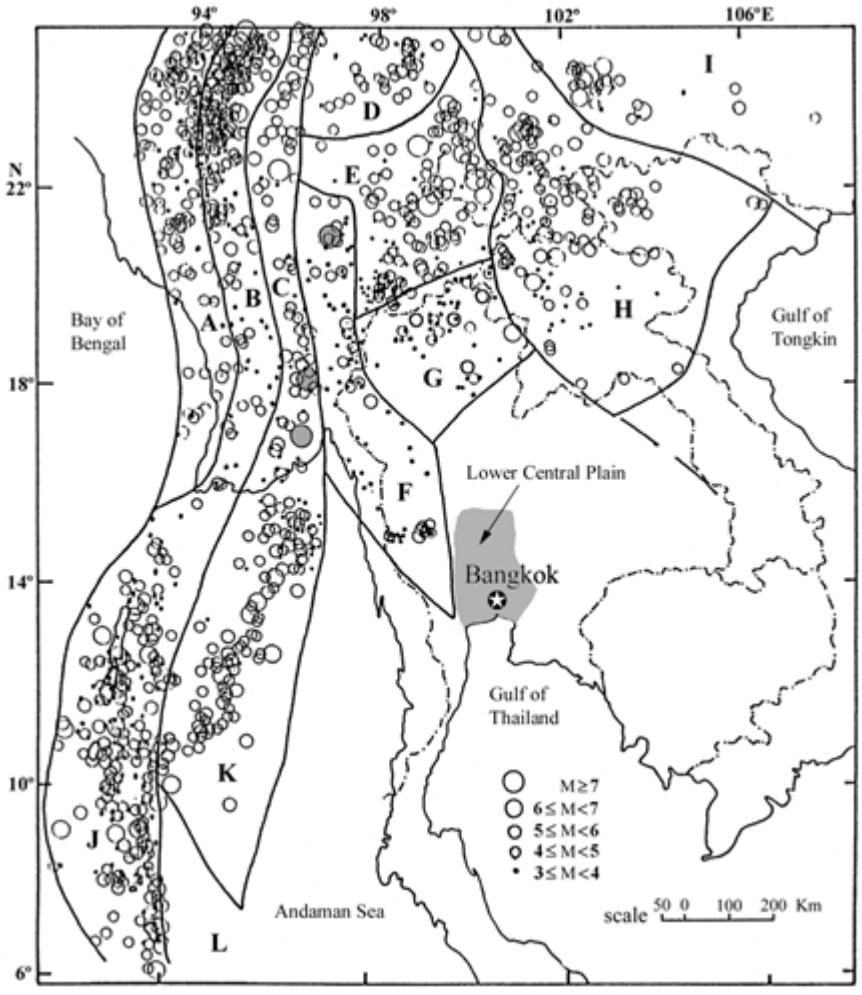

Figure 1.2 Seismic source zones (A-K) in the Thailand-Burma-Indochina region and earthquakes recorded during 1910 – 2000. (Pennung Warnitchai, 2004).

Morley (2007) interpreted satellite data images from Yunnan to Northern Thailand, show predominantly recent Cenozoic faults strike NNE-SSW, N-S to NNE-SSW and NE-SW to ENE-WSW with sedimentary basins aligned NE-SW to N-S. The patterns in the region are usually interpreted as strike-slip dominated deformation. Stepping patterns (en echelon and releasing bend) on sedimentary basins surrounding NE-SW to ENE-WSW trending faults indicate sinistral displacement (Figure 1.4).

Pailoplee et al. (2009) identified active fault zones using remote-sensing data on earthquake source parameters. Show Dien Bien Phu Fault zone (Fault no.4) was shown to be strike-slip fault caused by the Eurasian and Indian plates colliding (Polachan et al., 1991) with surface rupture length is 130 km. The slip rate is 2 mm/yr. Maximum possible earthquake magnitude (m_{max}) is 7.5. Ruptured area is 2,163 km^2 (Figure 1.5).

Recently Pailoplee, Channarong, and Chutakositkanon (2013) used a statistical investigation of recorded earthquakes to locate potential sources of future earthquakes and estimate the maximum possible magnitudes and recurrence intervals along the Thailand-Laos-Myanmar border. The results suggest that the areas that have the greatest potential to generate earthquakes are the northeastern part of Mong Pan and the dam areas of Luang Prabang and Pak Beng with a potential annual magnitude of m_b 4.0 - 5.0 and up to m_b 7.0 within 50 years and potentially short return period (1-500 years). Correlating with a low *b-value* area, there is a potential of future earthquakes in the northern part of Mong Pan and the Luang Prabang - Pak Beng dams (Figure 1.6).

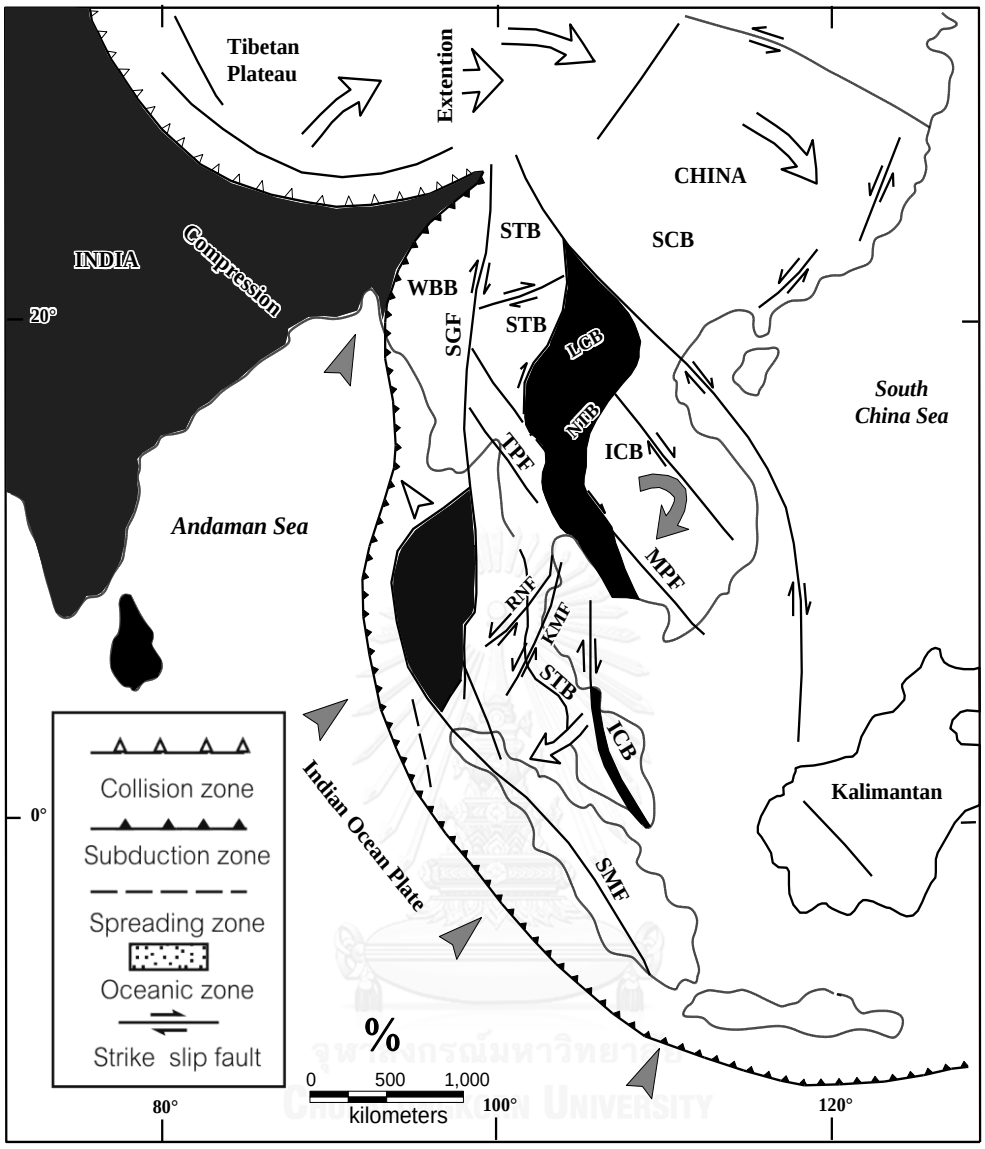

Figure 1.3 Major tectonic elements in Southeast Asia and Southern China. Arrows show relative directions of motion of crustal blocks during the Late Cenozoic. MPFZ - Mae Ping Fault Zone; NTFZ – Northern Thailand Fault Zone; TPFZ - Three Pagodas Fault Zone; UFZ - Uttaradit Fault Zone (after Fenton et al., 2003).

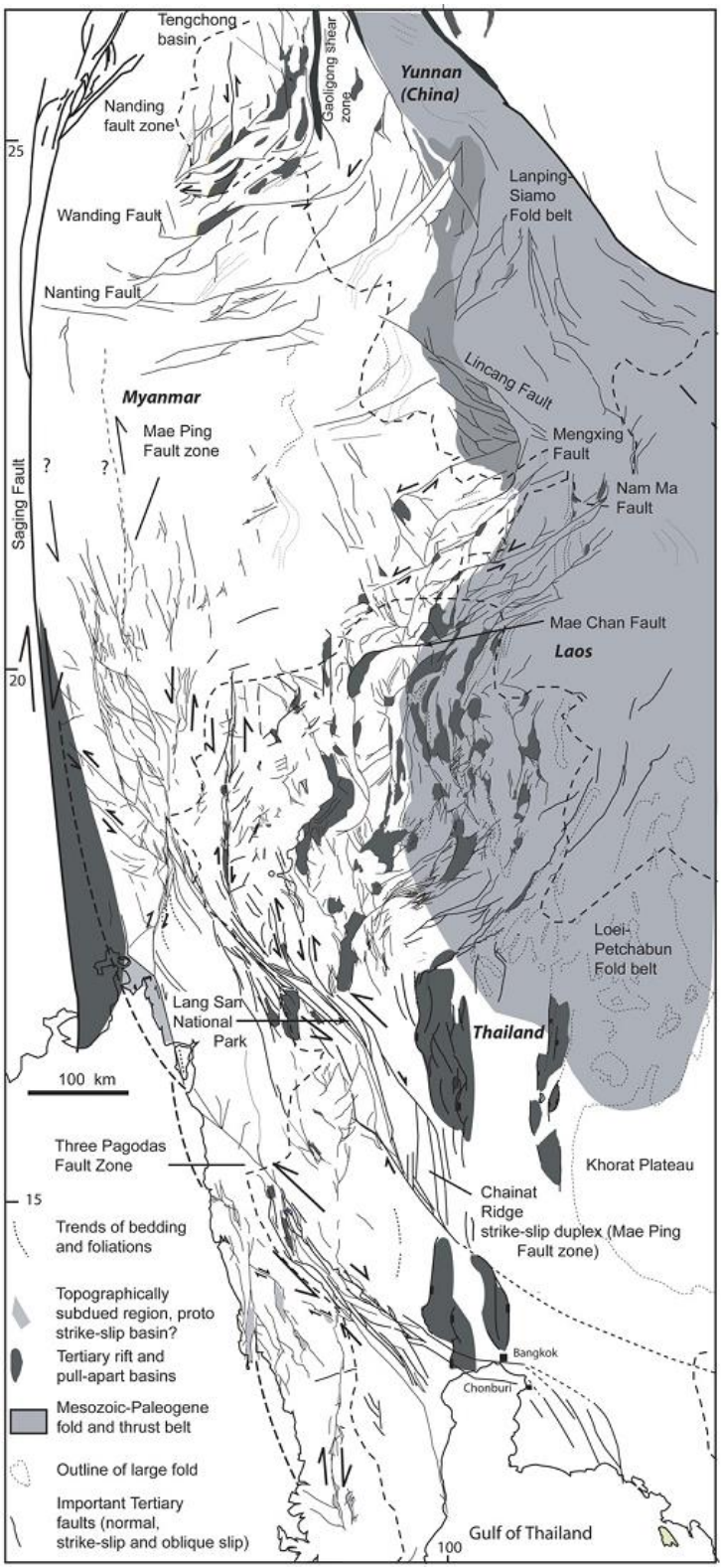

Figure 1.4 Regional map of northern South East Asia. Fault pattern largely derived from satellite interpretation aided by geological maps (Morley, 2007).

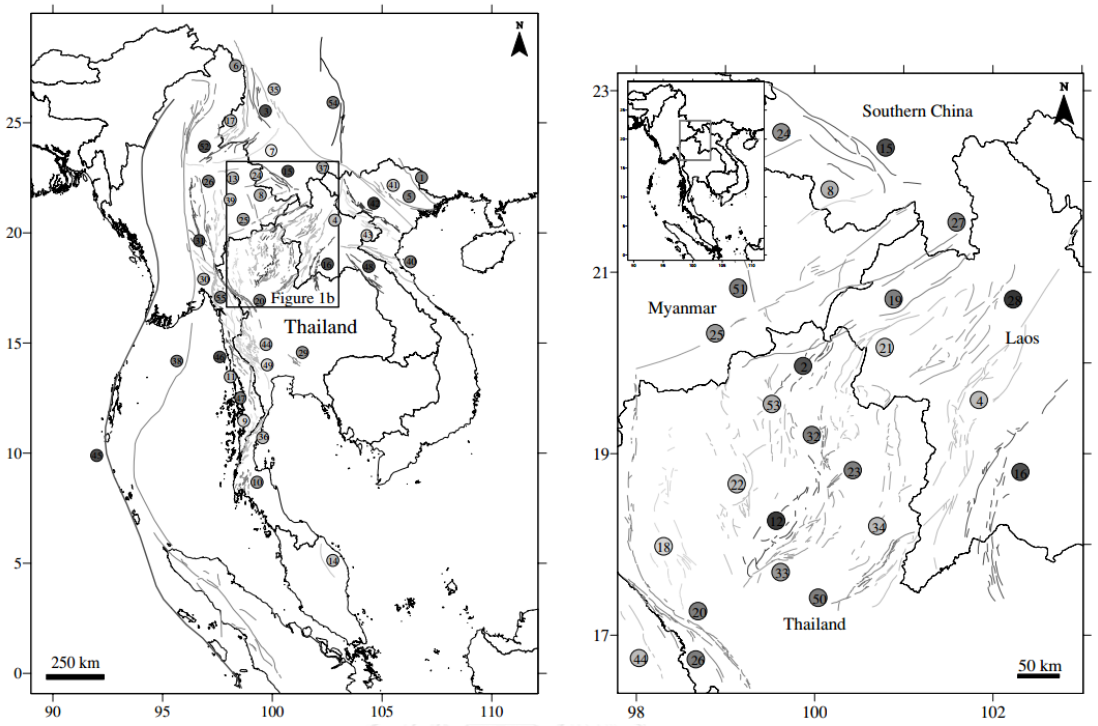

Figure 1.5 (left) Active faults in Thailand and adjacent areas interpreted from remote sensing data. (right) enlarged map showing active faults interpreted in northern Thailand and western Lao PDR (Pailoplee et al., 2009).

1.5 Thesis Outline

In this research work, three major tasks are involved. Compilation and analyses of geology, preexisting information, maps, and seismological data related to the study area form the first task. So in the first stage, geological maps, sections, and structures related to the study area are the outcome. Emphasis has been placed upon locations, geometry and types of the Cenozoic sedimentary basins where several communities and large man–made structures are located. In the second step, we characterize active faults using space–borne image interpretation. Verifications of these active faults can be done using aerial photographs and field checking. Thus orientation, type, distribution and evidence of active faults in the survey area have been delineated and documented. Structural

lineament and morphotectonic maps as well as fault segmentation in the study area are the principal output of this stage.

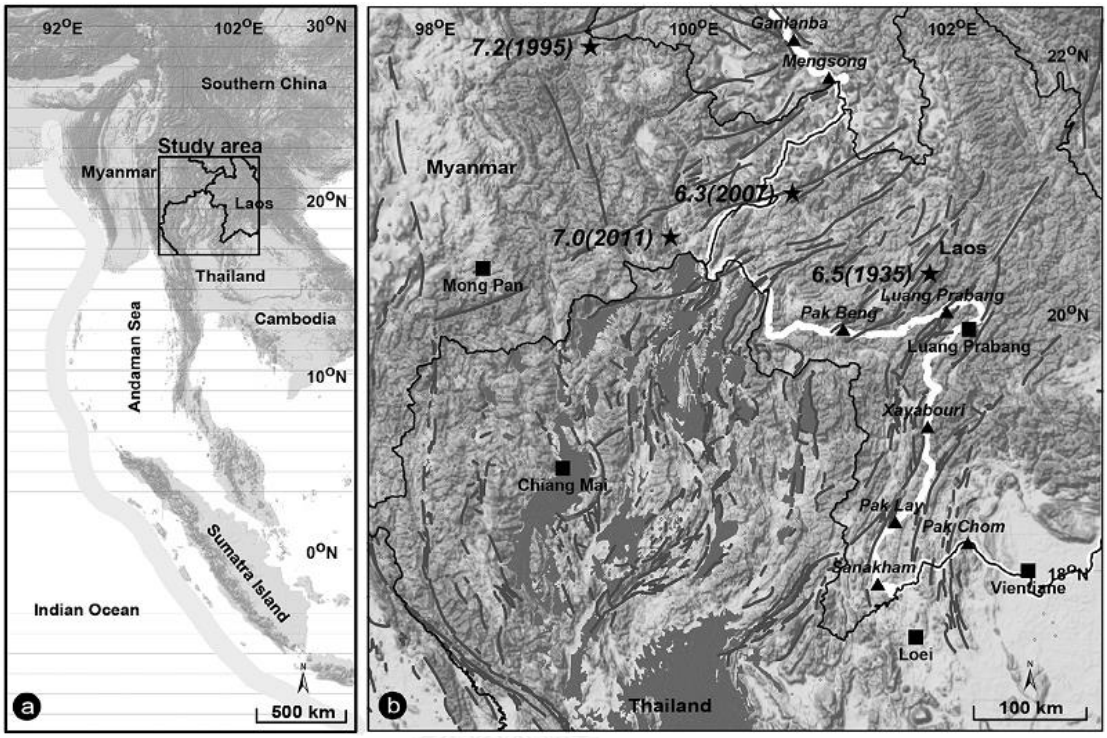

Figure 1.6 (a) Map of Mainland Southeast Asia showing the area of interest along the Thailand-Myanmar-Laos border within the Sumatra-Andaman Subduction Zone (b) Four hazardous earthquakes (black stars) with major cities as black squares in the study area. The seven proposed dams along the Mekong River main stream are marked with triangles. The grey lines are the boundaries of the intermountain basins. (Pailoplee et al., 2013)

The third task involves the result of field investigation on active faults. Concentration has been placed on lines of evidence gathered from field investigation, especially those related to outcrops of both man – made and natural exposures. Also include in this stage is to locate the most appropriate trench locations for paleoseismological exploration. The outcome of this work includes the report on several pieces of evidence and morphotectonic maps showing exploratory trenching locations related to fault lineaments.

In conclusion, 4 major outputs are involved; they are (1) data compilation and analyses, (2) maps of active faults based on remote sensing interpretation, (3) active fault information from field investigation, and (4) characteristic of active faults based on geological and geochronological investigations along with evaluation of earthquake source parameters from both paleosiesmological and seismicity investigations.

This thesis provides an emphasis on tectonic geomorphology and geochronology of the Xaignabouli fault zone in succession of Chapters as following:

Chapter I an introduction, objective, study area and output of the research.

Chapter II literature review of previous work

Chapter III methodology of thesis study

Chapter IV result of research

Chapter V discussion and recommendation

Chapter VI conclusion deduced from the result of research

CHAPTER II
LITERATURE REVIEW

2.1. Regional Geologic setting

The regional landforms of western of Lao PDR consist of mountain ranges and elongated basins with north to northeast strikes. The main rivers mostly follow the basin shape wherein they lie and are controlled by regional geology and structures. The structure of the study area is parallel to the main structure in the same direction. The geological map, scale 1:1,000,000 (Figure 2.1) revised by Wongsomsak and Charusiri (2000) was used to explain the regional geology and regional structural.

2.1.1 Geological Setting

Geology of the region as depicted as a geologic map, scale 1:1,000,000 consist of several units where most rock types are sedimentary rocks whose ages range from Lower Paleozoic to Upper Paleozoic sediment. Since this thesis does not focus on the geology of the concerned area, only a brief review of geology from a previous study is done (Figure 2.1).

2.1.1.1 Sedimentary Rocks

Lower Paleozoic Rocks

In the study area, this rock unit is widely exposed, particularly throughout northeast, central and southwest part of the area in Xaignabouli basin and Phiang basin. It is composed of metasediments and sedimentary rocks.

Upper Paleozoic Rocks

This rock unit is also dominantly observed in the northwest and southeast of the study area. It is composed of sedimentary and metasediments rocks.

2.1.2 Structural setting

In the study area, the major structure that can be well recognized in satellite images is the faults. The major faults are in the NNE-SSW and N-S directions.

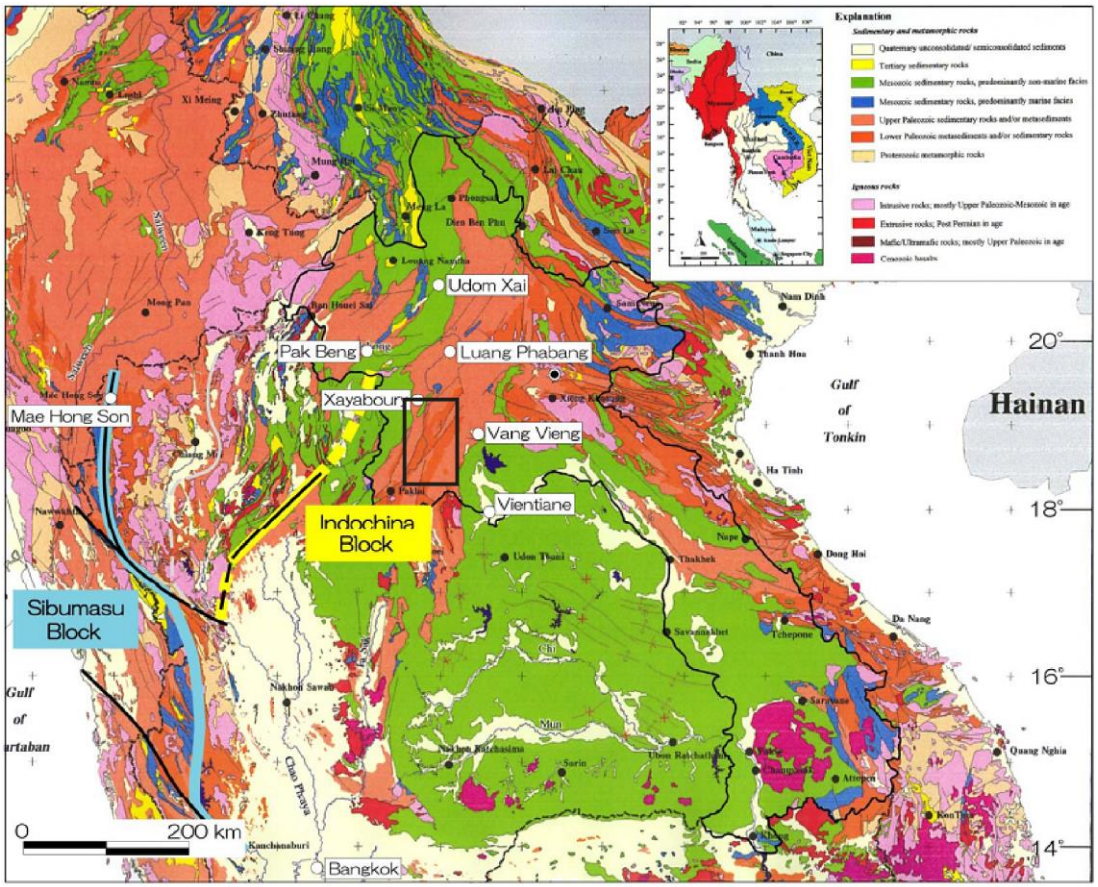

Explanation

Sedimentary and metamorphic rocks

- Quaternary unconsolidataed/ semiconsolidated sediments
- Tertiary sedimentary rocks
- Mesozoic sedimentary rocks, predominantly non marine facies
- Mesozoic sedimentary rocks, predominantly marine facies
- Upper Paleozoic sedimentary rocks and/or metasediments
- Lower Paleozoic metasediments and/or sedimentary rocks
- Proterozoic metamorphic rocks

Igneous rocks

- Igneous rocks, mostly Upper Paleozoic-Mesozoic in age
- Extrusive rocks, Post Permian in age
- Mafic/Ultramafic rocks; mostly Upper Paleozoic in age
- Cenozoic basalts

Figure 2.1 Geology of Lao PDR and nearby regions showing Xaignabouli area of western Lao PDR in located within the Loei - Luang Prabang fold belt (after Wongsomsak & Charusiri, 2000). Note that the study area is in the black box.

2.2 Tectonic setting

The collision between Eurasia and India, which led to the activation of major faults and plate reorganization in East Asia, represents the most significant tectonic event of the Cenozoic Earth (Burchfiel, 2004). In this context, many researchers have investigated the NW-SE trending transverse fault systems in Southeast Asia (Figure. 2.2) since the collision-extrusion tectonic model was proposed by P. Tapponnier et al. (1982).

The interaction between the Eurasian and Indo-Australian plates, and the more remote West Pacific and Philippine plates (Figure. 2.2) have defined the modern tectonic model of Southeast Asia. Thailand has an intraplate setting within the Eurasian plate which is enclosed by colliding boundaries, with the Sunda arc to the south and the Andaman thrust to the west. Australia is moving with a rate of 65-70 mm/yr towards Southeast Asia (McCaffrey, 1996) and Southeast Asia in turn may be moving with a rate of around 10 mm/yr towards Eurasia. The amount of seismogenic faults show continuing deformation within the Eurasian plate (Molnar & Qidong, 1984). Thailand is presently under transtensional tectonic stress with opening along right-lateral and left-lateral slip on northwest- and northeast-striking faults and north-south oriented basins, respectively (Packham, 1993; Polachan et al., 1991), which begun between the Late Cretaceous and Early Tertiary era (Cung et al., 1998; Polachan et al., 1991).

The Cenozoic tectonics of Southeast Asia and Thailand have their origin in the collision of Eurasia with India. Beginning around 50 Ma (Middle Eocene), it resulted in 2000-3000 km of shortening across the Himalayan Orogen (Peltzer & Tapponnier, 1988). During the first 20-30 million years of collision as India pushed into the southern edge of Eurasia, Indochina rotated about 25° clockwise and extruded to the southeast by approximately 800 km along the Red River and Wang Chao-Three Pagodas fault zones

(Peltzer & Tapponnier, 1988). As the collision progressed, extrusions migrated north towards the Altyn Tagh Fault. As the rotation continued the left-lateral sense of motion of the Red River fault was reversed to a right-lateral (Allen et al., 1984; Peltzer & Tapponnier, 1988).

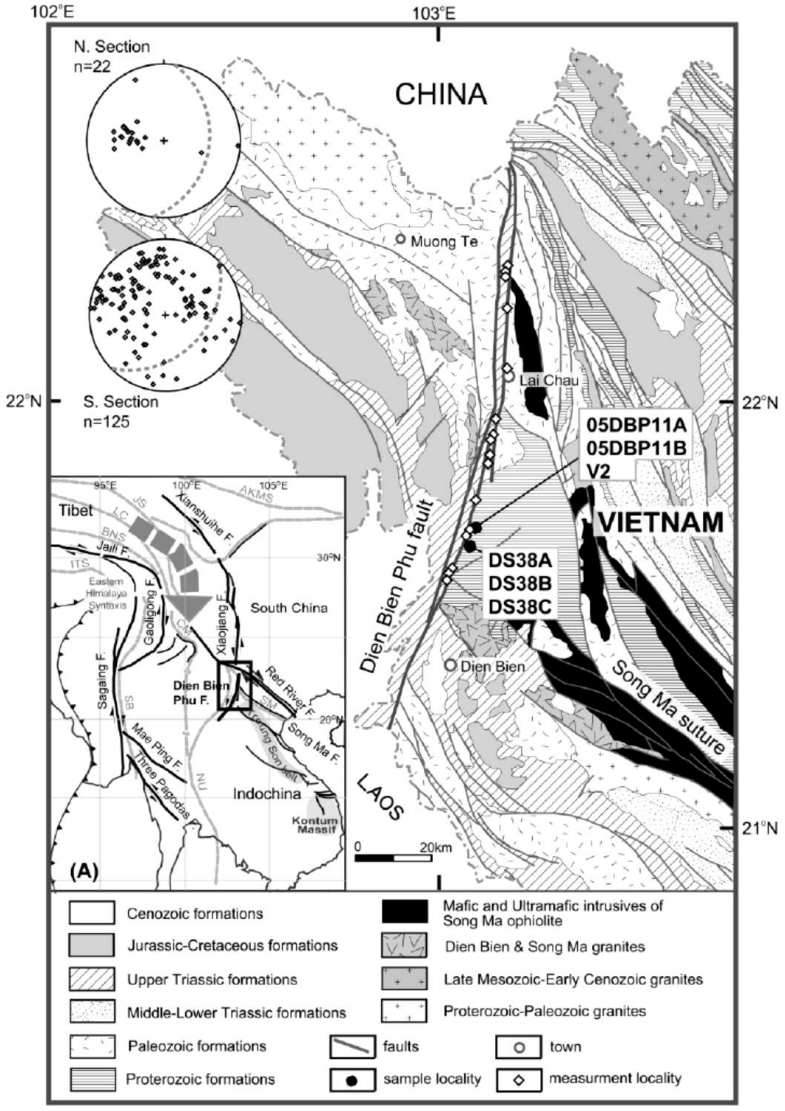

Figure 2.2 Inset: Tectonic framework of southeastern Asia, showing the distribution of major faults. The thick gray arrow indicates the movement direction of crustal fragments around the Eastern Himalaya Syntaxis. *AKMS* = Ayimaqin-Kunlun-Muztagh Suture; *BNS* = Bangong-Nujiang Suture; *CM* = Changning-Menglian Suture; *ITS* = Indus-Tsangpo Suture; *JS* = Jinsha Suture; *LC* = Lancangjiang Suture; *NU* = Nan-Uttaradit Suture; *SB* = Shan Boundary Suture; *SM* = Song Ma Suture. Area in box is

enlarged for main image: a simplified geological map of northern Vietnam, showing sample localities (filled circles). Equal-area stereonets show poles to foliation in areas north and south of the Dien Bien Phu fault (Lin et al., 2009).

The opening of the tertiary basins by transtensional stress was caused by a differential slip between the main strike-slip faults in the Red River, Mae Ping, Three Pagodas, and Sumatra fault zones (Figure 2.3) (Ducrocq et al., 1992). In Thailand, the tertiary basins are grabens or half grabens, typically bounded by north to northwest-striking normal faults (Lorenzetti, Brennan, & Hook, 1994; Polachan et al., 1991) with geometry and location controlled by the north-south-trending structural grain in pre-Triassic rocks and pre-existing northwest-southeast trending, strike-slip faults (O'Leary & Hill, 1989). Throughout Thailand basin evolution follows similar chain of events. The main phase of strike-slip tectonism with extensive fluvial sedimentation resulted in rapid extension (Oligocene-Early Miocene) followed by lacustrine sedimentation as basins became increasingly isolated (Early-Middle Miocene). A flood of rough terrigenous clastics took place as Lacustrine sedimentation ceased, which suggests a period of rapid, localized uplift (Middle-Late Miocene).

Recent GPS data suggest that the Tibetan extrusion is involved in a clockwise rotation (e.g. Clark et al., 2004), meaning that crustal flow is now bounded to the east by a sinistral strike-slip system consisting of the Xianshuihe, Xiaojiang, and Dien Bien Phu faults (DBFF) (Figure. 2.2).

However, geological correlations indicate that the DBFF has dextrally offset the Song Ma belt (Fontaine & Workman, 1997; C. Lepvrier et al., 2004) (Figure 2.2), implying a complicated movement for the fault. This complexity has apparently been magnified by the multiple collision events involved in the amalgamation of the South China, Indochina, (Shan Thai (Sibumasu), and Simao blocks during the Indosinian Orogeny (Carter & Clift, 2008; Carter, Roques, Bristow, & Kinny, 2001).

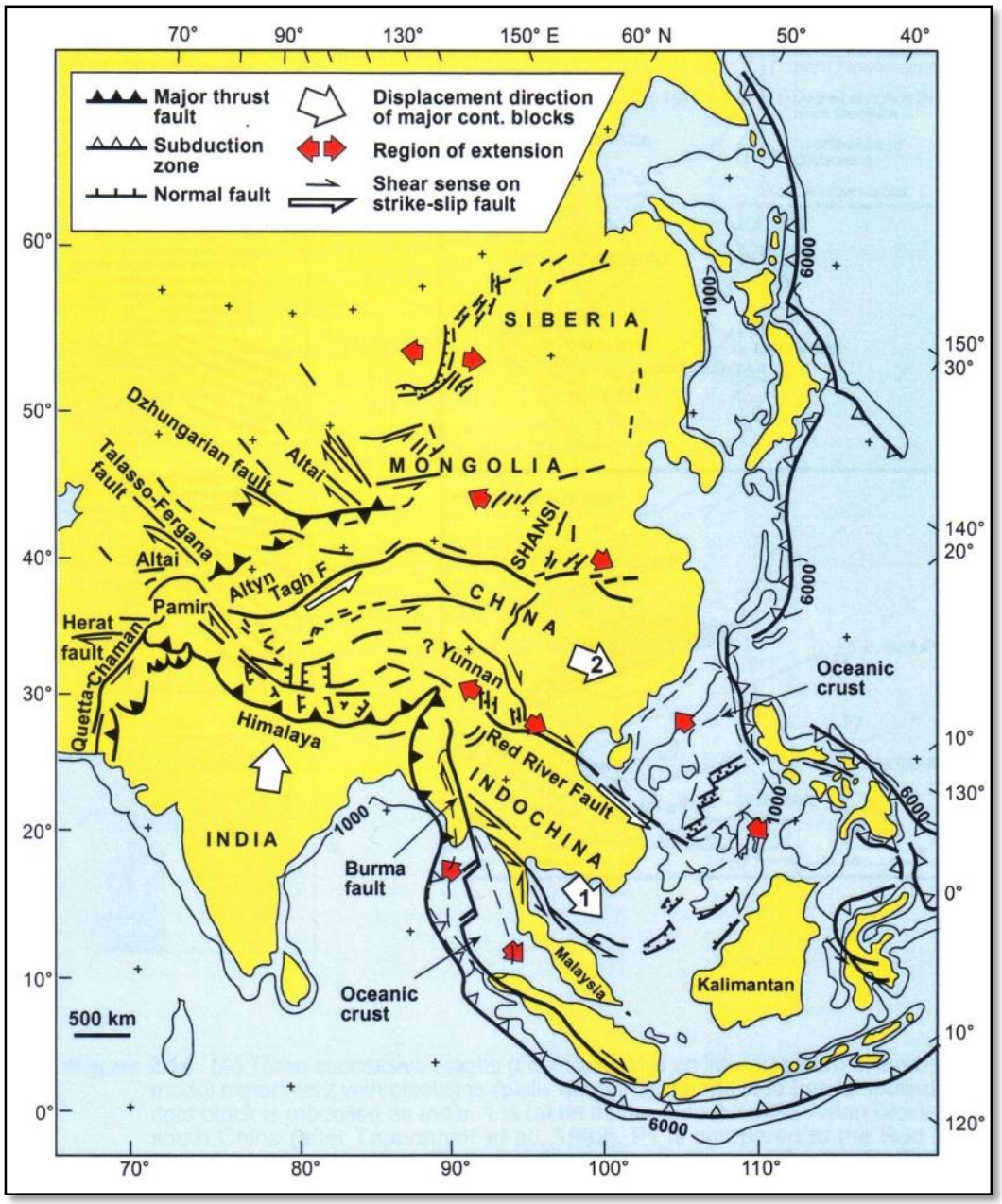

Figure 2.3 Tectonic map showing the extrusion model of central-east Asia and the relationship with regional Cenozoic structures (P. Tapponnier et al., 1982).

Geologically, the study Xaignabouli area is located in the so-called Loei-Paklay fold belt (Stokes et al., 1996) which stretches from the eastern part of northern Thailand to western Lao and is the same as the Loei fold belt of Bunopas (1981). However, P. Charusiri, V., Archibald, Hisada, and Ampaiwan (2002) introduced the term “Nakhonthai plate” which is more oceanic plate to replace the fold belt which is less meaningful. It is

therefore regarded in this study that the Xaignabouli area is situated within the so-called Nakhonthai plate. This plate collided with the Indochina plate during Late Triassic age in response to Indosinian Orogeny. The result of the compression tectonics was able to trigger the essential faulting event. In this circumstance we infer that numerous strike-slip faults in and around the Xaignabouli area have been formed in response to this collision tectonics. Generally, there are several fracture and fault sets in mainland SE Asia (Figure 2.4). However, based on P. Charusiri et al. (2002), only two major conjugate sets of faults are of importance, including one in the NE-SW direction and the other in the NW-SE direction, both of which took place during that Triassic time. P. Charusiri et al. (2002) also show evidence of slip movement in Thailand that the NE-SW trending fault set has the dextral sense of movement and the NW-SE trending fault set has the sinistral sense of movement.

2.3 Seismicity in the Xaignabouli Area

Seismotectonically, it is recognized that the Xaignabouli area is located in the Luang Phrabang – Nan zone where the structure is mainly in the NW-SE direction (Figure 2.5). It is also believed that the stress distribution and fault reactivation have continued towards the study area. However, not all faults in the barge area are considered to be active. In fact there are only some faults which are still active. Therefore, it is an aim of this geological study to find which faults in the study may have been active, when the latest movement occurred and how strong, and what the recurrence interval (or return period) for those active faults may be.

2.4 Dien Bien Phu Fault Zone

Orientated NNE to N and 160 km long and 6–10 km wide, cutting through sediment, the Dien Bien Phu fault zone (DBFF, sometimes spelled Dien Bien Fu), is one of the most seismically active zones in Indochina (Figure 2.6, Witold Zuchiewicz, Cuong, Bluszcz, & Michalik, 2004). Relatively small, narrow pull-apart basins occur (Figure 2.11) along the zone, the three largest of which have been studied in detail (Chan Nua, Lai Chau and Dien Bien Phu). All are bounded by sinistral and sinistral-normal faults, which are

responsible for shutter ridges and displaced terraces, offset and deflected drainage and alluvial fans.

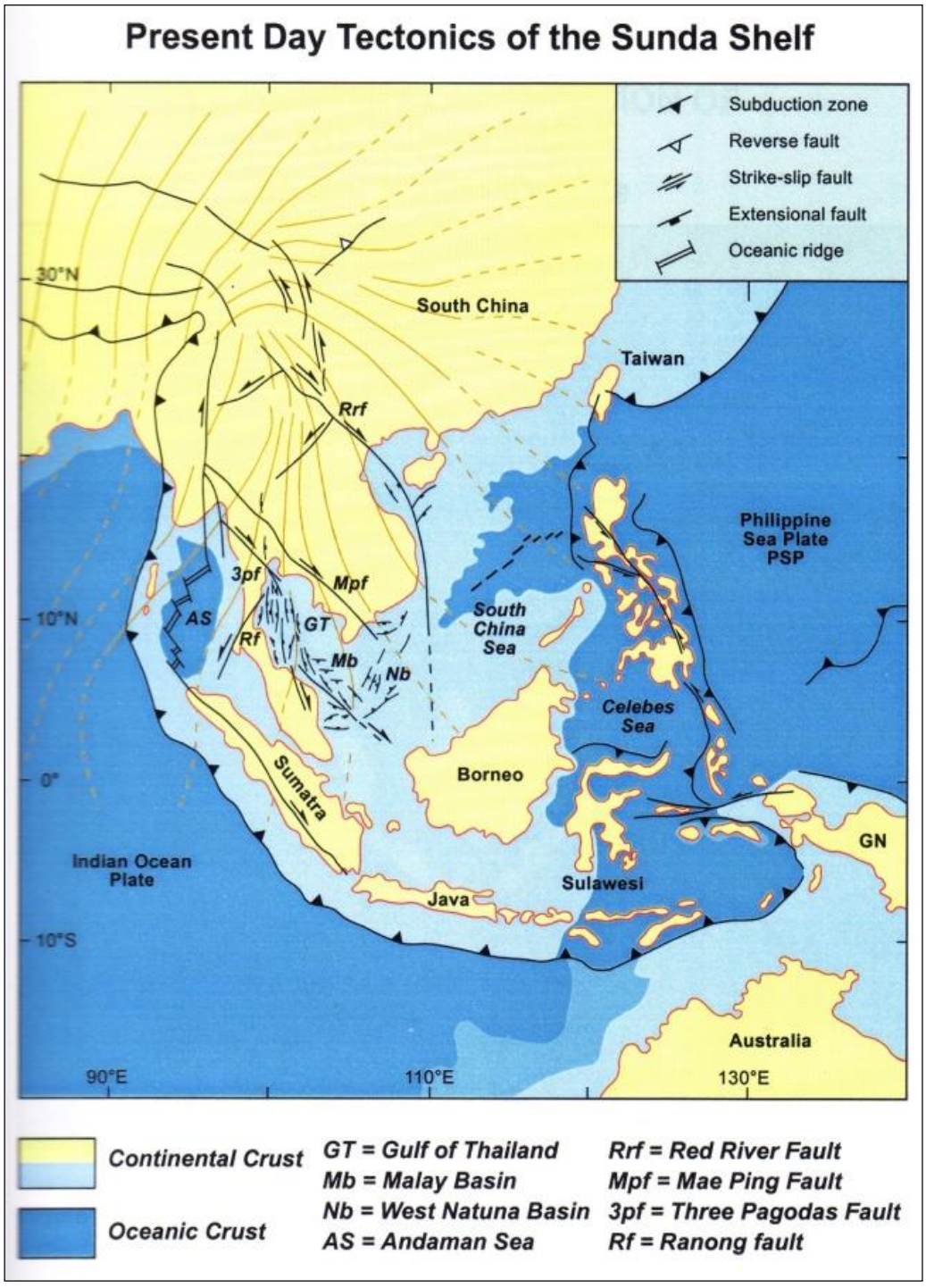

Figure 2.4 Tectonic map of Southeast Asia showing major structural elements in relation to direction of present maximum horizontal stress (after Srisuwon, 2002).

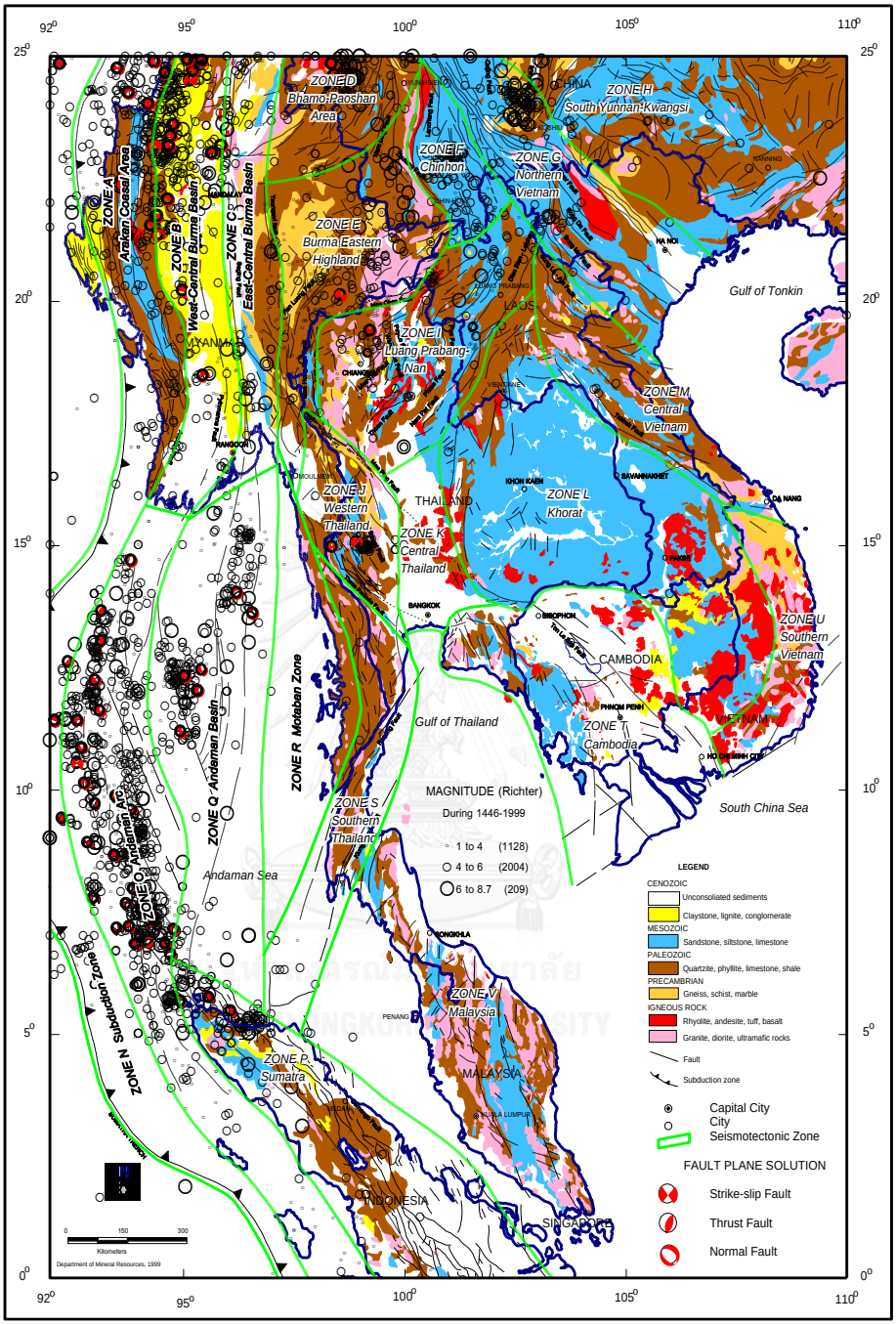

Figure 2.5 Seismic source zones and major fault zones in SE Asia (P. Charusiri, Kosuwan, Daorerk, Vajbunthoeng, & Khutaranon, 2000).

Well-preserved triangular facets on fault scarps demonstrate normal component of motion. A recent minimum sinistral offset ranging from 6-8 to 150 m to 1.2-9.75 km for

Holocene valleys and middle–late Pleistocene valleys respectively have been observed in different fault segments. Quaternary sediment thickness varies from 5–25 m to 130 m in the Lai Chau area and Dien Bien Phu Basin respectively. The middle terrace alluvia (23 m) of Nam Na River at Muong Te bridge in the Lai Chau Basin have been dated at 23–40 to 13 ka through OSL-SAR (optically stimulated luminescence/single aliquot regenerative dose technique). These were normal-faulted by about 11 m after 13 ka and are mantled by varicolored 8–12 m thick slope loams with colluvial wedges of angular debris. The wedges were most likely shaped by at least three paleoseismologic events postdating 6 ka. Using the same method, alluvium of the upper Holocene terraces in the Dien Bien Phu Basin has been dated to 6.5–7 and 1.7–1.0 ka, with younger terrace sediments of 0.5–0.2 ka. The narrow pull-apart basins in the south part of the DBFF are bounded by sinistral and sinistral-normal faults, which reveal minimum rates of left-lateral strike-slip ranging from 0.6-2 mm/year in Holocene and 0.5–3.8 mm/year in Pleistocene times. Holocene uplift may reach 0.4–0.6 mm/year west of Dien Bien Phu and 1 mm/year north of Lai Chau. It is difficult to obtain more precise estimates due to inadequate age control of the displaced drainage. Although of opposing sense of movement, the Quaternary strike-slip rates are analogous with those of the Red River fault. Considering the geometry and presence of two Late Cenozoic phases of strike-slip faulting with opposing sense of motion, we hypothesize that Dien Bien Phu and the Red River faults are conjugate faults with the capability of producing comparatively strong earthquakes.

The NNE to N orientated Dien Bien Phu fault (DBFF) zone extends from Chieng Chai in the north to Tay Trang Pass in the south (Figure 2.7), continuing into Laos and Thailand. Although Wang et al. (1998) believed that the DBFF is probably approaching the Gulf of Thailand, we only infer that the fault extends to the northcentral Thailand.

The DBFF zone cuts late Proterozoic, Palaeozoic and Mesozoic aged sedimentary and metamorphic rock in northwest Vietnam (Figure 2.8). In northern Lao the DBFF zone cuts through Middle and Late Paleozoic sedimentary rocks as well as Palaeozoic and Upper Triassic granitoids. In comparison with the lately dextral Red River (Song Hong)

fault zone (RRFZ), the DBFF zone is a mainly sinistral and probably conjugate fault of RRFZ (Figures 2.6 and 2.7; see also Hùng & Vinh, 2001; Phan Trong Trinh et al., 1999).

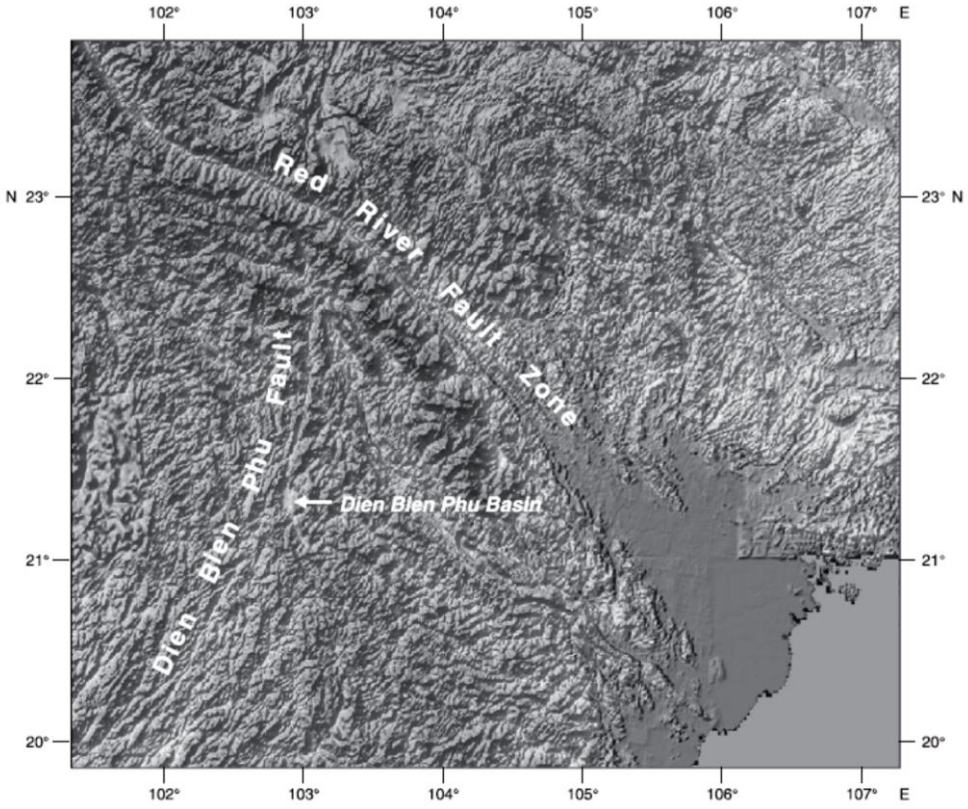

Figure 2.6 Satellite radar (SAR) image of the Red River and Dien Bien Phu faults, based on 30-second GTOPO 30 grid data provided by USGS (Witold Zuchiewicz et al., 2004).

The sense of movement of the DBFF zone in Quaternary times remains a matter of debate and the pre-Pliocene history is poorly restricted. Dextrally displacing the NW-SE-trending Song Ma suture, the NNE-SSW-trending DBFF zone is widely considered one of the most seismically active faults in Indochina (Witold Zuchiewicz et al., 2004).

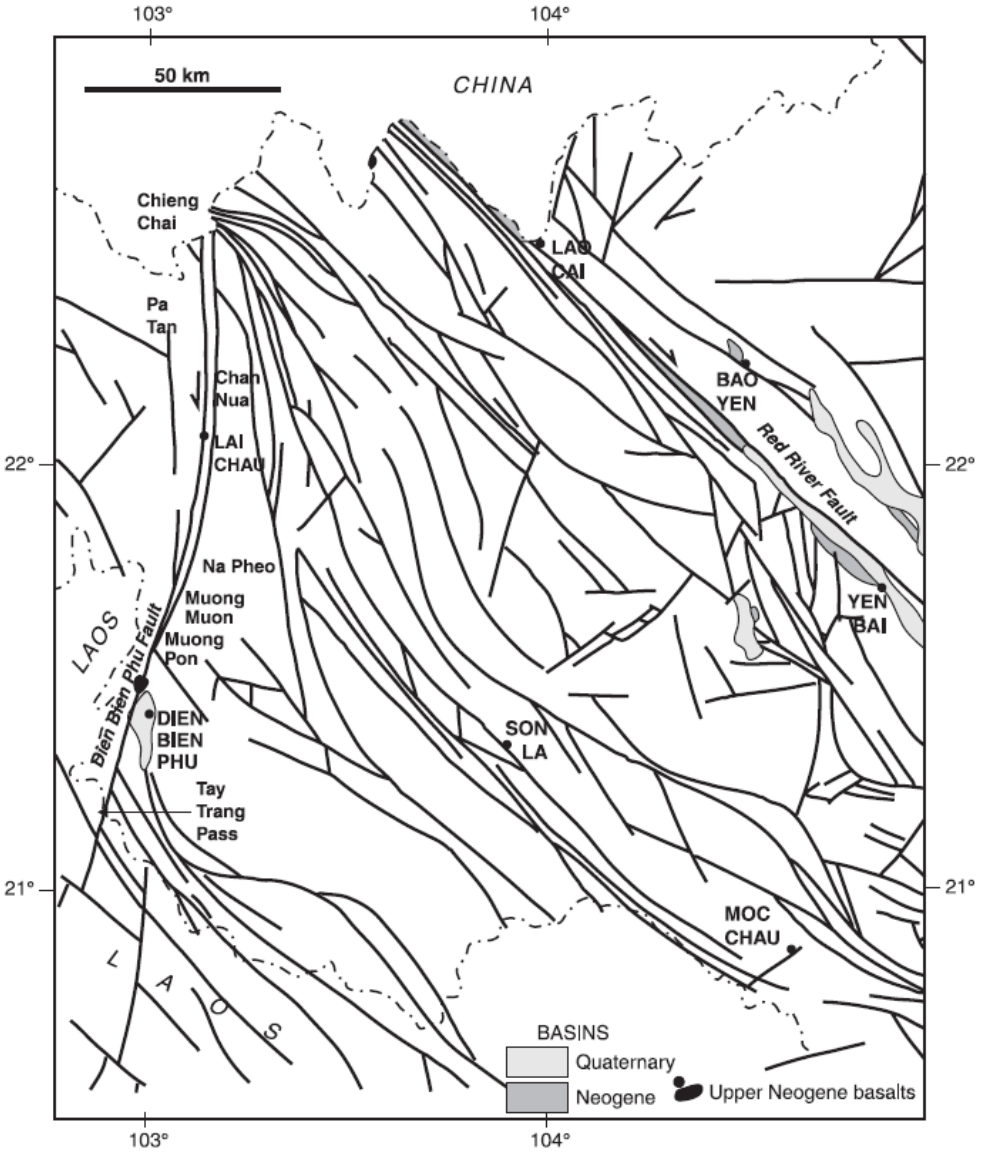

Figure 2.7 The conjugate Dien Bien Phu Fault (DPFF) and Red River Fault zones in Vietnam (based on the work of Tien & Nguyen, 1991; Witold Zuchiewicz et al., 2004).

Occasional structural sketches (Hùng & Vinh, 2001) and geological maps at scales 1:200,000 (cf. My et al., 1978; Tuyet et al., 1978; Son, 1978) and 1:1 M (Tien & Nguyen, 1991) show individual faults in the DBFF zone with entirely different patterns, while interpretations of late Cenozoic sense of slip (sinistral; e.g. Hùng & Vinh, 2001; vs. dextral, e.g. Son, 2000; Ph T Trinh, Lacassin, Tapponnier, Leloup, & Yem, 1993) as well

as the character of Quaternary sedimentary basins (graben vs. pull-apart) are far from clear (Figures 2.9 and 2.10).

The NNE-SSW- to N-S-trending Dien Bien Phu fault (DBFF) dextrally offsets the Song Ma suture zone in northwestern Vietnam, which divides the Indochina and South China blocks (Figure 2.9) and is characterized by metamorphosed mafic and ultramafic masses (Hutchinson, 1975; C. Lepvrier et al., 2004; Trung, Tsujimori, & Itaya, 2006). Despite fossil records of fish that indicate a geographic association between the two blocks during the Devonian period (Thanh, Janvier, & Phuong, 1996), Argon–argon dating substantiates that merging of the two blocks actually took place in the Early Triassic (Claude Lepvrier et al., 1997).

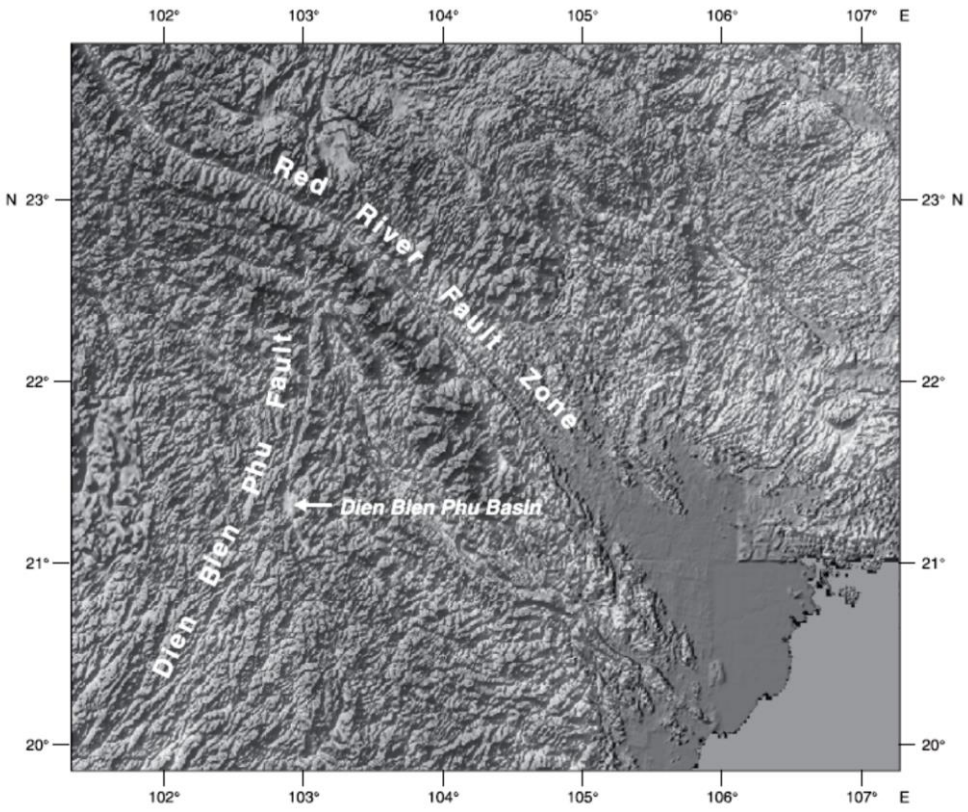

Figure 2.8 Satellite radar (SAR) image of the Red River and Dien Bien Fu faults, based on 30-second GTOPO 30 grid data provided by USGS. (Zuchiewicz et al., 2004)

Although seismic and geomorphic data from the Dien Bien Phu fault suggest a sinistral slip accompanied by a component of normal faulting (Peltzer Tapponnier, Peltzer,

& Armijo, 1986; Zhang et al., 2004; Witold Zuchiewicz et al., 2004), no sinistral ductile deformation is observed in the field except sinistral brittle deformation and a series of small, narrow pull-apart basins filled with Quaternary sediments. Estimated slip rates (0:4–3:8 mm/yr) of sinistral movement along the Dien Bien Phu fault are broadly comparable with those of present-day dextral movement along the Red River fault, indicating a conjugate relationship between the two faults since the Holocene (Witold Zuchiewicz et al., 2004).

There are granitoid intrusions of the Dien Bien Phu (Palaeozoic) and Kim Bai (Upper Triassic) complexes (My, Ky, Hoanh, Tuyet, & My, 1978; Tuyet, Hoi, Hung, & Thong, 1978, Figures 2.9 and 2.10) in the DBFF zone fault zone. In the SE part, exposures of granitoid and granite intrusions in Silurian–Devonian flyschoid shales and acid volcanic tuffs are found, followed northwards in the Song Ma suture by ultramafic rocks that are thrust upon Palaeozoic strata. Even further north they are substituted by Triassic shales and limestones, strongly folded Permian mafic volcanics and Cretaceous continental red beds belonging to the tightly folded Song Da orogenic belt (Leloup et al., 1995; Figure 2.10). The main and related subsidiary faults have strike-slip and oblique-slip character. In the northern part of the zone the principal fault plane dips 60–70j to the west and in the southern 70–80j (even to 90j) (Hùng & Vinh, 2001). Mesozoic rock exposure are offset dextrally by 45–50 km (Wemmer, Sievers, Thang, & Trinh, 1999) or 50–100 km (Fontaine & Workman, 1997), however the fault is presently of sinistral and normal-sinistral character, the normal component increases to the north (Hùng & Vinh, 2001; Peltzer Tapponnier et al., 1986; Wang et al., 1998); see also Figure 2.10). Certain seismologists still assert that the fault is dextral (Son, 2000).

Dextral faulting ended in either in Early Cretaceous (Leloup et al., 1995; Wemmer et al., 1999) or in Late Miocene times (Hùng & Vinh, 2001; Kiem, Quy, Tuyet, & Van, 1999; Phan Trong Trinh et al., 1999). The amount of Quaternary sinistral offset has been estimated at 250–800 m (Ph T Trinh et al., 1993) to >2 km (Hùng & Vinh, 2001; W Zuchiewicz & Cuong, 2002). More exact dating of the change of the sense of slip is not possible due to lack of Tertiary strata along the fault zone. The age control of Quaternary

sediments is far from sufficient apart from initial palynological determinations performed on infrequent drilling cores in the DBFF Basin (cf. Dy, Tu, Thuan, & Tan, 1999). Pliocene–Quaternary offset estimates are based only on position of shutter ridges and geomorphic studies of drainage deflection. Exposures of Upper Neogene (8.2 Ma) follow the fault zone in the north of Dien Bien Phu town, and in town by the earliest Pliocene tholeiitic basalts (5.4–5.2 Ma; Hoang, Flower, & Carlson, 1996; Lee, Angelier, Chu, Yu, & Hu, 1998; to 5.2 Ma Pécskay, Balogh, & Tóth, 2002), as well as thermal springs (Punya Charusiri, Buenkhuntod, Won-In, Thayakupt, & Niampan, 2003) and increased methane, radon and carbon dioxide emanations (Hùng & Vinh, 2001). The strongest Vietnamese earthquakes, of magnitudes up to M_S 6.8 (Trieu, 2001; Trieu, Xuan, Thang, Dung, & Tuyen, 1999 ; see also Figure 2.11) are also associated with the area.

Seismic events of M_S up to 5–6 (max 1935 AD, Ms 6.8) occurs in the area and shows strike-slip focal mechanism (Trieu et al., 1999). In both the Dien Bien Phu and Lai Chau area the average density of earthquakes is 4 per 1 sq. km. An earthquake in Dien Bien city in 1935 led to the creation of ground cracks up to 20 cm wide and 50 m long (Xuyen & Dy, 1994). In 2001 earthquakes occurred on February 19 in the south of Dien Bien Phu and on April 3, north west of Lai Chau (M_S 5.3, I=7º and M_S 4.9, focal depth 8 km respectively). In the western part of the basin, minor damage to housing was caused by the February event. A maximum horizontal compressive stress with N–S orientation is implied by the cracks in walls, matching a sinistral fault with NNE orientation. Landslides and debris flows were triggered by the April event.

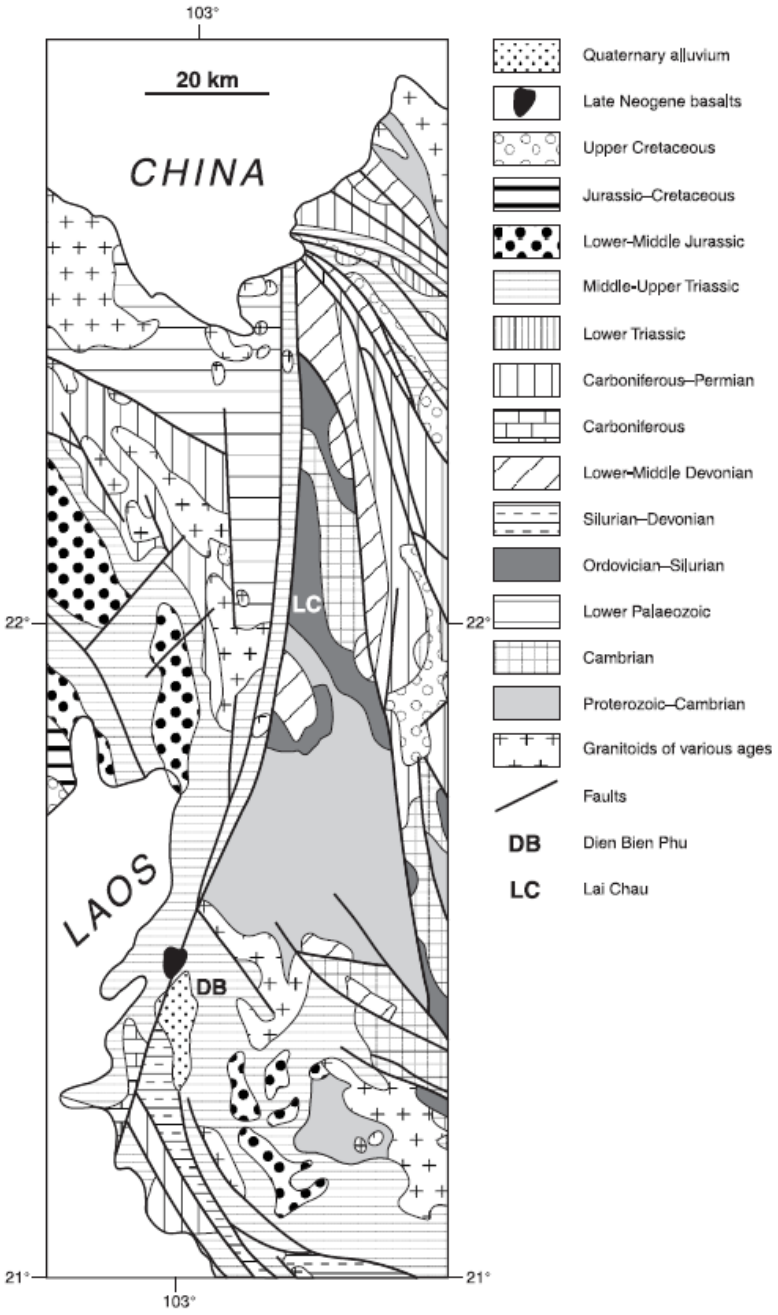

Figure 2.9 Simplified geological map of the Dien Bien Phu fault (DBFF) system in northwestern Vietnam (based on the work of Tien & Nguyen, 1991)

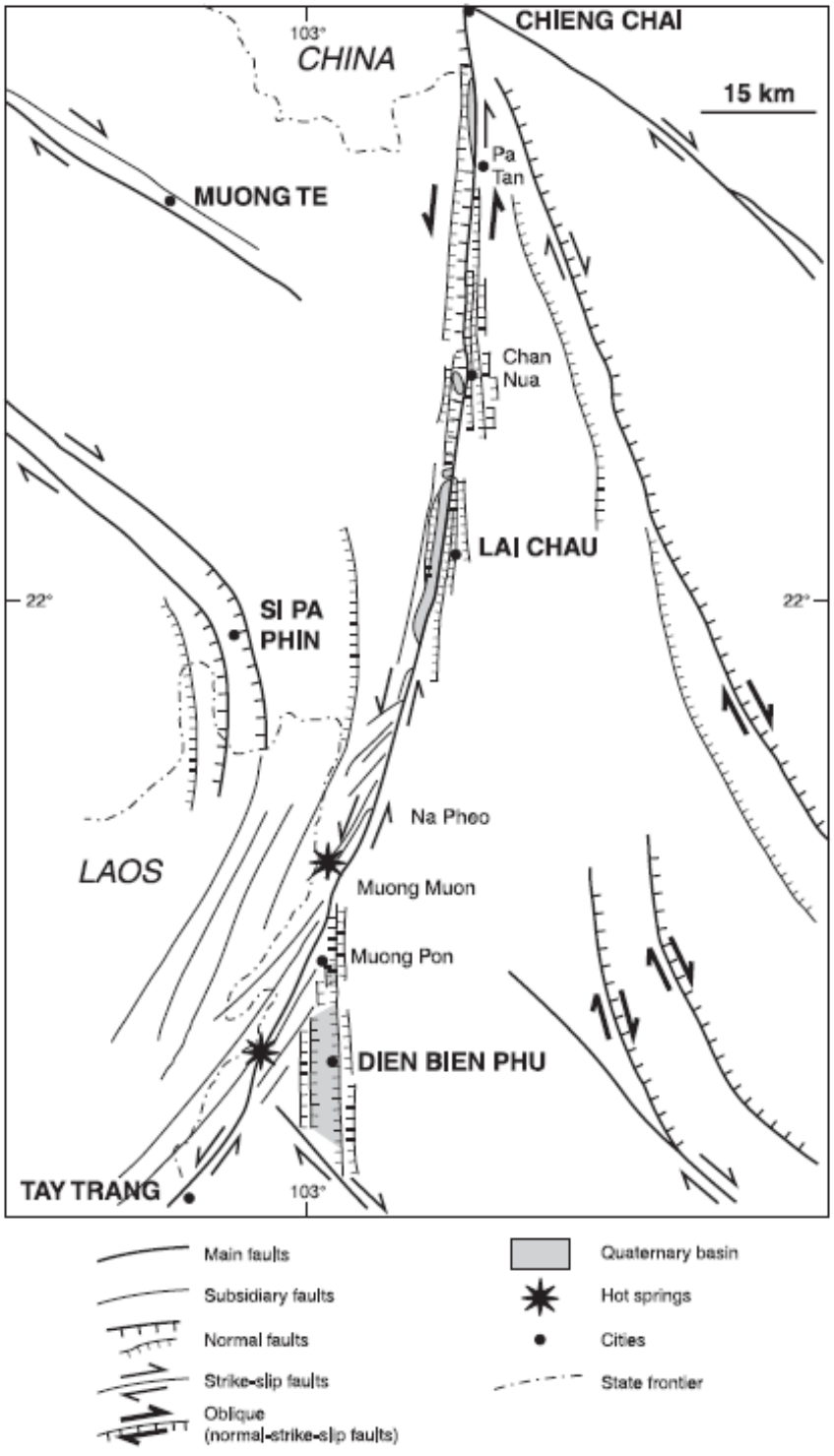

Figure 2.10 Simplified structural sketch map of the Dien Bien Phu fault (DBFF) zone mainly in northern Vietnam (Hùng & Vinh, 2001).

Additionally, Global Positioning System (GPS) measurements from 2002 to 2004 were used by Duong, Yun, and Cho (2002) to estimate recent crustal movement along the DBFF zone in northwest Vietnam (Figure 2.12). The result indicates that the DBFF zone is almost certainly active in the present day as a sinistral strike-slip fault as described earlier by Hùng and Vinh (2001) and Burchfiel (2004). The GPS data shows that regionally the DBFF zone in the Indochina block together with South China block is moving east – southeastward (Figure 2.13) similar to the earlier report by Michel et al. (2001).

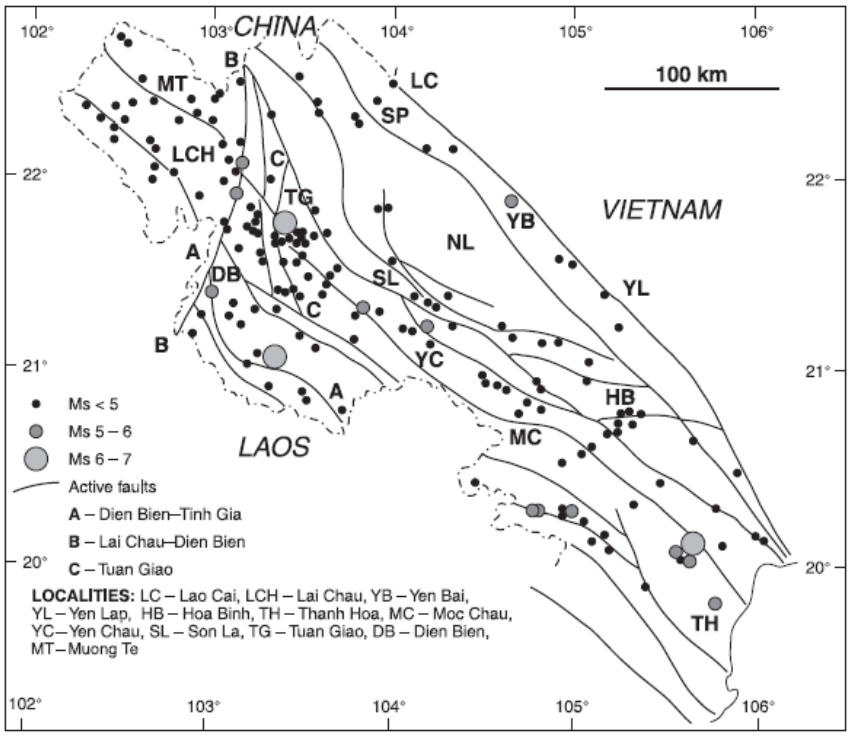

Figure 2.11 Simplified pattern of seismicity in relation to active faults in NW Vietnam (based on the work of Trieu et al., 1999).

The remote-sensing data are compiled and analyzed in previous studies by P. Charusiri et al. (2002) (Figure 2.14) and Pailoplee et al. (2009) (Figure 2.15, 2.16) to infer the active faults in northern, western Lao PDR and nearby area.

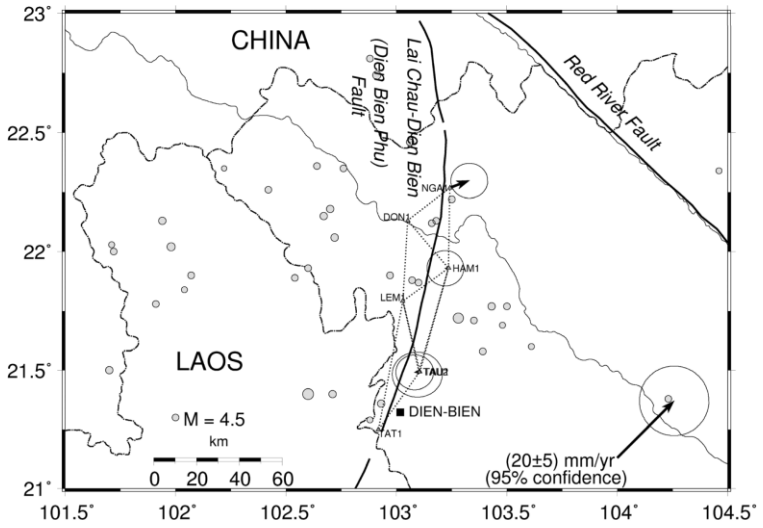

Figure 2.12 Map of northern Lao and northwest Vietnam showing location of Dien Bien Phu Fault (DBFF) and GPS network in the study area with stations (shaded triangles) and their names, earthquake epicenters (shaded circles) with magnitude M > 3.5 from the USGS catalog (1973–Mar. 2005), faults (heavy lines), rivers (thin lines), international borders (dashed lines), and the velocities in a local reference frame defined by DON1, LEM1, and TAT1.

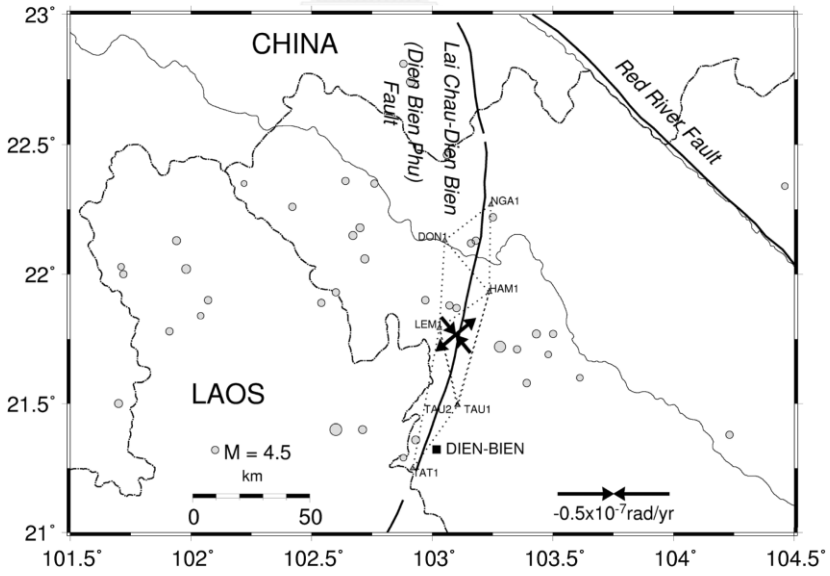

Figure 2.13 Map of northern Lao and northwestern Vietnam showing the location of the NE-SW trending Dien Bien Phu Fault and the maximum extension, compression strain parameters estimated from our ITRF 2000 velocity solution for the whole network. GPS network, earthquake epicenters, faults, rivers, international borders are the same as in Figure 2.13.

New geological, geochemical and geochronological data from P. Charusiri et al. (2002), has resulted in new suture zones (or tectonic lines) being proposed in Thailand and Lao PDR (Figure 2.17). In Thailand they occur as branch sutures, consisting of the Loei, Nan, Sra Keao and Chiang Mai sutures zones and represent the tectonic lines that border the Shanthai, Indochina, and other intervening blocks. In northern Thailand two new blocks, Nakhonthai and Lampang-Chiang Rai, have been clearly defined by P. Charusiri et al. (2002).

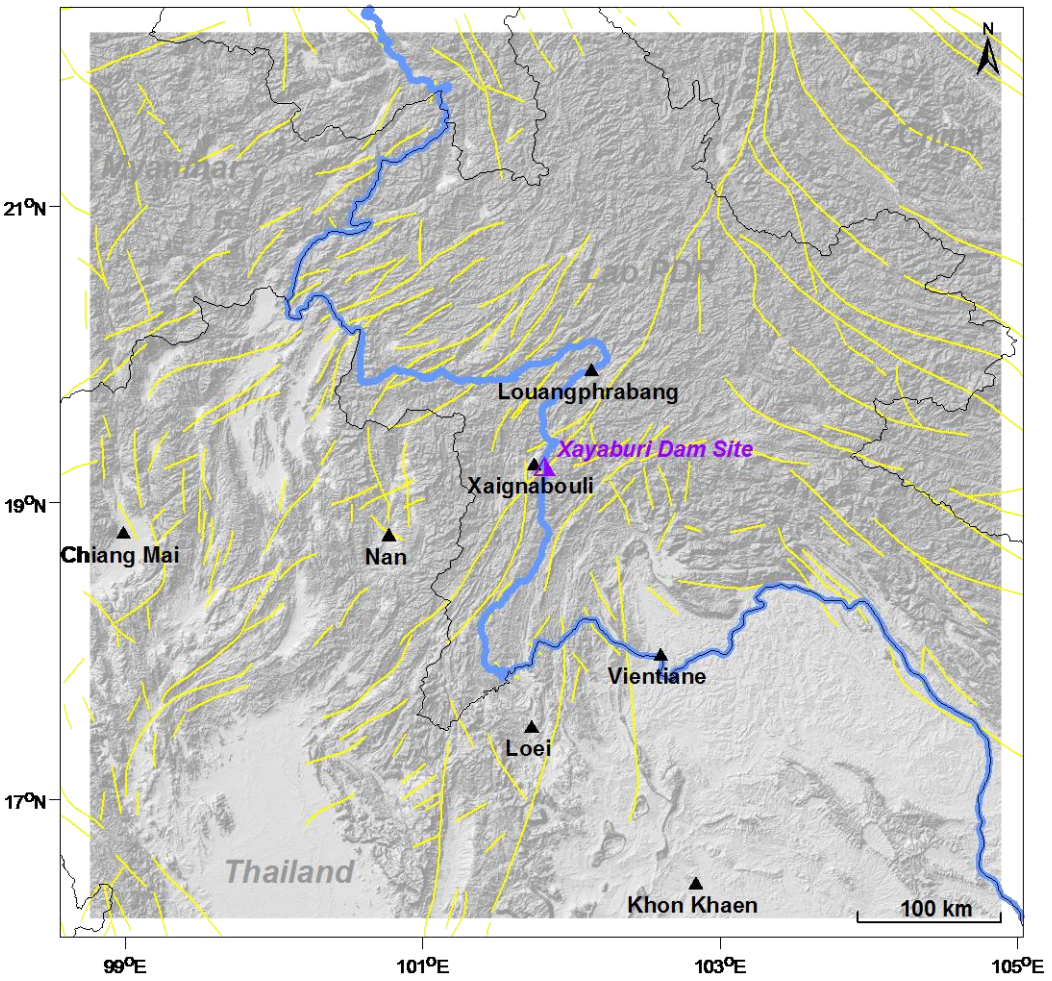

Figure 2.14 Structural lineaments of northern Thailand and northern Lao area interpreted from satellite – borne image (after P. Charusiri et al., 2002). Noted that due to the scale of the image used in the past, some faults cross-cut the main structural features which make difficulties in morphotectonic study.

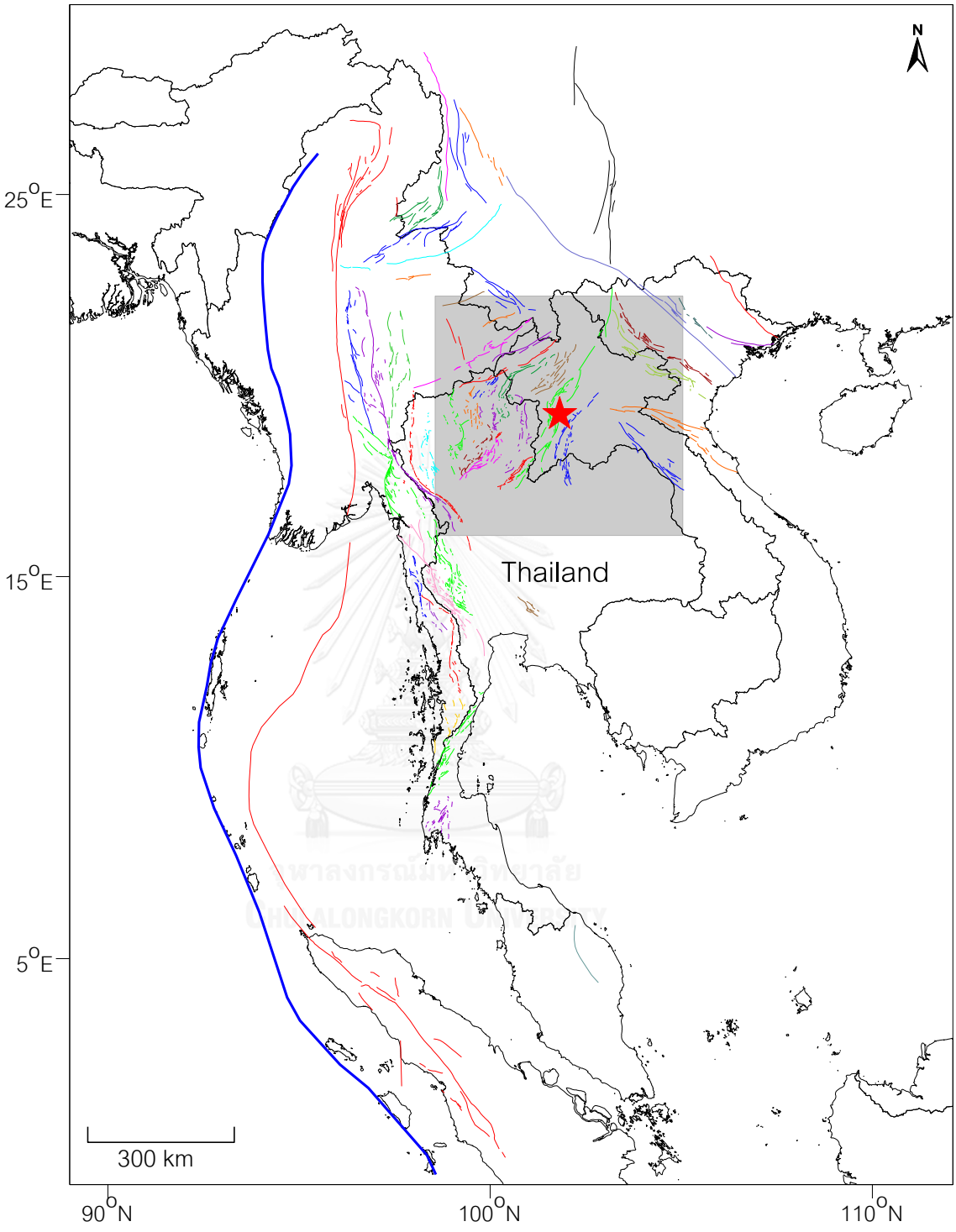

Figure 2.15 Map of the study region showing 55 active faults interpreted from remote sensing data proposed by Pailoplee et al. (2009). In the map, individual fault zones are distinguished by color.

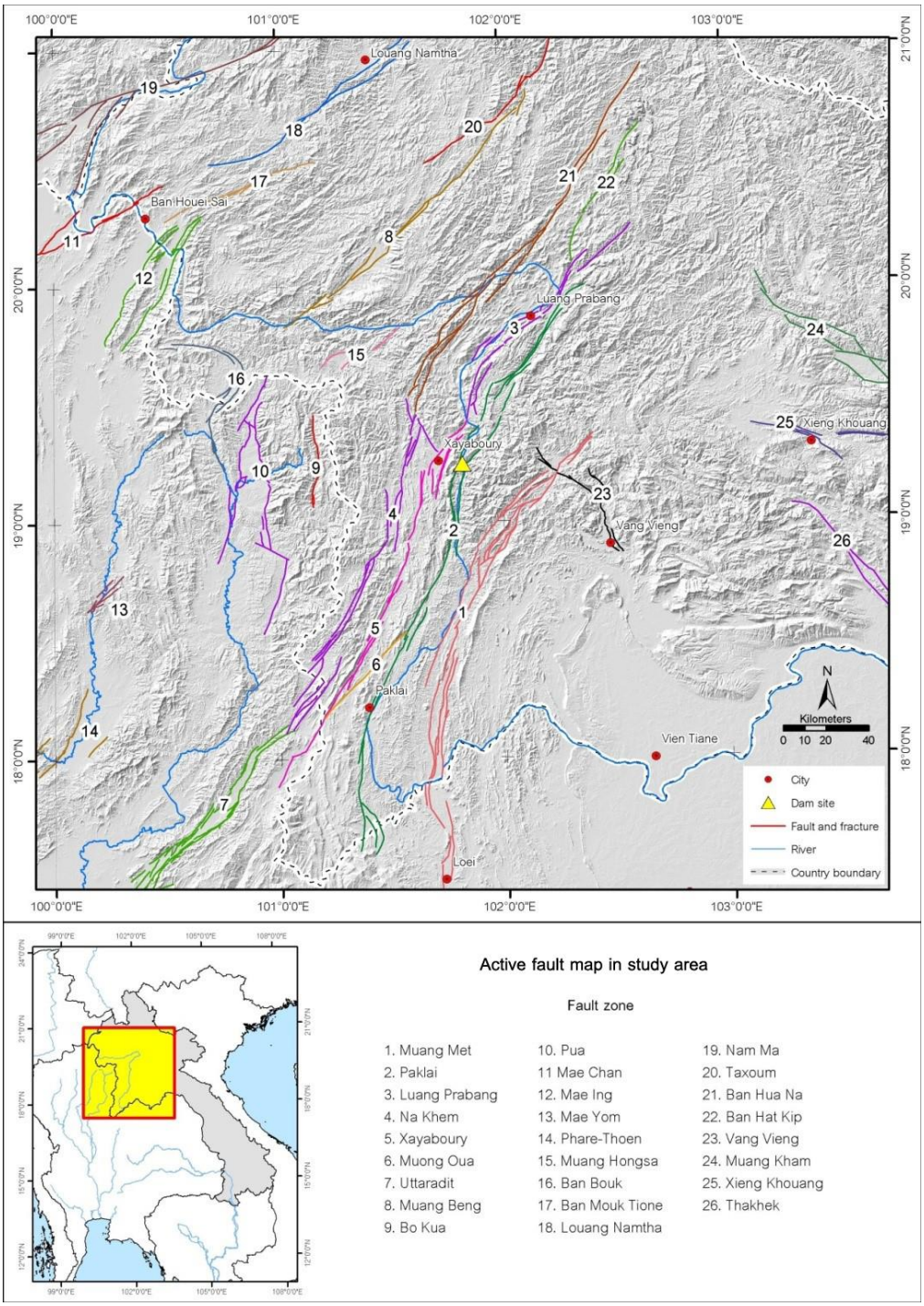

Figure 2.16 Map showing distributions, segments (shown by number), and orientations of active faults within the study area and its nearby regions both in northern Lao and northern Thailand as identified by Pailoplee et al. (2009). Note that no 4 is the Dien Bien Phu Fault (DBPF) and the inserted map showing the location of the study area within the South East Asian region.

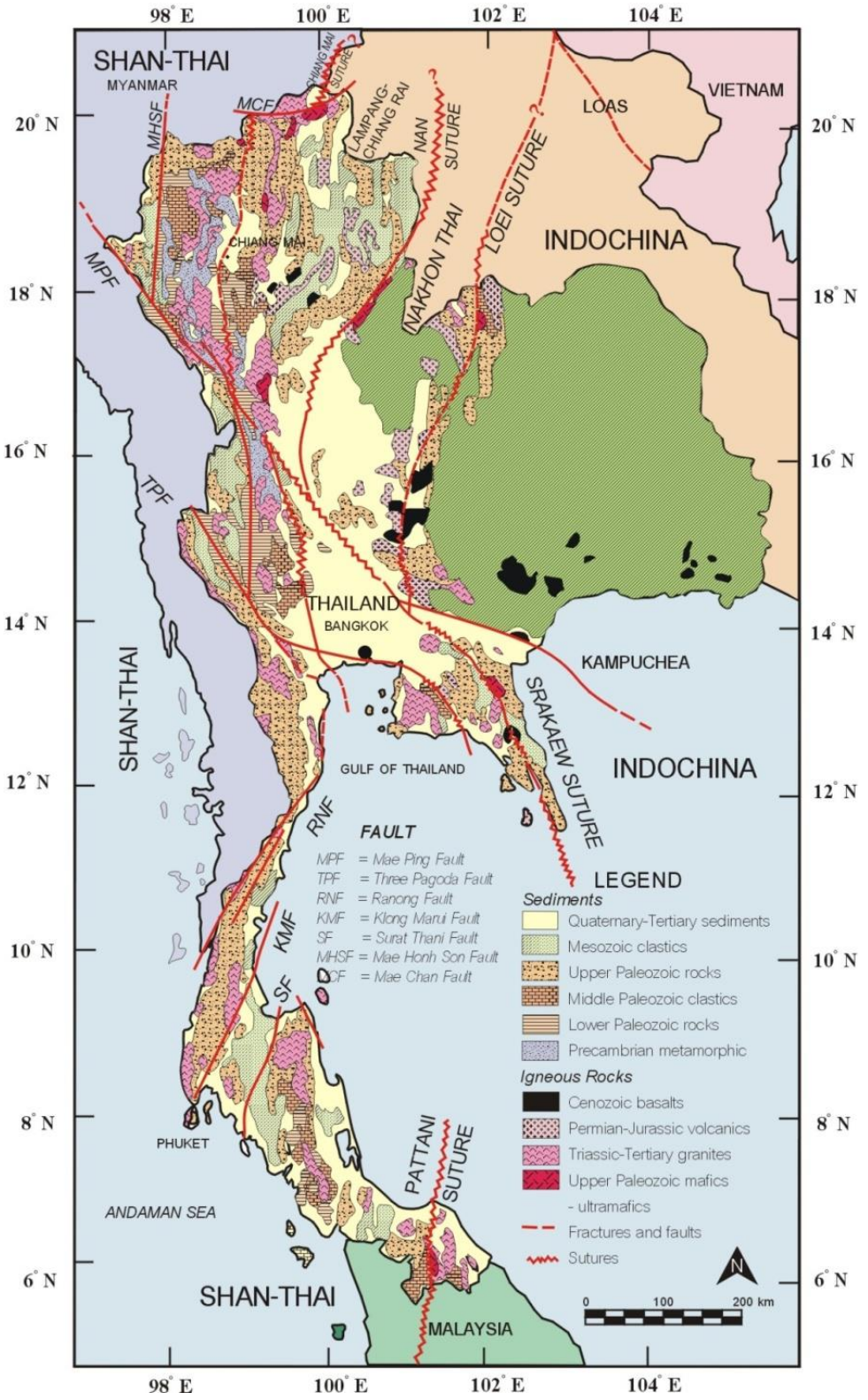

Figure 2.17 Map of Thailand showing major tectonic units, 1 = Shan-Thai plate, 2 Lampang-Chiang Rai plate, 3 = Nakhon Thai plate, and 4 = Indochina plate. (P. Charusiri et al., 2002).

CHAPTER III
METHODOLOGY

The study methodology is divided into seven steps (Figure 2.1). This procedure focuses on geological investigations (i.e. paleo-seismology) according to the method proposed by McCalpin (1996) (step 1 in Figure 1.2). The major and most important task is to compile all available information necessary for detailed geologic, tectonic and paleoseismological investigations of the study area as well as interpretations of satellite images and aerial-photographs. Verification of the interpreted crustal faults existing in Xayaburi region is largely based on field and remote sensing interpretations, which will determine the site of interest selected for paleoseismological. Field geologic and paleoseismological investigation are conducted in the region pertinent to the seismic safety at the study area and fault trenching and dating for active faults. The results are described in stratigraphy associated with faulting. OSL geochronological techniques are applied to constrain the dates of paleoseismological results, such as latest movements and slip rates of the paleoearthquakes.

Moreover, all possible active faults that may affect the study area are compiled. The active fault lines proposed in the previous published maps and documents are re-interpreted using enhanced remote sensing data.

The first step involves data collection to support further stages of the study. The data is compiled by reviewing literature of previous work, selecting topographic maps, analyzing geological maps, screening earthquake epicenters, acquiring remote-sensing images and aerial photographs, and other related technical and nontechnical documents.

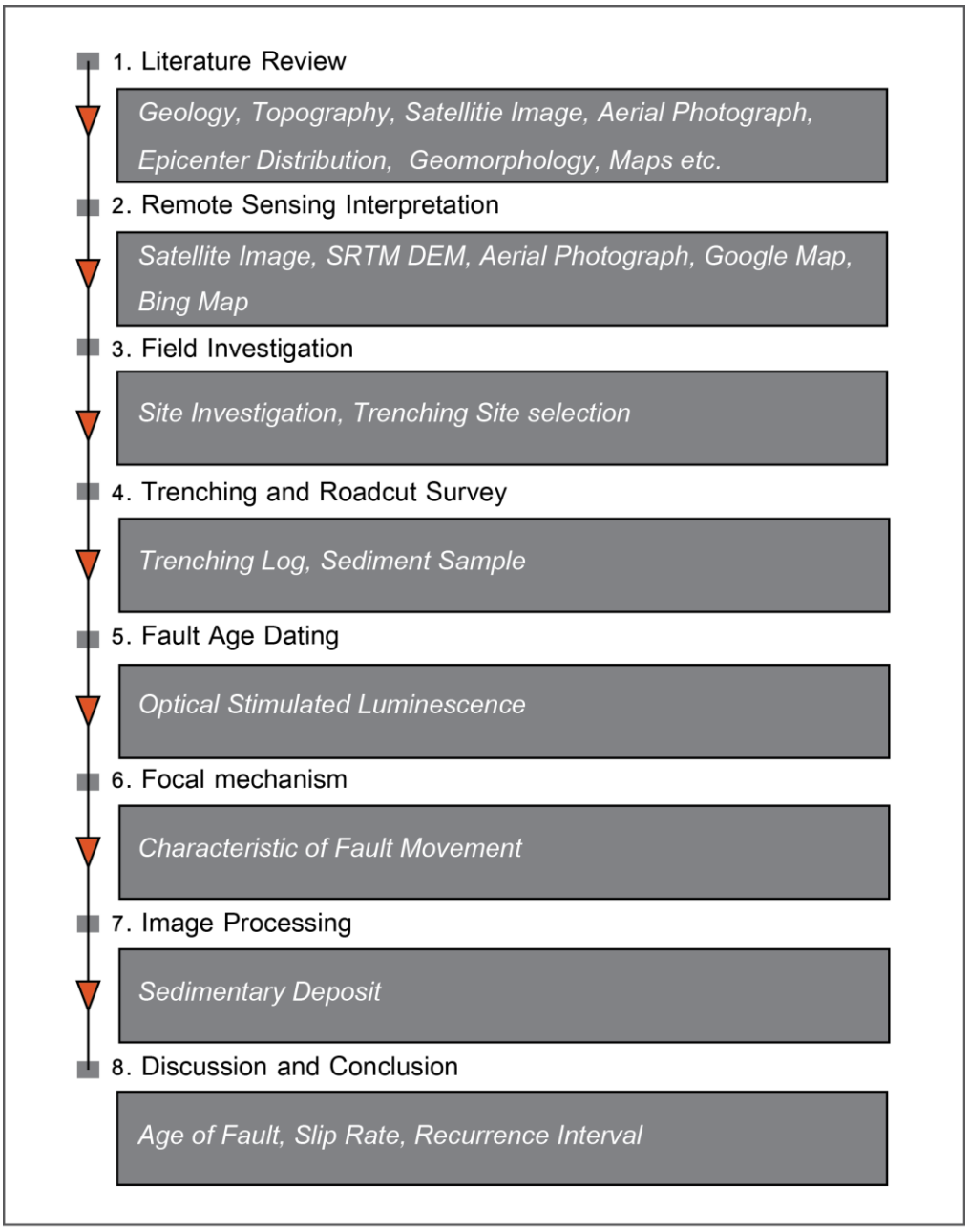

Figure 2.1 Simplified flow chart showing the methodology applied in this study.

3.1 Remote sensing interpretation

Commencement of this second step of remote-sensing interpretation is the study of fine details using digital satellite imageries and interpretation on a large scale with aerial photographs. Basic data for the interpretation is enhanced with SRTM DEM to determine lineaments, their attitude and orientation as well as delineating Cenozoic basins.

Interpretation is also performed using Google Earth data to find geomorphology evidence of active tectonic landforms.

The remote-sensing data are compiled and analyzed in this study to infer the active faults in study area. The purpose is to define lines of morphotectonic evidence on the earth surface, such as fault scarps, triangular facets, shutter ridges and offset streams etc. (Figure 3.2). The next step is to re-locate, re-shape, and re-group the active fault zones reported in the previous studies. The names and regional locations of individual fault zones are cited mostly from previous publications as proposed by P. Charusiri et al. (2002) (Figure 2.14) and Pailoplee et al. (2009) (Figure 2.15, 2.16). The first section is supposed to investigate geological lineaments and Cenozoic basins interpretation in a regional scale using Landsat 7 ETM^{+}, ASTER and SRTM DEM imageries. The second section describes fault segmentation of the Xaignabouli Fault and criteria used. The last section is focused on the detailed study of tectonic geomorphology and results on morphotectonic interpretation of individual selected segments. In addition, morphotectonic maps, which include fault branches and neotectonic evidence of fault movements, are also shown in this chapter.

3.1.1 Satellite image interpretation

3.1.1.1 Satellite images acquisition

A multitude of cameras, instruments and sensors are installed in satellites orbiting the earth. The remote sensing data provided from these are very useful for various applications, such as climate monitoring, mapping and monitoring of disasters (Figure 3.1).

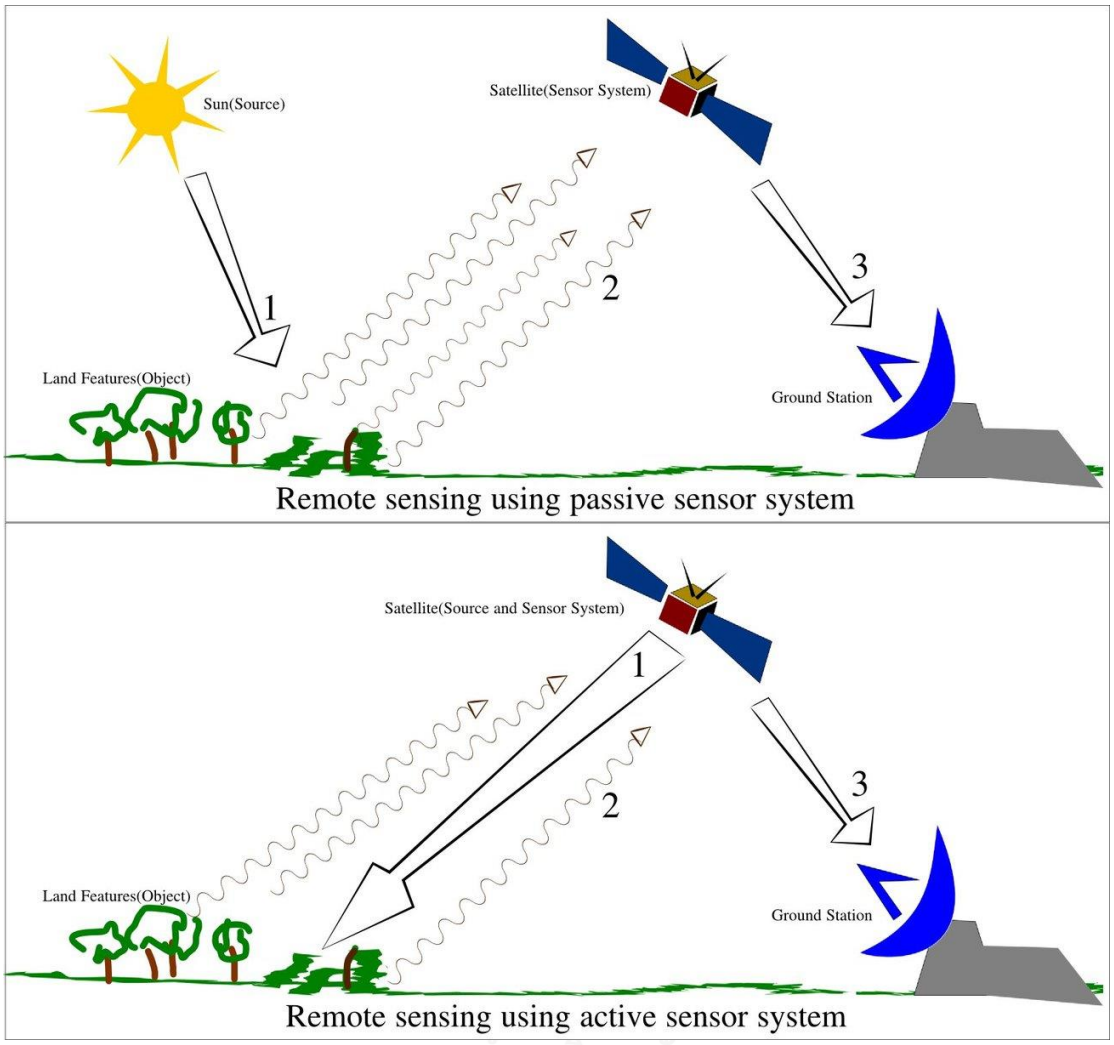

Figure 3.1 Illustration of Remote Sensing (Arkarjun, 2013)

The Landsat 7 satellite was successfully launched from Vandenburg Air Force based on April 15, 1999. A single scene image from the satellite covers a land area of about 185 x 180 kilometers. Landsat 7 was designed to collect eight spectral bands of reflected electromagnetic radiation: The first bands 1, 2 and 3 consist of the visible wavelengths, followed by band 4, 5 and 7 for infrared. The two remaining bands are band 6 for thermal infrared wavelength and band 8 for panchromatic as listed in Table 3.1.

Table 3.1 Spectral bands of Landsat 7

Band No.	Wavelength Interval (μm)	Spectral Response	Resolution (m)
1	0.45 - 0.52	Blue-Green	30
2	0.52 - 0.60	Green	30
3	0.63 - 0.69	Red	30
4	0.76 - 0.90	Near IR	30
5	1.55 - 1.75	Mid-IR	30
6	10.40 - 12.50	Thermal IR	120
7	2.08 - 2.35	Mid-IR	30
8	0.52-0.92	Panchromatic	15

Satellites record the electromagnetic radiation emitted or reflected by the surface or objects. The data is converted to images or rasters, where each element represents a measurement in that point. Data points can be visible wavelengths (e.g. color), but also heights, surface material or temperature.

Digital Elevation Model (DEM) is a digital representation of the topography of the surface of the earth. These models can be created by data collected using remote sensing techniques such as LIDAR. In this thesis DEM data from the study area plays a significant role.

3.1.1.2 ASTER Imagery

The Advanced Spaceborne Thermal Emission and Reflection Radiometer (ASTER) is an imaging instrument on NASA's Terra satellite, which was launched in December 1999. It's a collaboration between NASA and Japan's Ministry of Economy, Trade and Industry and Japan Space Systems and part of the Earth Observing System (EOS).

The data collected by ASTER is used to create detailed maps of land surface temperatures, reflectance and elevation. It provides high-resolution images ranging from 15-90 meters in 14 different bands, from visible to thermal infrared.

3.1.1.3 STRM DEM

A DEM is generated using the two components of band 3, with 30 meter horizontal postings and an accuracy between 10 m and 25 m root mean square error (RMSE).

ASTER Global DEM images are available free to all to users worldwide via electronic download through the USGS. The DEM data for this thesis was retrieved through the USGS Global Data Explorer.

Several remote sensing data sources have been used for the current investigation. The joint interpretation of Digital Elevation Model (DEM) and different satellite images (i.e., MODIS, LANDSAT, and IKONOS) are analyzed for identifying the candidate morphotectonic index (Figure 3.2) implying the possible active fault segments in the DBFF zone (Figures 3.3-3.7). The purpose is to investigate whether or not the studied faults in the area can be linked to the so-called "Nan-Uttaradit suture zone" (Figure 2.17) which is major tectonic line of Thailand (P. Charusiri et al., 2002).

In this study, lineaments and Cenozoic basins were examined by visual justification with Google Earth maps. For image processing and enhancement, the author used methods such as hill shading and topographic modeling. These methods help improve the image appearance and are useful for delineation of major structures and Cenozoic basins.

3.1.2 Lineaments

In an attempt to understand regional geological lineament patterns and characteristics in the study area and nearby areas, SRTM DEM data was consulted for lineament interpretation approach. The SRTM DEM data was used to create a hill shade image or virtual terrain model as show in Figure 3.3-3.7. Those images as mentioned above covers the western part of Lao PDR and nearby area.

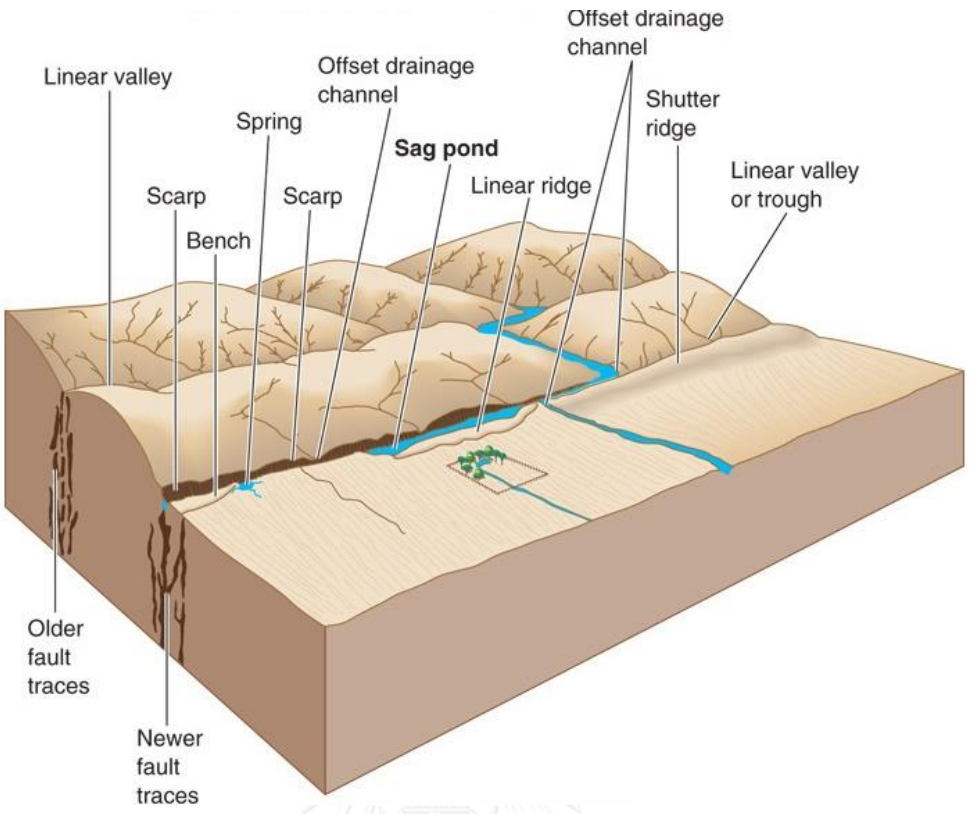

Figure 3.2 Characteristics of morpho-tectonic landforms associated with active faulting (Vedder & Wallace, 1970).

3.1.3 Cenozoic basins

The study of Cenozoic basins uses regional Google Earth images and DEM data. They are well recognized in remote sensing images by relatively low-relief and gentle slopes to flat lying area (Figure 3.6) when compared with those of the older rocks (mountainous area).

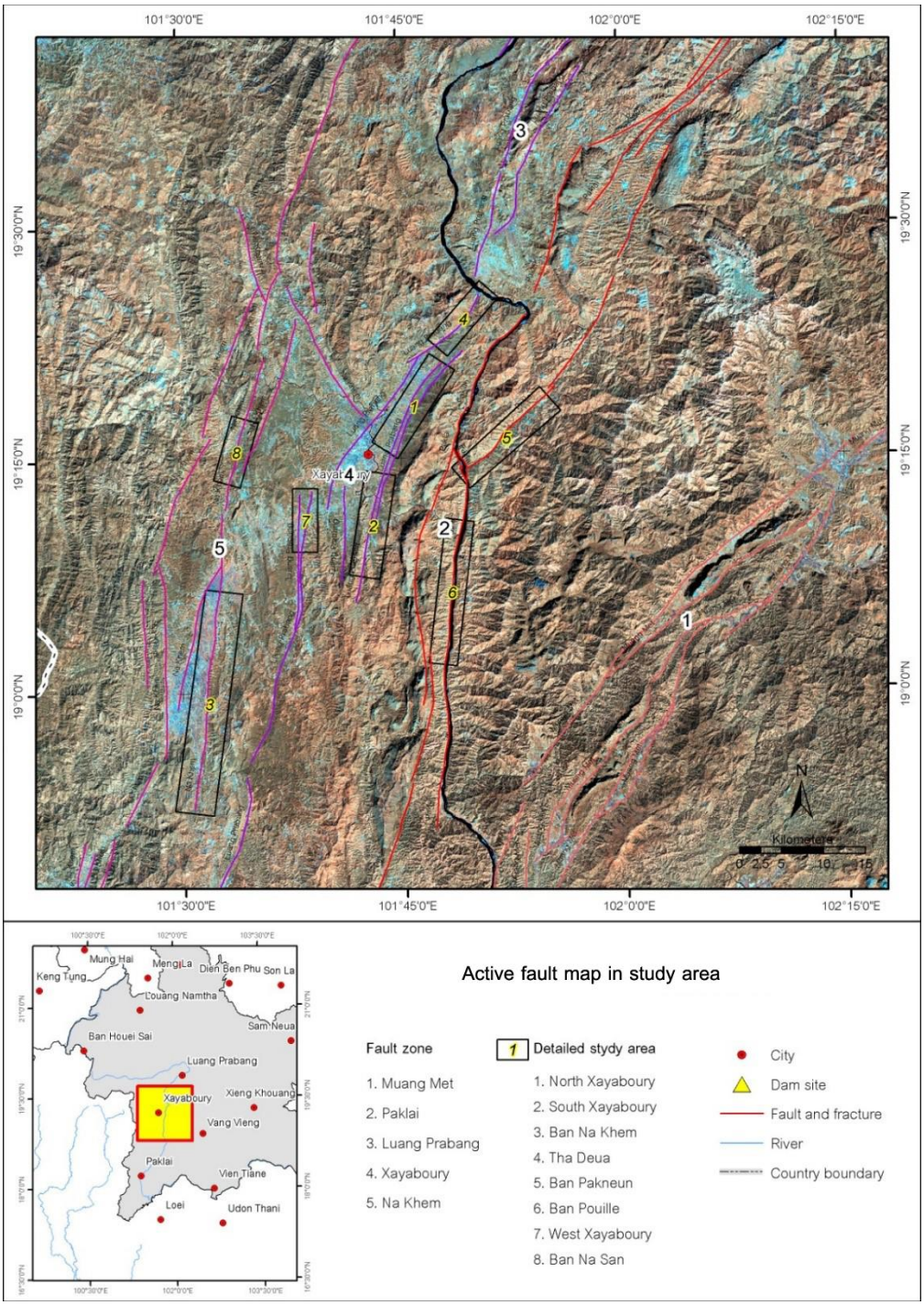

Figure 3.3 Enhancement Landsat 7 ETM+ (B457) by using the false-colored composite image data of bands 4 (red), 5 (green), and 7 (blue) showing physiographic features of the study area in the western part of LAO PDR.

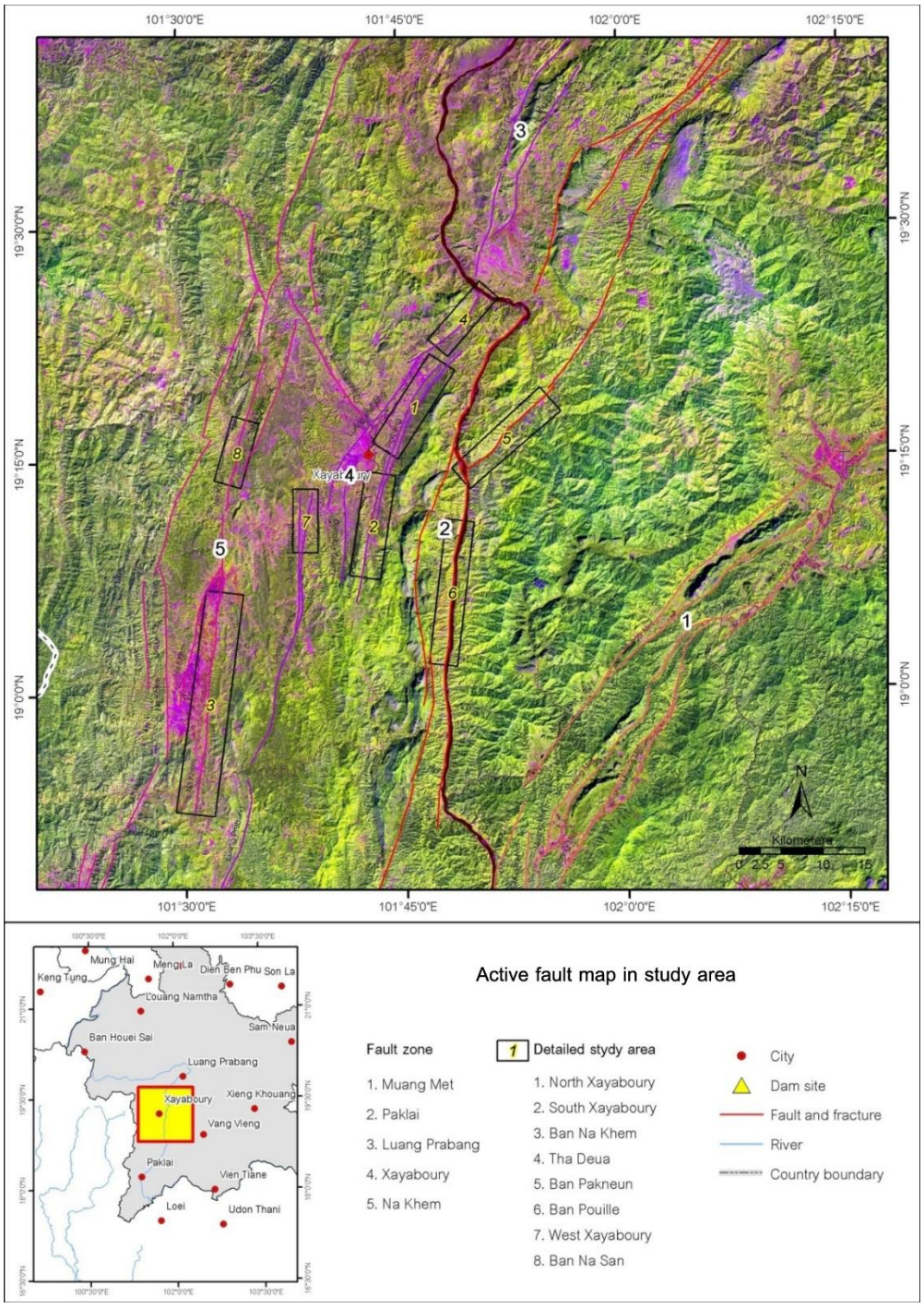

Figure 3.4 Enhanced Landsat 7 ETM+ (PCA123) by using the false-colored composite image data of bands 4 (red), 5 (green), and 7 (blue) showing physiographic features of the study area in the western part of LAO PDR.

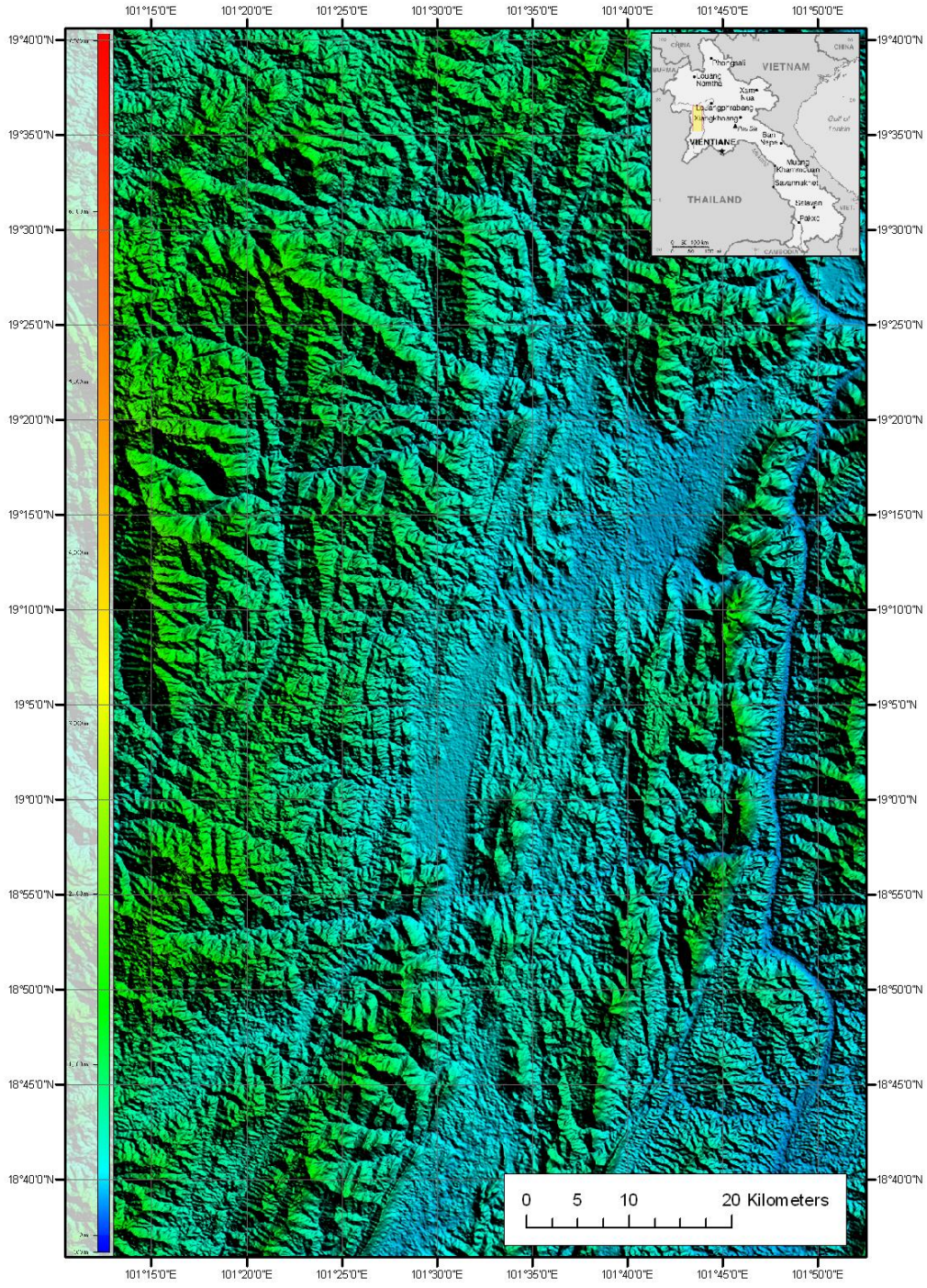

Figure 3.5 Enhanced SRTM map showing physiographic features of the study area covered the western part of Lao PDR. Note that two of basins are Phiang (south) and Xaignabouli (north) in the study area.

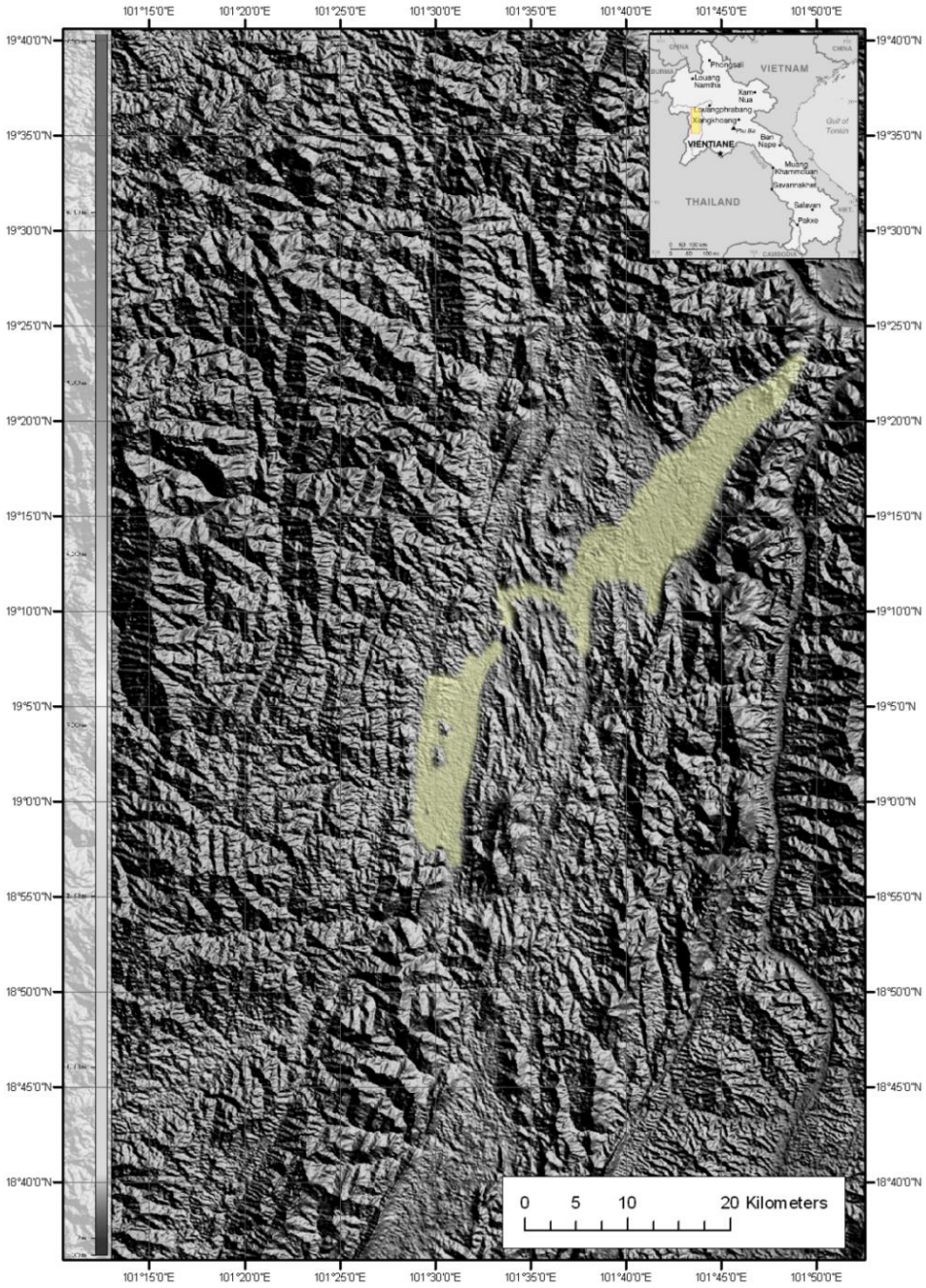

Figure 3.6 Shade relief image from SRTM DEM data showing contrasting hard-rock geology and structures between Phiang Basin in southwestern and Xaignabouli Basin in northeastern blocks of western Lao PDR. Also shown is a series of the EW-trending faults in the western block that is quite distinct and cut the major structure and lithologies.

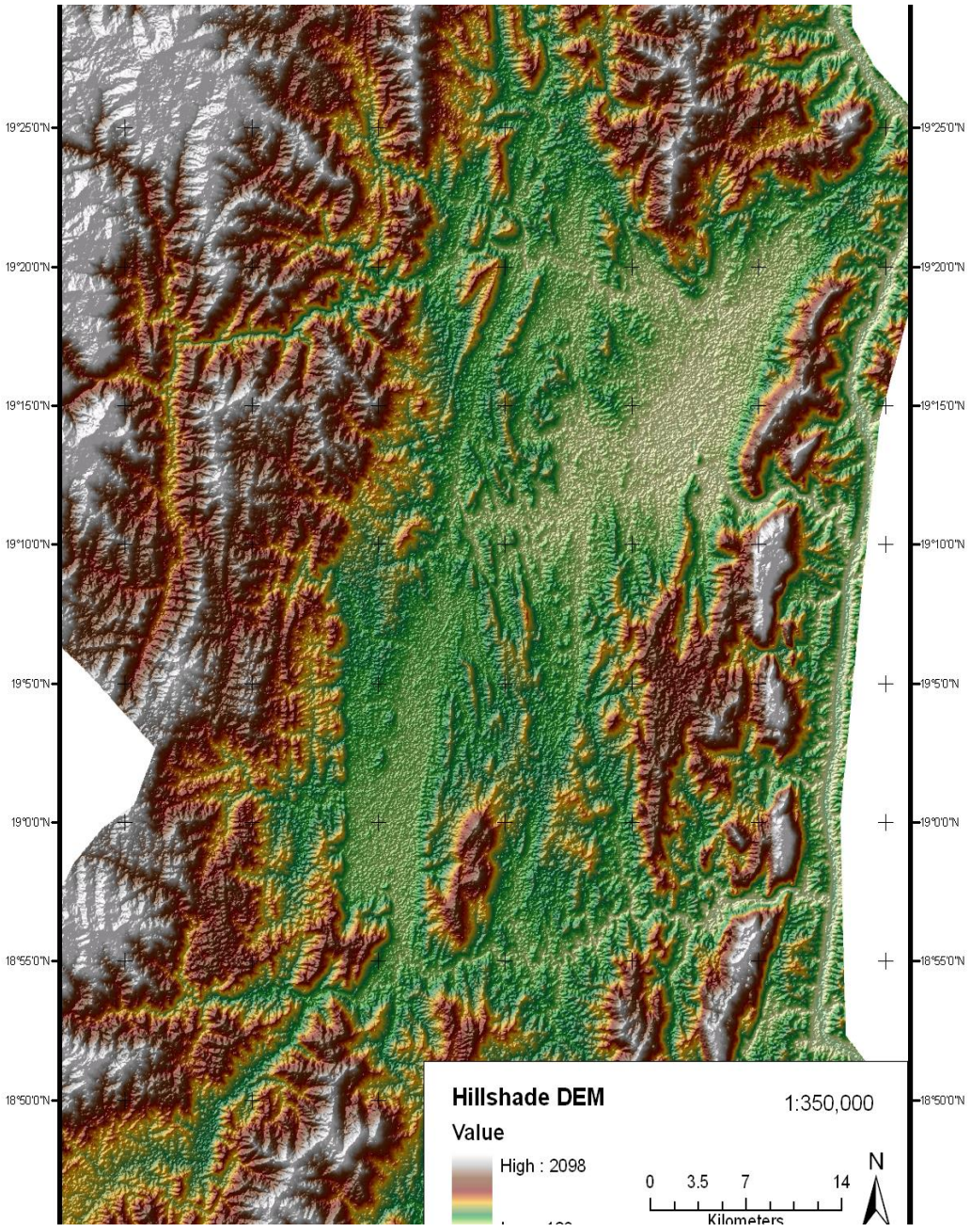

Figure 3.7 Index hillshade map of DEM showing the study area as measured by ASTER Global DEM. The data are posted on a 1 arc-second grid and referenced to the 1984 World Geodetic System (WGS84)/ 1996 Earth Gravitational Model (EGM96) geoid. ASTER GDEM is a product of METI and NASA.

3.1.4 Determination of Maximum Credible Earthquakes

To determine the Maximum Credible Earthquakes ($MCEs$), the relationship between moment magnitude (Mw) and fault rupture length at the surface (SRL) proposed by Wells and Coppersmith (1994) are applied (see equation 3.1). The SRL (or surface rupture length) used for the Mw calculation is the length of the longest fault segment in individual fault segments. The rupture area A_f, which is also required for SHA, is determined by using the empirical relationship between the obtained Mw from equation 3.1 and A_f (Wells & Coppersmith, 1994) of equation 3.2:

$$Mw = 5.08 + 1.16\log(SRL) \quad \text{(Eq. 3.1)}$$

$$\log(A_f) = -3.49 + 0.91Mw \quad \text{(Eq 3.2)}$$

where Mw is moment magnitude, SRL is surface rupture length of fault segment (km), and A_f is rupture area of the fault (km^2).

3.2 Paleoseismic investigation

This step is to conduct field investigations and chose suitable sites for the following trenching step.

3.2.1 Field evidence of tectonic geomorphology

This procedure focuses on geological investigations (i.e. paleo-seismology) according to the method proposed by Vedder and Wallace (1970) (Figure 3.2). The major important task is to compile all available information necessary for detailed geologic, tectonic and paleoseismological investigations of the study area as well as interpretations on satellite images and aerial-photographs. Verification on the interpreted crustal faults existing in Xaignabouli region is based largely on the field and remote sensing interpretations.

A few thin sections were prepared for the identification of faults under microscopic scale to show supporting evidence of faulting from mesoscopic scale and similar faulting evidence found in the outcrops.

3.3 Trenching

This step starts with compilation of previous field data related to fault evidence. Subsequently identifying sequences of faulting in the selected area with exploratory trenching. This is followed by collection of geological data and samples.

3.3.1 Site selection for paleoseismic trenching

Trenching sites was selected by using satellite image and aerial photographic interpretation in conjunction with field reconnaissance, fourteen potential trench sites, i.e. six trenches (T5, T6, T7, T8, T9 and T11) at Phiang basin, and eight trenches (T11, T12, T13, T14, T15, T16, T17 and T18) at Xaignabouli basin were selected. Their locations are summarized in Table 3.2.

3.3.2 Geochronological dating

Dating is the fifth step with the main purpose of collecting samples for dating using the Optical Stimulated Luminescence (OSL) method. The dating method follows that of Takashima and Watanabe (1994) commencing at collecting suitable geological samples related to active fault, treatment of quartz-enriched samples for dating, and analyzing both of equivalent and annual doses of quartz concentrates.

The methodology of analysis is composed of 2 main procedures, including equivalent dose evaluation and annual dose evaluation as explained below.

Table 3.2 Location of the trenches and exposures for paleoseismological investigations.

No.	Location	Coordinate		Type of Excavation
		East	North	
T1	Western bank of Khong River	795972	2130444	Trench
T2	Western bank of Khong River	796240	2129994	Trench
T3	Western bank of Khong River	796224	2130254	Trench
T4	Western bank of Khong River	796028	2130261	Trench
T5	Ban Kang, Phiang district	767079	2112107	Trench

T6	Ban Dongngoen, Phiang district	767410	2113032	Exposure
T7	Ban Saeng Chaloen, Phiang district	767527	2114202	Trench
T8	Ban Saeng Chaloen, Phiang district	768501	2115897	Exposure
T9	Ban Phonhin, Phiang district	764922	2113244	Trench
T10	Ban Phonhin, Phiang district	765212	2114199	Exposure
T11	Chinese maket, Xaignabouli district	786064	2132183	Exposure
T12	PTT gas ststion, Xaignabouli district	786047	2132471	Exposure
T13	Ban Nahai, Xaignabouli district	786104	2133071	Exposure
T14	Soldier monument, Xaignabouli district	783117	2132341	Exposure
T15	Ban Vangxoy, Xaignabouli district	787895	2137850	Exposure
T16	Ban Vangxoy, Xaignabouli district	788118	2138350	Exposure
T17	Ban Naleng Noy, Xaignabouli district	788967	2139205	Exposure
T18	Ban Wang Kham, Xaignabouli district	783546	2126351	Exposure

3.3.2.1 Crushing and Sieving

Upon arrival in the OSL laboratory, 23 sediment samples in total were dried by baking to 40-50 °C in a dark room. Water content is also measured for all samples being dated because it is the one significant parameter for annual dose determination. The formula of water content calculation is shown in equation 3.3 as below;

$$\frac{\text{(weight of a wet sample- weight of a dried sample) X 100}}{\text{weight of a dried sample}} \qquad \text{(Eq. 3.3)}$$

After getting dried samples, each sediment sample was crushed by using a rubber-hammer and the resulting material sieved to isolate the grain size fractions in two parts. About 300 g of sediments were collected with grain sizes that passed through a 20 mesh (<841μm) and then separated in plastic containers for annual dose determination. The remainder from the annual dose collection was carefully re-sieved to isolate grain size fractions between 60-200 mesh (74-250μm) according to Aitken (1985). This latter portion

was kept in beakers for purifying quartz grained and equivalent dose determination, respectively.

On completion of this sample management step, each sample was extracted into 3 portions, including one calculated numerical value of the water content and the other 2 portions consisting of one portion for annual dose analysis (grain size<841μm, 300g) and one portion for equivalent dose analysis (grain size 74μm-250μm). In the annual dose, the sample portion is ready and can pass to the measurement step but for the portion for equivalent dose determination it is necessary to perform chemical treatment (detailed in the next section).

3.3.2.2 Equivalent Dose Determination

The equivalent dose operations are separated into 3 continuous steps consisting of 1) chemical treatment, 2) sample preparation for equivalent dose measurement, and 3) equivalent dose measurement as well. Each step is described in full detail below:

In this OSL dating procedure, we decide to select quartz mineral as suggest by Aitken (1985) for representation of the OSL signal of the sediment sample. The main objective of chemical treatment is, therefore, to extract quartz mineral from sediment samples before the OSL signal measurement procedure. The detailed steps of the chemical treatment are: (Figure 4.8).

a) Washing the sample by distilled water 10 times to remove some organic materials and clay particles;

b) Chemically cleans the sample in diluted 35% HCl at 50-60 °C for a period of 15-30 minutes and re-wash several times with distilled water to eliminate carbonates and deep-rooted organic material;

c) Etching the sample in 24% HF at 50-60 °C for 15-30 minutes and re-wash it several times with distilled water. HF is used to dissolve the plagioclase and outer layer of quartz grains; and

d) After washing with water and drying in the dark room, the dried sample was then separated to remove dark minerals (e.g. zircon, garnet, and metallic minerals) by

using an isodynamic separator from Department of Mineral Resources (Frant'z isodynamic magnetrometer). After finishing the sample treatment, it is ready for equivalent dose determination.

Evaluation of equivalent dose commences with measurement of OSL intensities on 3 sample portions: 1) natural sample portion, 2) residual sample portion and 3) artificial irradiation sample portion. The OSL emission of quartz were measured in subdued red light room by using the Riso TLD dosimeter installed at Department of Geology Faculty of Science, Chulalongkorn University (Figure 3.8). About 20 mg of sample was filled in aluminum planchettes and placed on a molybdenum heater. The filter system applied in this research study is a blue filter (Toshiba IRA-10). The light emission is amplified and measured by photomultiplier and recorded simultaneously with the temperature added to the sample. The graph shows a relationship between OSL intensity and known-add dose which is called "growth curve" as shown in the appendix.

Figure 3.8 Riso TLD dosimeter at Department of Geology, Faculty of Science, Chulalongkorn University, used for OSL glow curve measurement.

3.3.2.3 Annual Dose Evaluation

Sediments are normally continuously exposed to ionizing radiation originating from their radioactive contents and a small fraction originating from cosmic

rays (Aitken, 1985). The natural dose rate (annual dose) is primarily contributed from three radioactive elements: uranium (U), thorium (Th) and potassium (K_2O). The decay of uranium and thorium emits α, $\beta$and γ radiation while potassium emits β and γ. The natural dose rate in most sediments is measured in the order of mGy/year.

3.3.3 Fault age interpretation

From the chronological determination data, we can interpret the dates of faulting in the study area by using cross-cutting relations to determine the relative ages of rock strata.

3.3.4 Determination on slip rates

By using recurrence interval of fault, and average slip in each major rupture along a fault, can estimate a slip rate with equation 3.4:

$$\text{Slip rate} = \frac{\text{Average slip per major rupture}}{\text{Recurrence interval}} \qquad \text{(Eq. 3.4)}$$

3.4 Image processing

This step is to identify sedimentary deposits and facies from photographic images of outcrops by using Optical stratigraphy method.

3.4.1 Optical stratigraphy technique

Trenches are excavated across active fault zones to determine the recurrence interval and frequency of paleo-earthquakes. An accurate determination of these parameters can be used to predict future earthquakes. Traditionally, trench walls are hand logged to separate sediment into stratigraphic units. Here we suggest an algorithm based on one proposed by Willis et al. (2004) to autonomously separate sediment in trench walls using high-resolution digital photos of the wall. The algorithm consists of two steps, a preprocessing step using fundamental image processing techniques: histogram equalization, thresholding, morphological operations, edge detection, and watershed transform to enable higher level processing to determine the shape and properties of rocks via specific weighted averages known as image moments. The algorithm

successfully segments rocks from each other and from the background matrix and by estimating their size and orientation by calculating the geometric image moments of various orders (Flusser, 2006) colluvial wedges can be identified.

3.4.2 Step of image processing

Digital images of a fault trench wall were processed in MATLAB using various image processing operations. The images are initially transformed to grayscale, where the color channels are combined in to a single luminance, or intensity value. Histogram equalization is then performed on the single channel image, which adjusts the dynamic range of the image by mapping luminance value so that the output has a uniform distribution of intensities, thereby improving the global contrast of the image. A threshold is then applied to intensity value, obtain binary images. These first steps mitigate variance in lighting and other optical conditions in the source image, and also reduce the computational cost for more complex operations.

As a first segmentation step, erosion and dilation morphological operations were applied to the binary images to isolate objects. The first step is erosion which reduces objects and in the process, removes small objects and noise and also breaking up any spurious connections between objects. This is followed by a dilation to restore the original size of the remaining objects. When the objects have been isolated, Canny edge detection is detect the outlines (Figure 3.9).

The remaining objects were filtered for area (Figure 3.10), where objects smaller than a threshold value are discarded. Then the 0^{th}, 1^{st} and 2^{nd} order image moments were calculated to determine area, centre of mass and axes of orientation. By analyzing the axes we determine a basic shape of the object and focus on oval-shaped objects which indicate rocks that have been oriented in the direction of the wedge. By calculating the angle between the axes, a direction vector of the rock can be estimated.

The moment values are then combined and plotted as bi-directional arrows going through the object centre, in the direction of the major axis, with a magnitude relative to

its area as seen in Figure 3.11 (left). Together these vectors indicate the colluvial wedge as it extends through the trench wall.

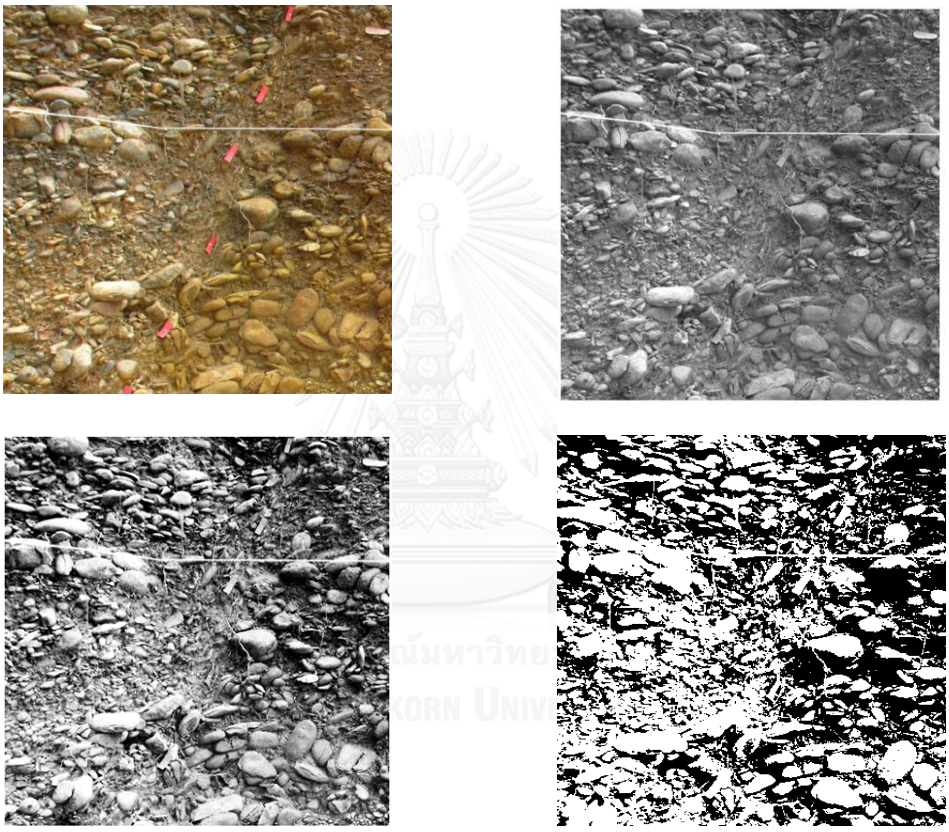

Figure 3.9 Original image section of a trench wall (top left), Grayscale transformation image (top right), Enhanced image by using Histogram Equalization (bottom left), Thresholded (bottom right)

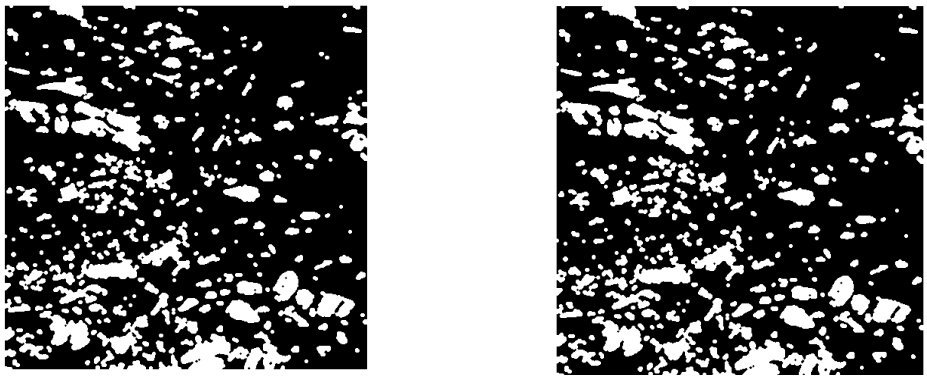

Figure 3.10 Two morphological operations are performed: opening to remove small components of objects (left) and erosion to thin objects (right)

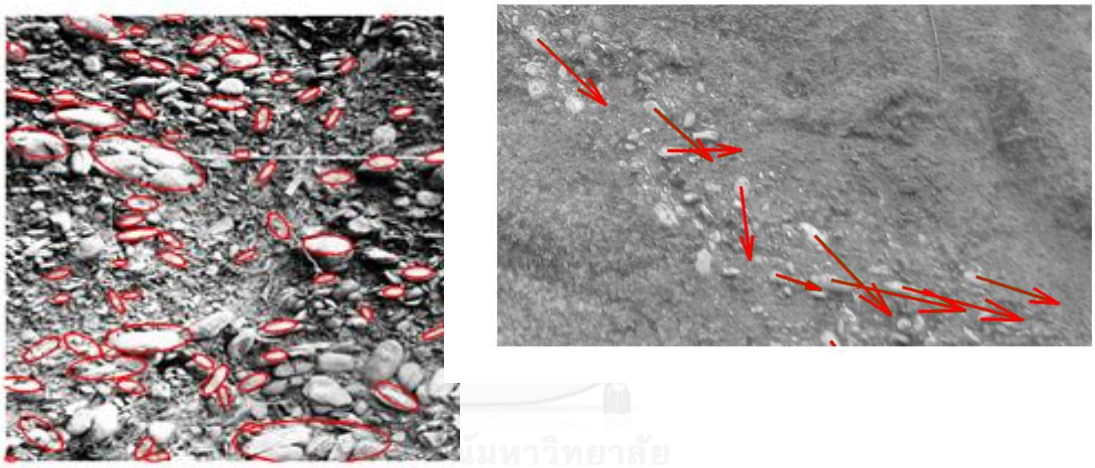

Figure 3.11 Detected rocks (left) a fault line and estimated direction in the form of overlaid vectors on the original image (right)

3.5 Focal mechanism

This step is to make a focal mechanism of the related fault earthquake events in the study area from a solution of the moment tensor, which itself is estimated by an analysis of observed seismic waveforms to describe the seismic wave generating deformation in the source region and also a fault-plane solution.

The focal mechanism is studied on the basis of P-wave first motion, S-wave polarization angle, and long-period surface-wave data. For the inversion model

“FOCMEC” was used, a Fortran77 computer program developed by Snoke, Munsey, Teague, and Bollinger (1984). It performs a search of the focal sphere based on certain criteria given the polarities of P, SV and SH together with amplitude ratios of SV/P, SH/P and SV/SH. Readings need to be provided from several stations together with their azimuths and takeoff angles at the source.

The selectable search criteria include parameters like maximum polarity error count, acceptable deviation between observed and calculated amplitude ratios and region of the focal sphere to be searched. The search is performed systematically by testing all possible focal mechanism, uniform in angle with selectable step size and bounds. The developers have made applications to find the best-constrained solutions for fault-plane of earthquakes recorded at local to regional distances (Chapman, Powell, Vlahovic, & Sibol, 1997).

If the station density is low the number of possible solutions can be high, however it can be greatly reduced if P and S amplitudes from vertical-component seismograms are available. The final output is a summary of the found acceptable solutions, which can be plotted by an auxiliary program as an equal-area Lambert-Schmidt projection of the focal sphere.

CHAPTER IV
RESULTS

4.1 Remote sensing interpretation

4.1.1 Satellite image interpretation

The processed satellite images show the image of the study are which easy to delineate of major structures and Cenozoic basins (Figure 4.1). DEM with the resolution of 30 x 30 m was applied for re-tracing lineaments and fault segments in the regional scale (Figure 4.2) whereas satellite images of different types can support the morpho-tectonic evidence associated with surface faulting in more detail. Satellite images illustrate clearly the offset stream, triangular facet, linear valley, offset spur, sag pond and fault scarp in the Xaignabouli Fault Zone (Figures 4.4-4.12).

4.1.2 Lineaments

The interpretation result for neotectonic evidence from SRTM DEM and Landsat 7 ETM^{+} images is shown in Figure 3.6 and 3.7. The hill shade image interpretation is used to define orientation and direction of the investigated fault segments and to support delineating the large scale neotectonic features (McCalpin, 1996). The result shows several neotectonic features including triangular facets, fault scarps, offset streams, and shutter ridges. Based on combined interpretation of DEM, BING and Google Earth, a series of faults trending in the NE-NW direction is present (Figure 4.1). The major lineaments or fault lines are in the northeast direction and extend from northern Thailand including surveyed area though Thailand-Lao border to the western part of Lao PDR. The author considered these fault zones caused the opening of Cenozoic basins. And the two minor trends of lineaments and faults lie in the north-northeast and south-southwest direction with short length than major trend. As shown in Figure 4.1, most of lineaments which oriented in northeast-southwest and northwest-southeast direction situate in the area of base rocks, whereas the lineaments in north-south direction situate along basin boundary such as Phiang and Xaignabouli Basin.

4.1.3 Cenozoic basins

Based on Bing and Google Earth images and DEM data interpretation, the study region contains with two Cenozoic basins as Phiang and Xaignabouli Basin (Figure 4.1). Two basins have elongate shape and oriented in the northeast-southwest direction or following the main structure.

Phiang Basin is about 15 km eastern area near Thai-Lao border and is obviously seen in satellite and DEM images because both basins are bounded by fault lines (see Figure 4.1)

The Phiang and Xaignabouli Basin orients in northeast-southwest direction, the upper part of the both basins is narrow about 2 km and the lower part is much wider about 5 km and the length is about 25 km in Phiang Basin and 22 km in Xaignabouli Basin. If compare, Xaignabouli Basin has low relief and morphotectonic evidences are occurred in this basin is not sharp as the Phiang Basin.

4.1.4 Determination of Maximum Credible Earthquakes

Based on satellite image interpretation, several lines of morphotectonic evidence show that the fault segments belonging to the DBFF zone have the wide range of SRL from 3.4 km (the Ban Nakhan-2 segment) up to 130.4 km (the Lai Chau segment) (see Table 3.2). As a result, the determined fault segments of the DBFF zone can generate the credible earthquakes with the maximum Mw of ca. around 5.8 to 7.5. It is also estimated that the A_f can vary from 58 to 2,271 km2 (Table 4.1).

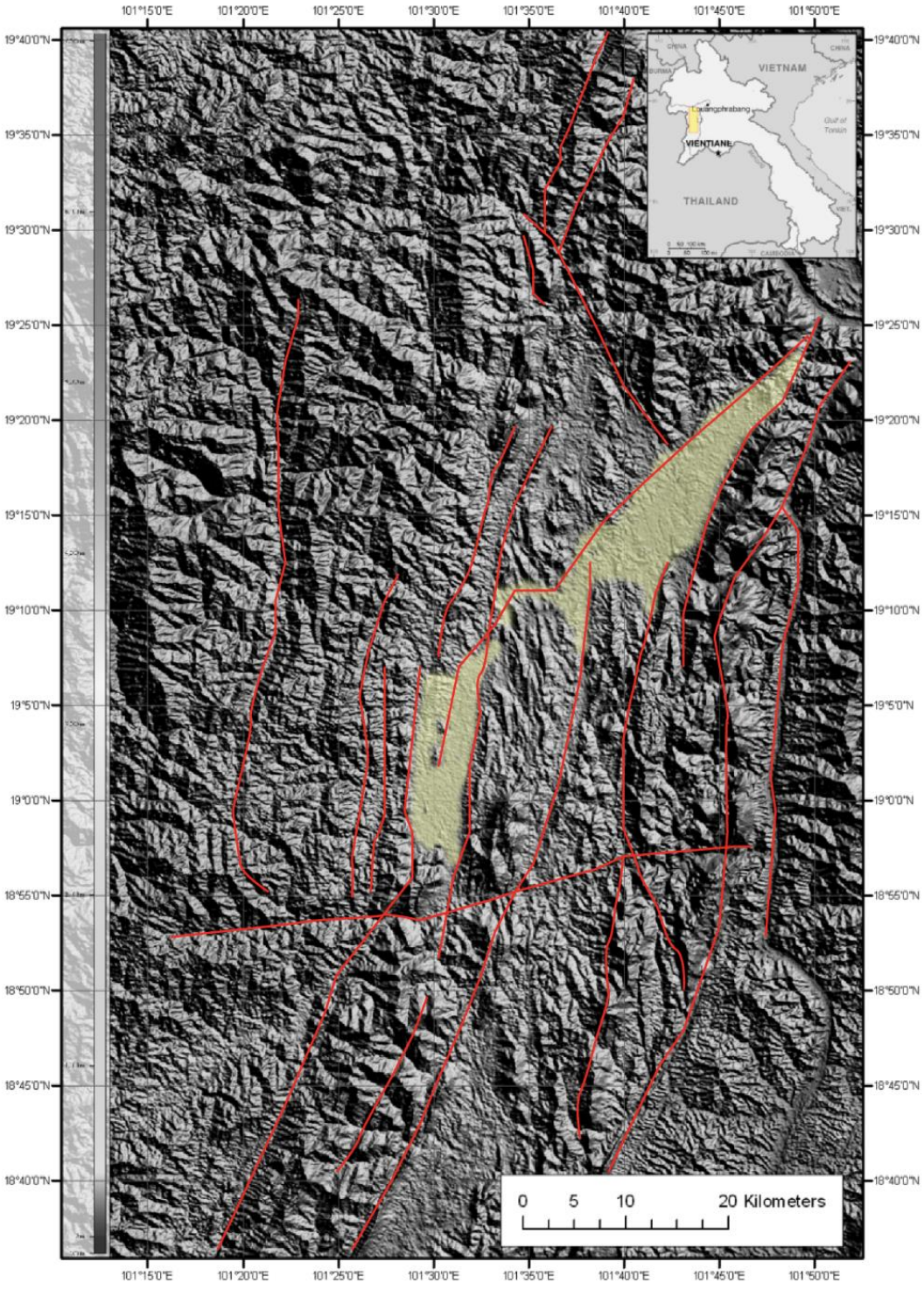

Figure 4.1 Map of the study region showing distribution of lineaments and Cenozoic basins interpreted using the enhanced SRTM DEM data.

Table 4.1 Sixty fault segments of Dien Bien Phu Fault (DBFF) zone with essential information of earthquake source parameters identified in this study.

No.	Fault segment	SRL (km)	MCEs	Af (km2)	R (km)
1	Ban Houaykha	49.4	7.1	854	74.7
2	Dein Bein Fu-2	76.4	7.3	1325	126.4
3	Dein Bein Fu-1	20.1	6.6	345	145.6
4	Dein Bein Fu-3	50.6	7.1	875	81.7
5	Nam Thang	8.1	6.2	138	23.2
6	Houay Sok Tieng	4.8	5.9	81	23.2
7	Muang Phiang-4	10.2	6.3	175	34.1
8	Houay Meng	8.2	6.2	140	34.1
9	Nam Khan	25.2	6.7	433	36.4
10	Ban Nakhan-2	3.4	5.8	58	30.3
11	Ban Nakhan-1	4.3	5.9	73	31.9
12	Ban Vanghoua	6.0	6.0	102	27.6
13	Muang Phiang-1	6.0	6.0	102	27.6
14	Muang Phiang-2	11.0	6.3	188	28.4
15	Houay La	2.4	5.6	40	28.2
16	Ban Nato	2.8	5.7	48	26.2
17	Muang Phiang-3	19.0	6.6	325	29.5
18	Ban Mokkok	8.0	6.2	136	29.5
19	Ban Nalom	15.5	6.5	265	29.5
20	Nam Tan	5.0	5.9	84	29.5
21	Muang Phiang-5	19.2	6.6	330	29.5
22	Phou Vaysom Gnai	28.6	6.8	491	52.9
23	Ban Naven	29.6	6.8	510	50.6

No.	Fault segment	SRL (km)	MCEs	Af (km2)	R (km)
24	Ban Houayxao	9.2	6.2	156	23.4
25	Ban Houaynak	15.1	6.5	258	50.6
26	Ban Naso	5.8	6.0	99	34.0
27	Ban Houaylap	49.2	7.1	849	41.5
28	Ban Namkha	20.4	6.6	351	34.9
29	Ban Nakheng	10.6	6.3	181	40.0
30	Ban Donxai	12.1	6.4	207	42.4
31	Ban Houayving	8.9	6.2	151	42.4
32	Ban Bouloy	30.0	6.8	516	58.5
33	Ban Hat Deng	12.4	6.4	211	58.5
34	Phou Sang	4.2	5.9	71	20.6
35	Phou Khu Nkao	22.5	6.7	386	28.2
36	Nam Houng	26.7	6.8	460	16.8
37	Huay Gnoun	52.7	7.1	911	42.4
38	Ban Lat Rua	45.6	7.0	788	85.0
39	Phou Khomfat	10.3	6.3	176	43.4
40	Ban Ray	5.5	6.0	94	43.4
41	Nam Houang	5.1	5.9	86	43.4
42	Ban Huai Pong	19.2	6.6	329	85.0
43	Ban Kok Mon Kaeo	3.3	5.7	56	85.0
44	Ban Kok Mi	3.1	5.7	52	85.0
45	Ban Huai Dua	9.5	6.3	162	85.0
46	Khao Daen	8.7	6.2	148	85.0
47	Nam Pho	46.1	7.0	796	29.7

No.	Fault segment	SRL (km)	MCEs	Af (km2)	R (km)
48	Houay Xa	4.0	5.8	67	19.5
49	Houay Ho	17.3	6.5	297	29.7
50	Houay Dok	5.9	6.0	101	20.5
51	Ban Houaysala	7.6	6.1	129	29.7
52	Ban Houay Khuei	20.3	6.6	349	29.7
53	Ban Namxong	51.5	7.1	889	83.9
54	Ban Khok	7.1	6.1	120	83.9
55	Ban Pa Kabak	6.4	6.1	108	83.9
56	Mon Kwang	3.9	5.8	67	83.9
57	Ban Huai Dua	10.9	6.3	185	83.9
58	Ban Dong Yang	6.8	6.1	115	83.9
59	Ban Mayom	14.4	6.5	247	83.9
60	Lai Chau	130.4	7.5	2271	235.8

Remarks: “Fault Segment” are proposed by Pailoplee et al. (2009). “SRL” is surface rupture length of fault segment (km). Based on the empirical relationship between SRL and Mw, “MCEs” is the possible maximum earthquake magnitude expected (Well and Coppersmith, 1994) while “Af” is the rupture area (km^2) expected from empirical relationship between Mw and Af (Wells & Coppersmith, 1994). “R” is the closest distance from individual fault segment to the Xaignabouli area.

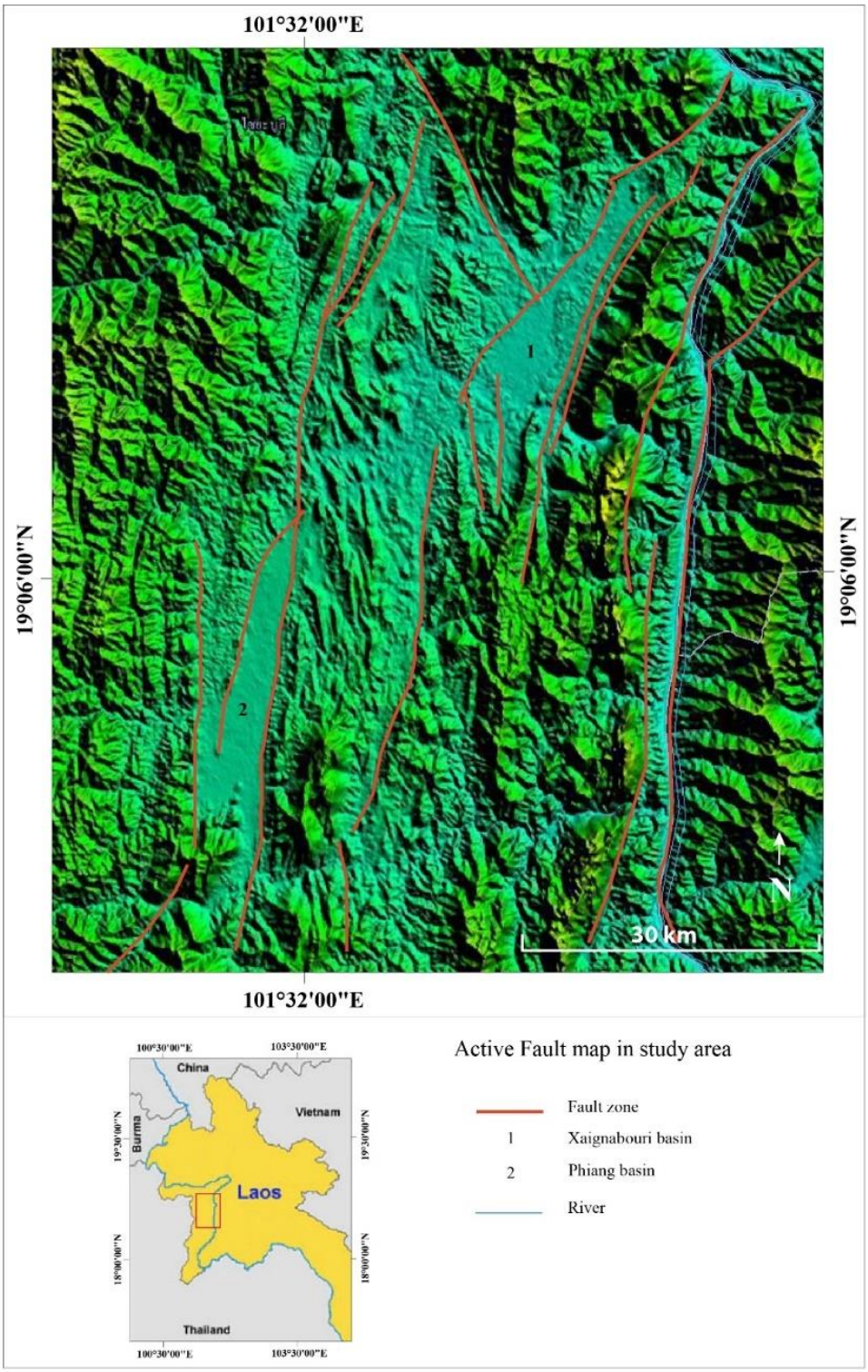

Figure 4.2 Detailed interpreted map from SRTM DEM and Google images showing study area of interest with well – defined morphotectonic features related to active faults, Xaignabouli area, Lao PDR.

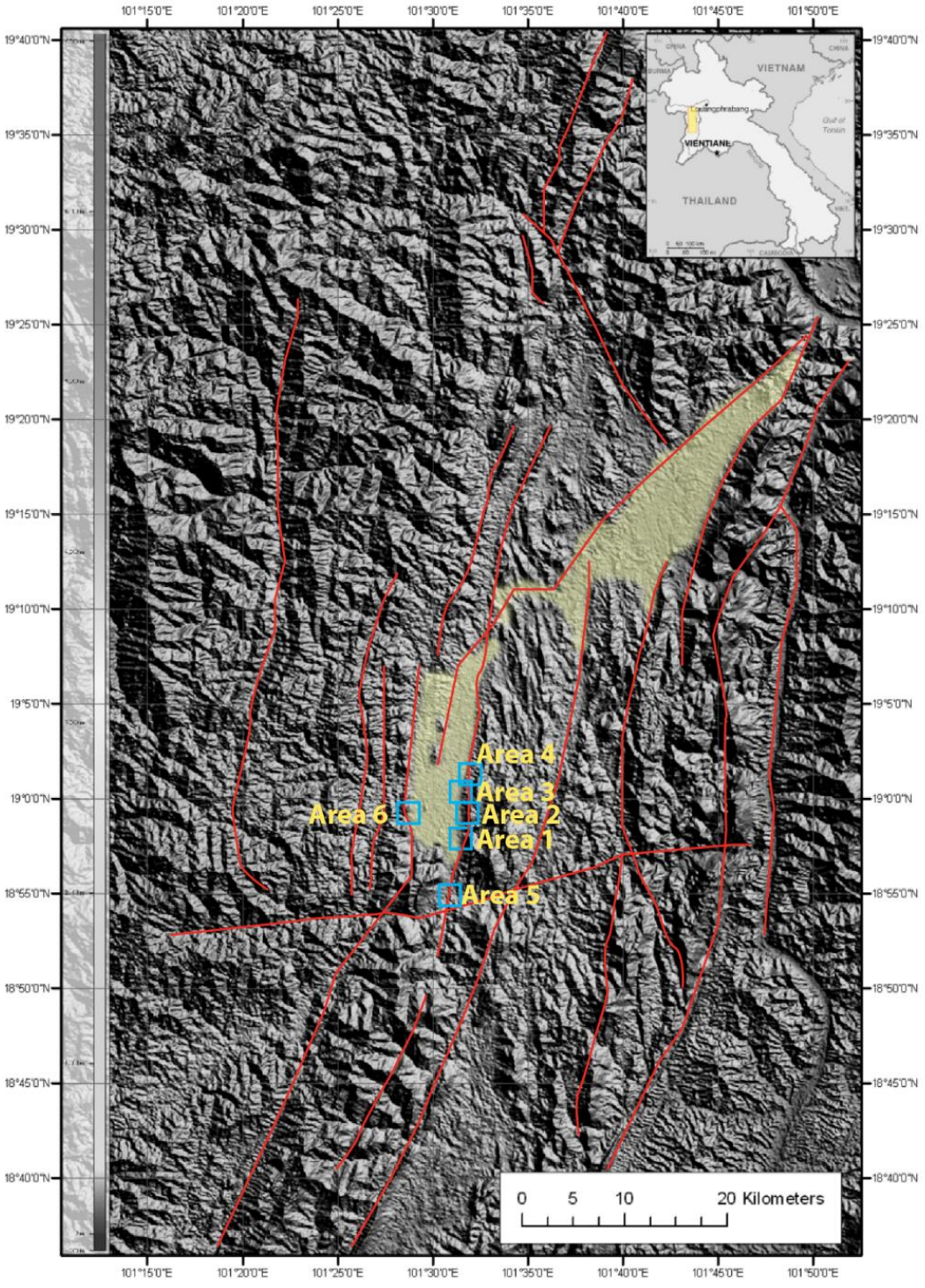

Figure 4.3 Map showing location of the Xaignabouli fault zone (red line) and its major inferred active fault segments. Boxes with number indicate selected areas for remote-sensing and google earth images interpretation for detailed paleoseismic data.

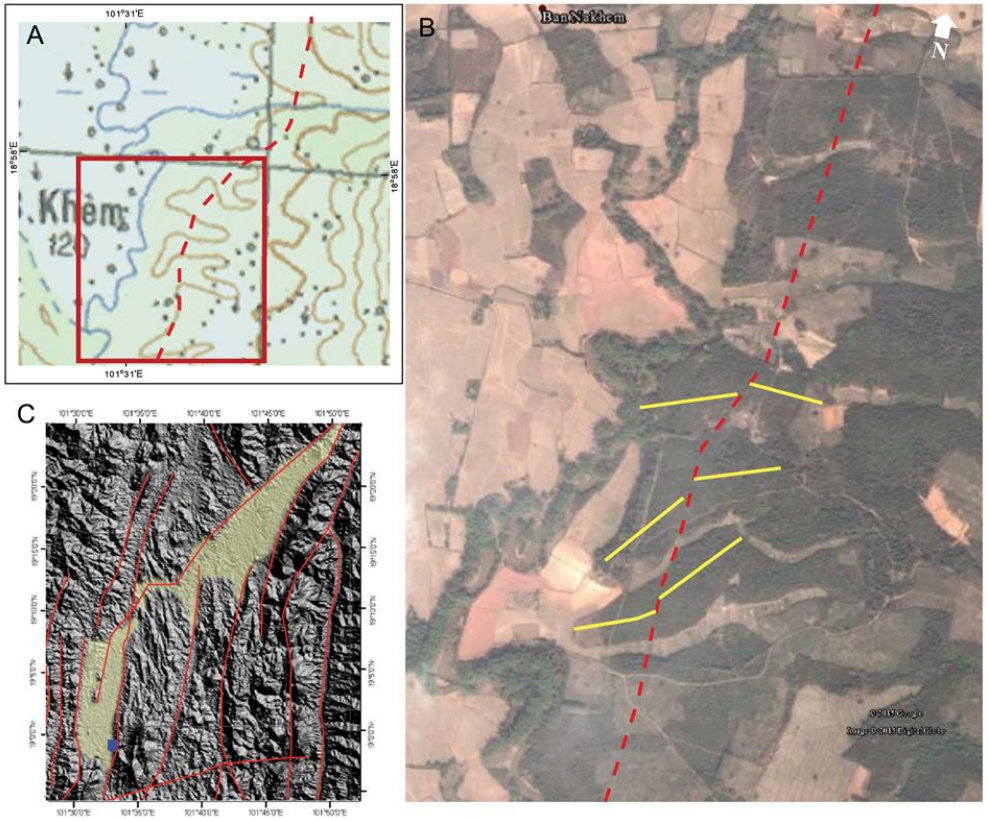

Figure 4.4 (A) Topographic map, (B) Google Earth map and (C) location of the interpretation area in blue box along the fault segment in Area 1 Ban Nakhem show offset spur, Phiang basin.

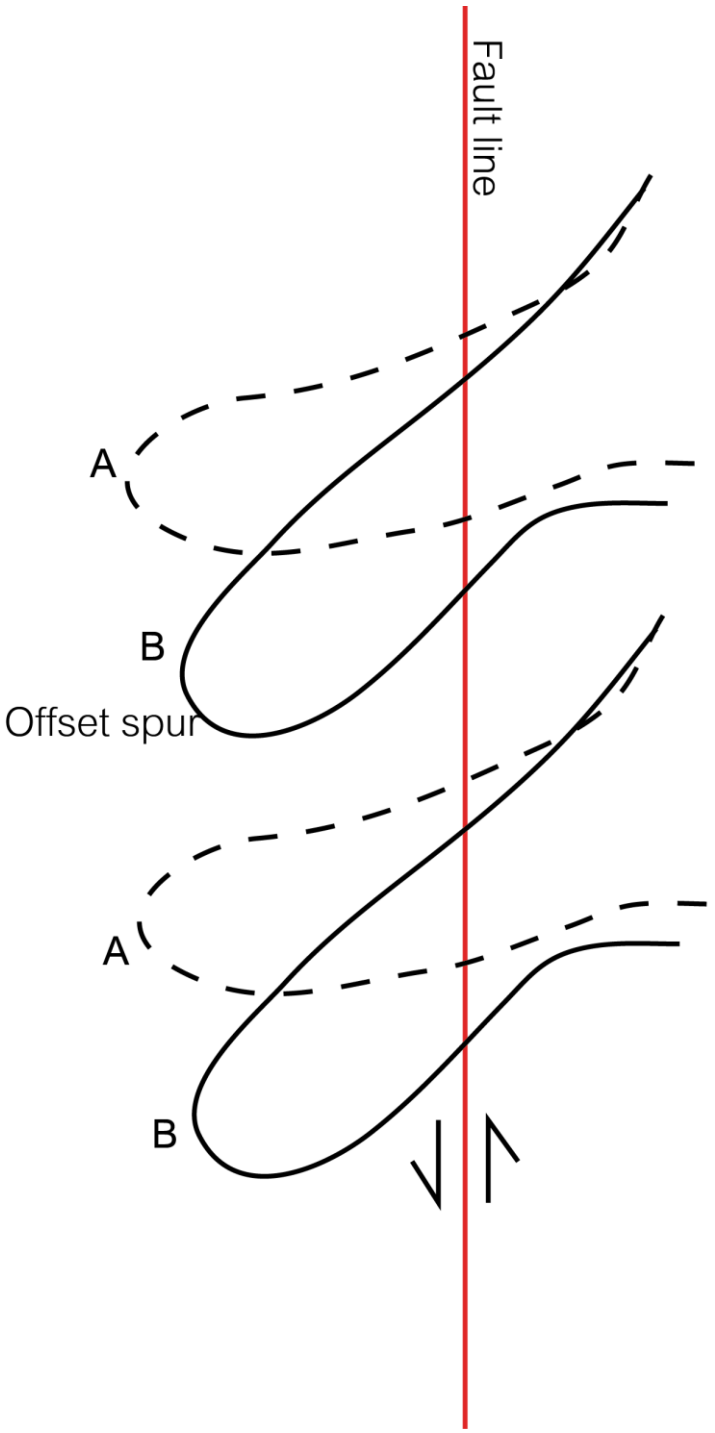

Figure 4.5 The interpretation of offset spur along the fault segment in Area 1 Ban Nakhem, Phiang basin. (A) Spur before faulting and (B) Offset spur after faulting.

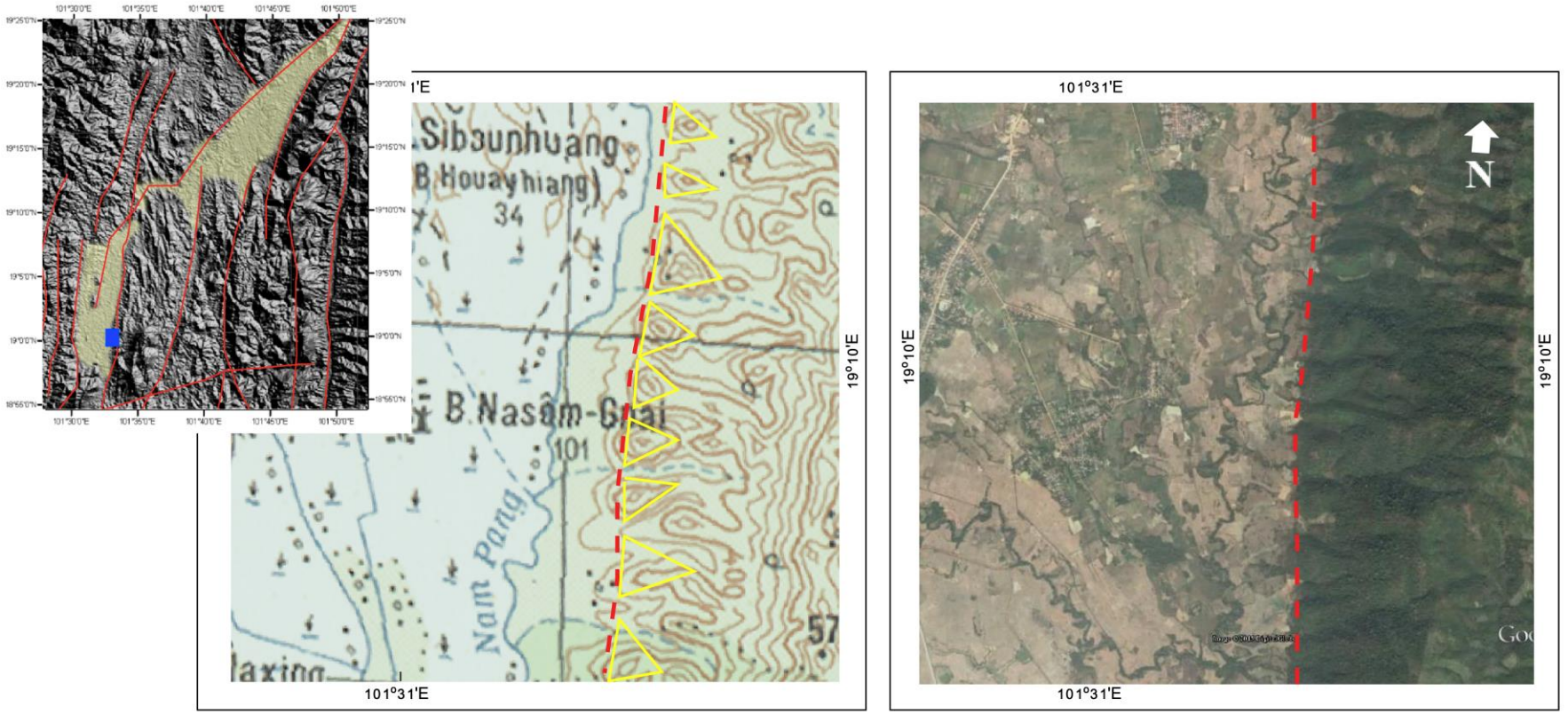

Figure 4.6 Location of the interpretation area in blue box (left), topographic map (middle) and Google Earth map (right) along the fault segment in Area 2 Ban Nasom show triangular facets, Phiang basin.

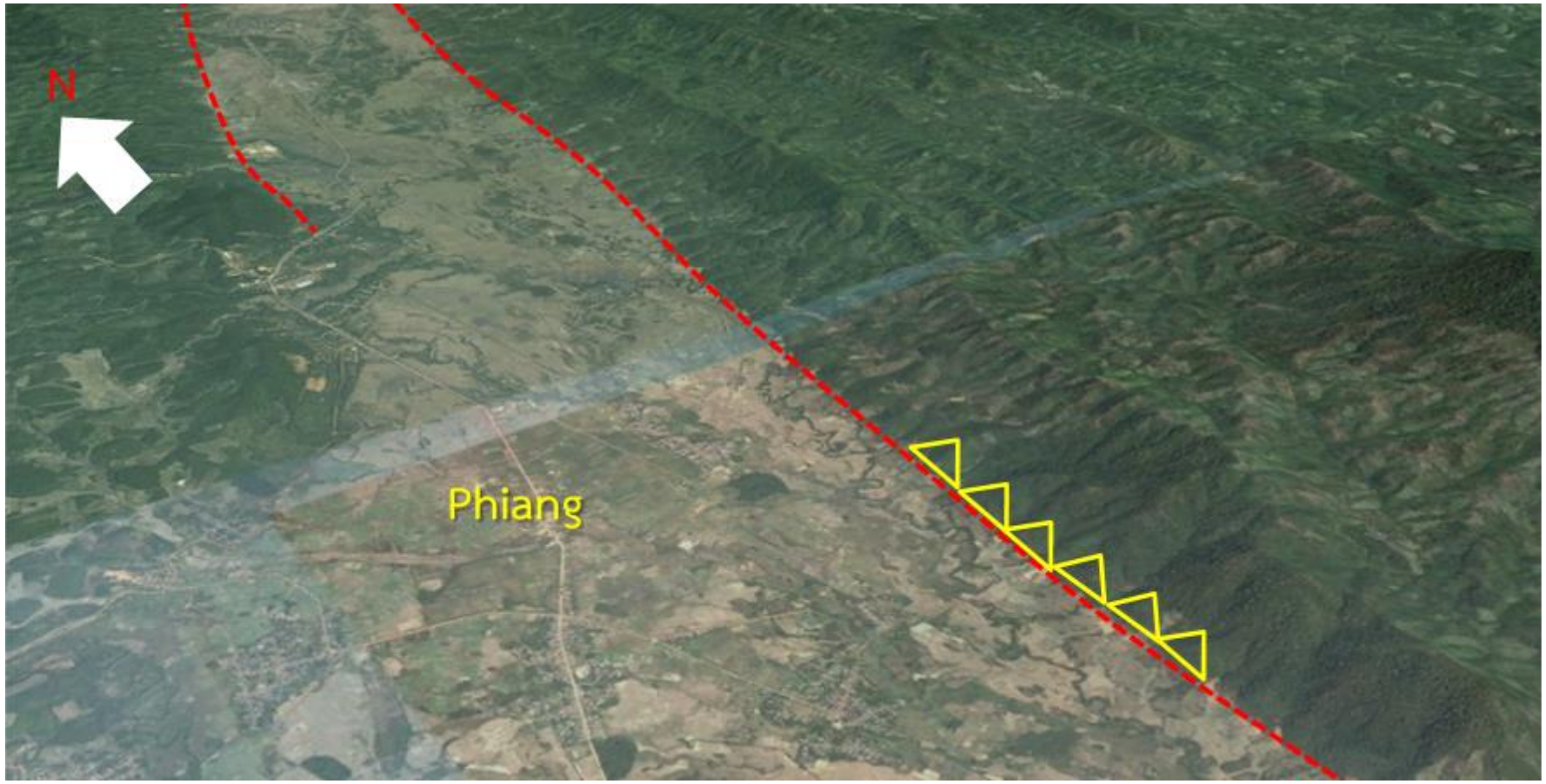

Figure 4.7 Google Earth map along the fault segment in Area 2 Ban Nasom (Figure 3.21) show triangular facets (side view), Phiang basin.

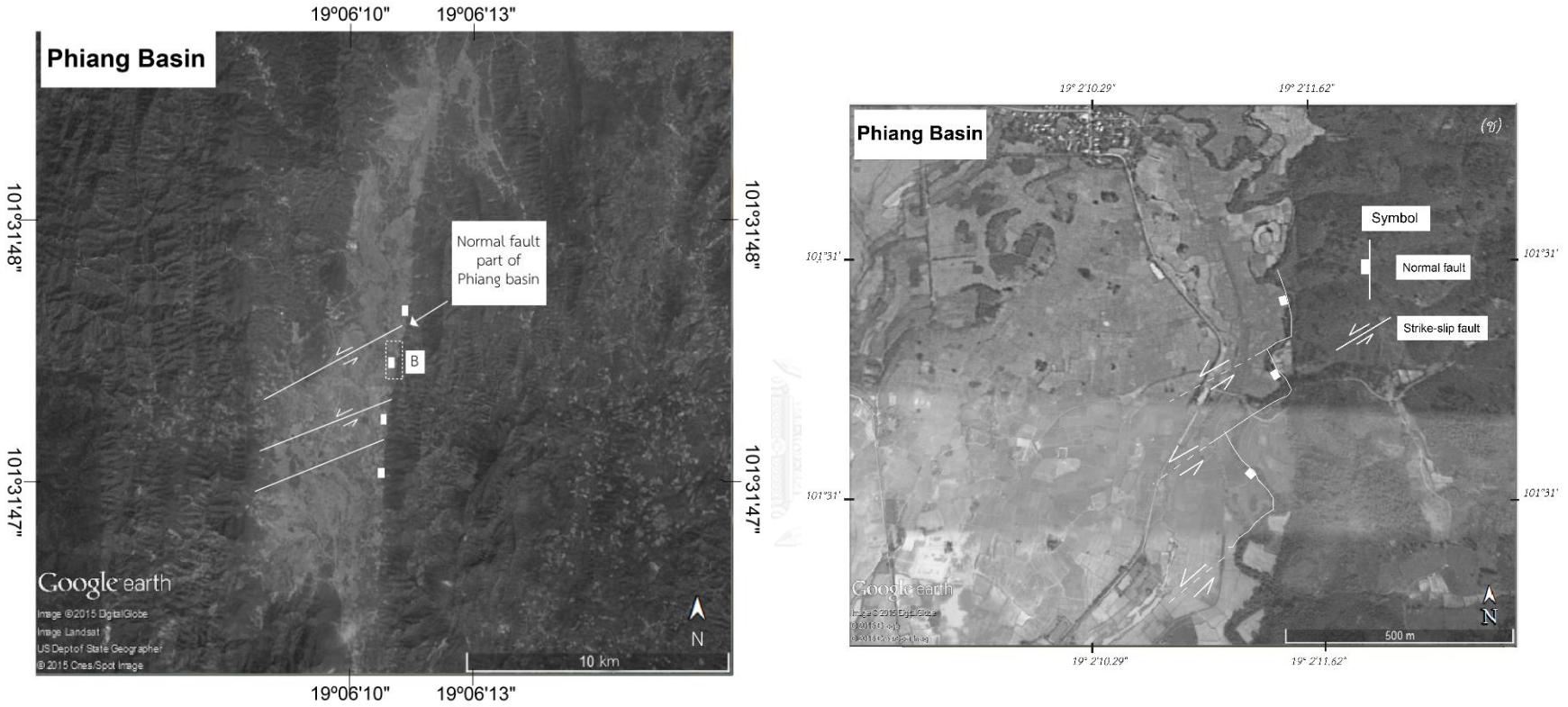

Figure 4.8 Google Earth map (left) interpretation in Phiang basin shows the strik-slip fault movement creating a half-graben basin. (right) Close-up of area indicated with letter B.

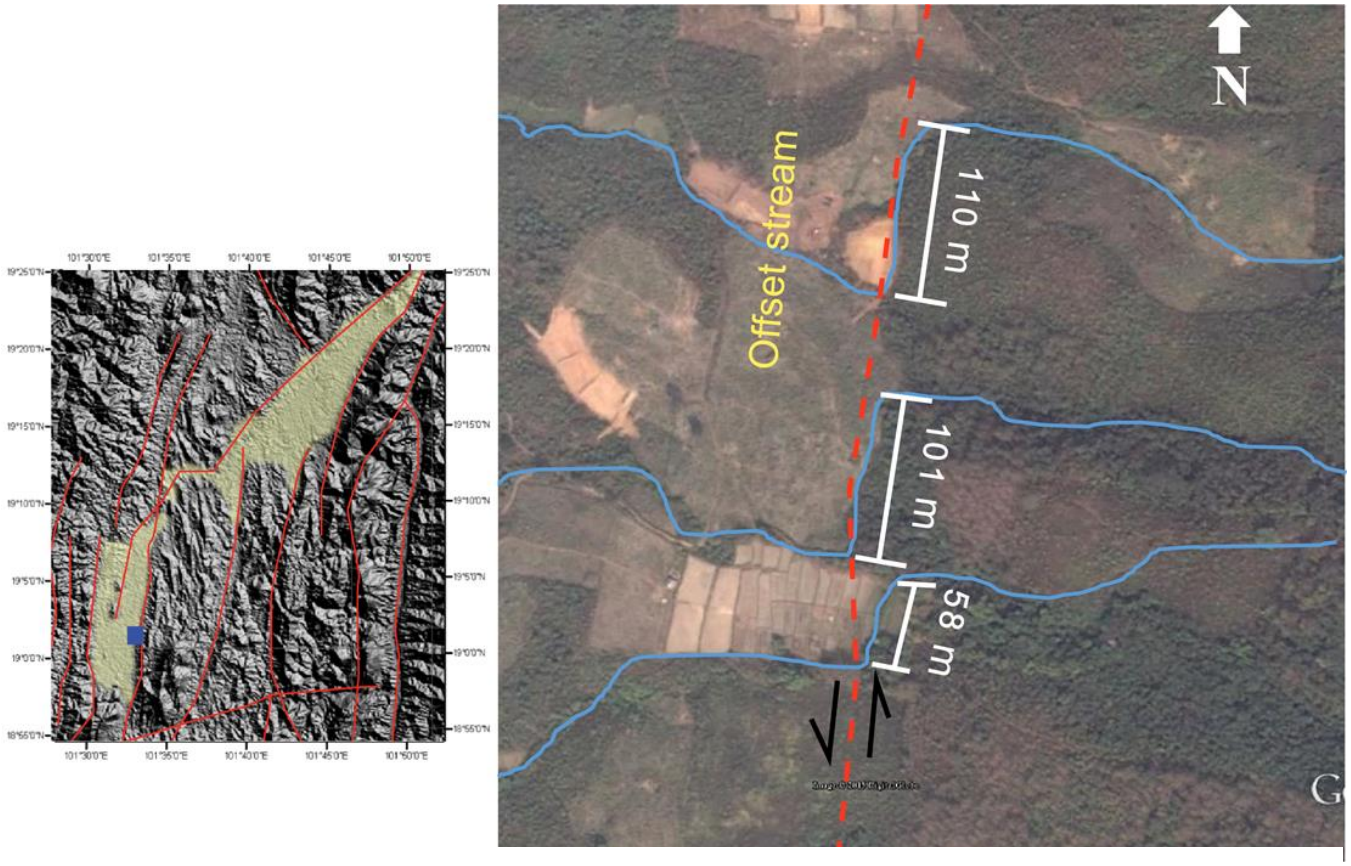

Figure 4.9 Location of the interpretation area in blue box (left) and Google Earth map side view (right) along the fault segment in Area 3 Ban Nakhem show offset streams 58, 101 and 110 meters, Phiang basin. Indicated left lateral fault movement

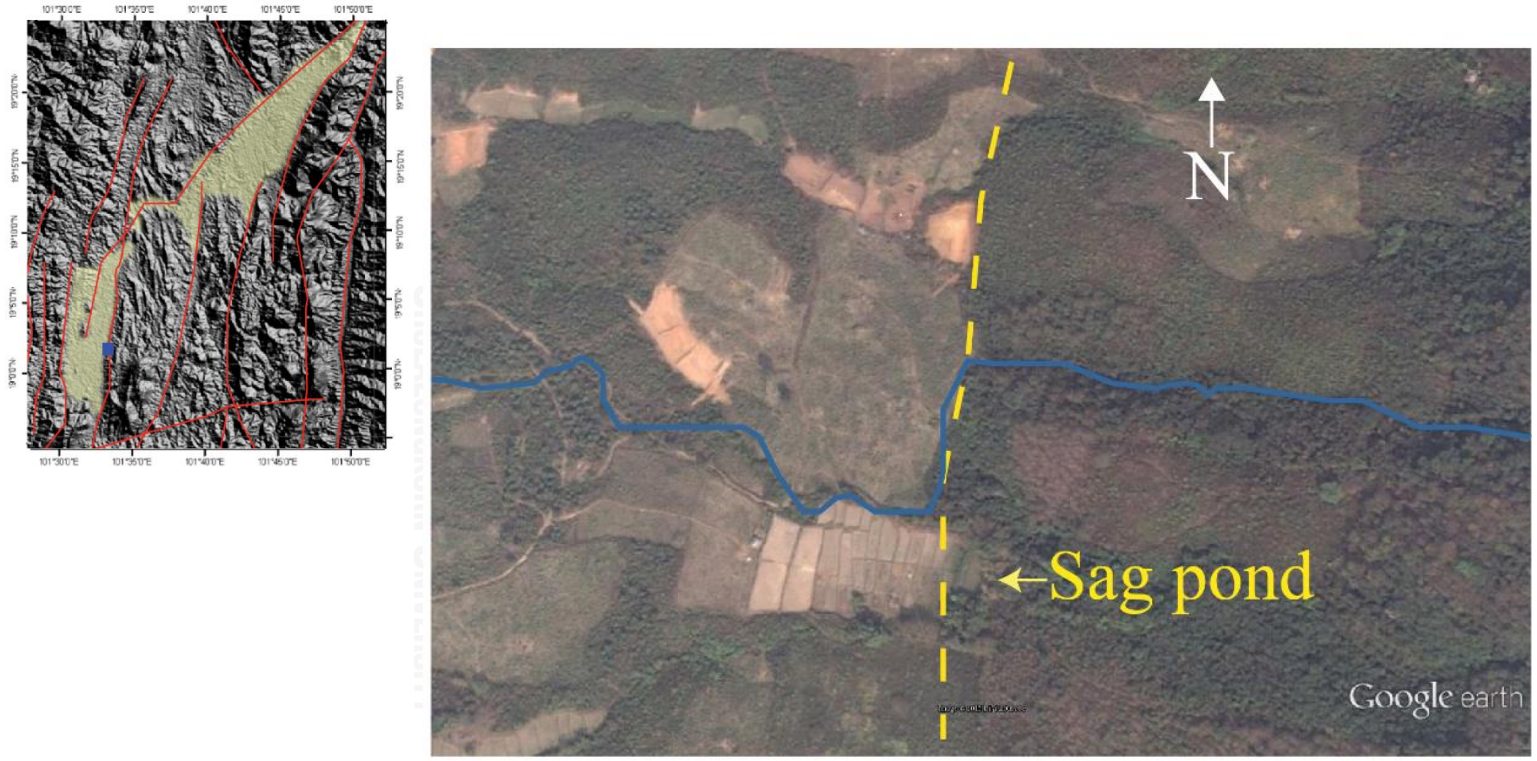

Figure 4.10 Location of the interpretation area in blue box (upper left) and Google Earth map top view (right) along the fault segment in Area 4 Ban Khem show sag pond, Phiang basin.

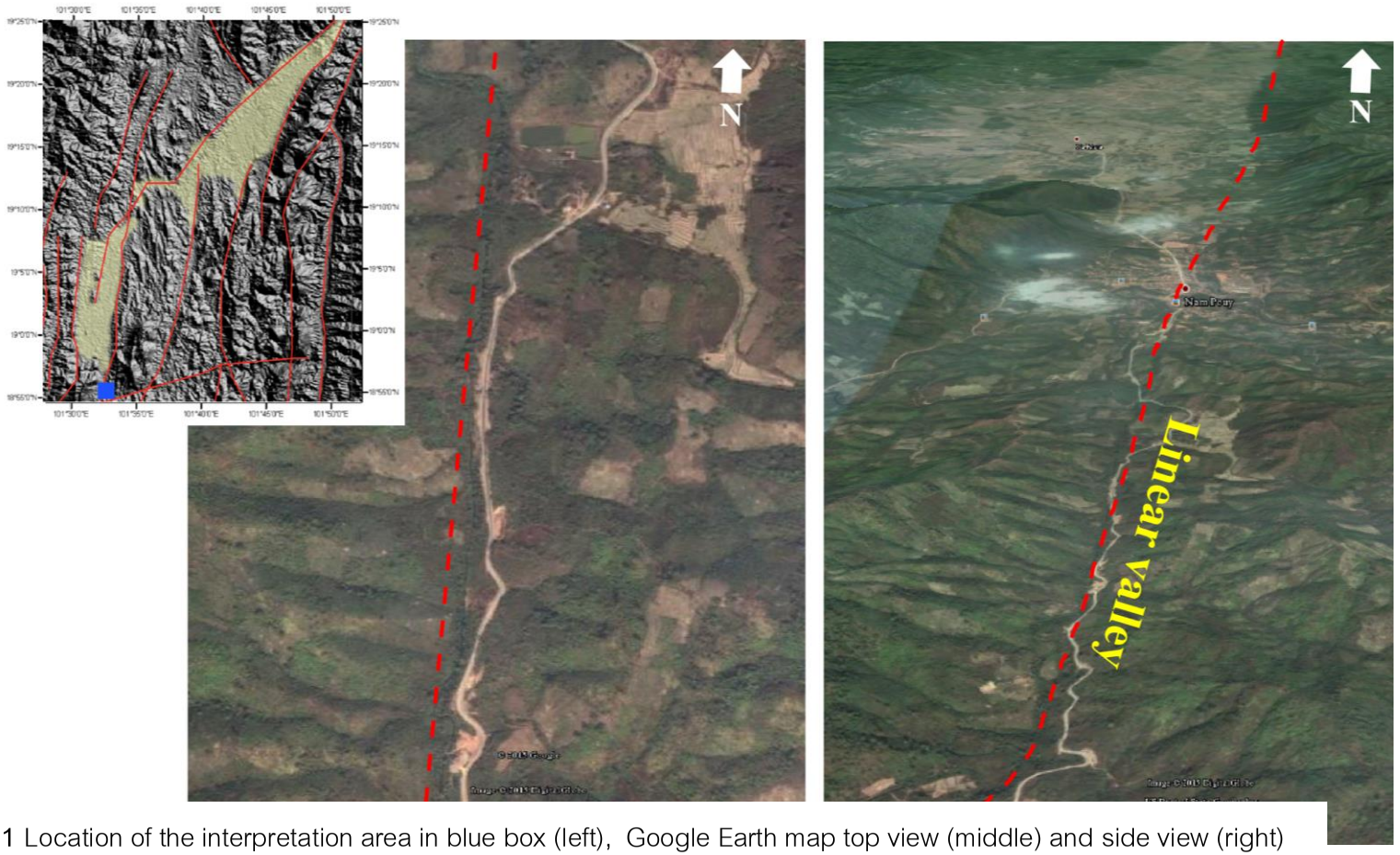

Figure 4.11 Location of the interpretation area in blue box (left), Google Earth map top view (middle) and side view (right) along the fault segment in Area 5 Ban Nam Pouy show linear valley, run along the road in southern of Phiang basin.

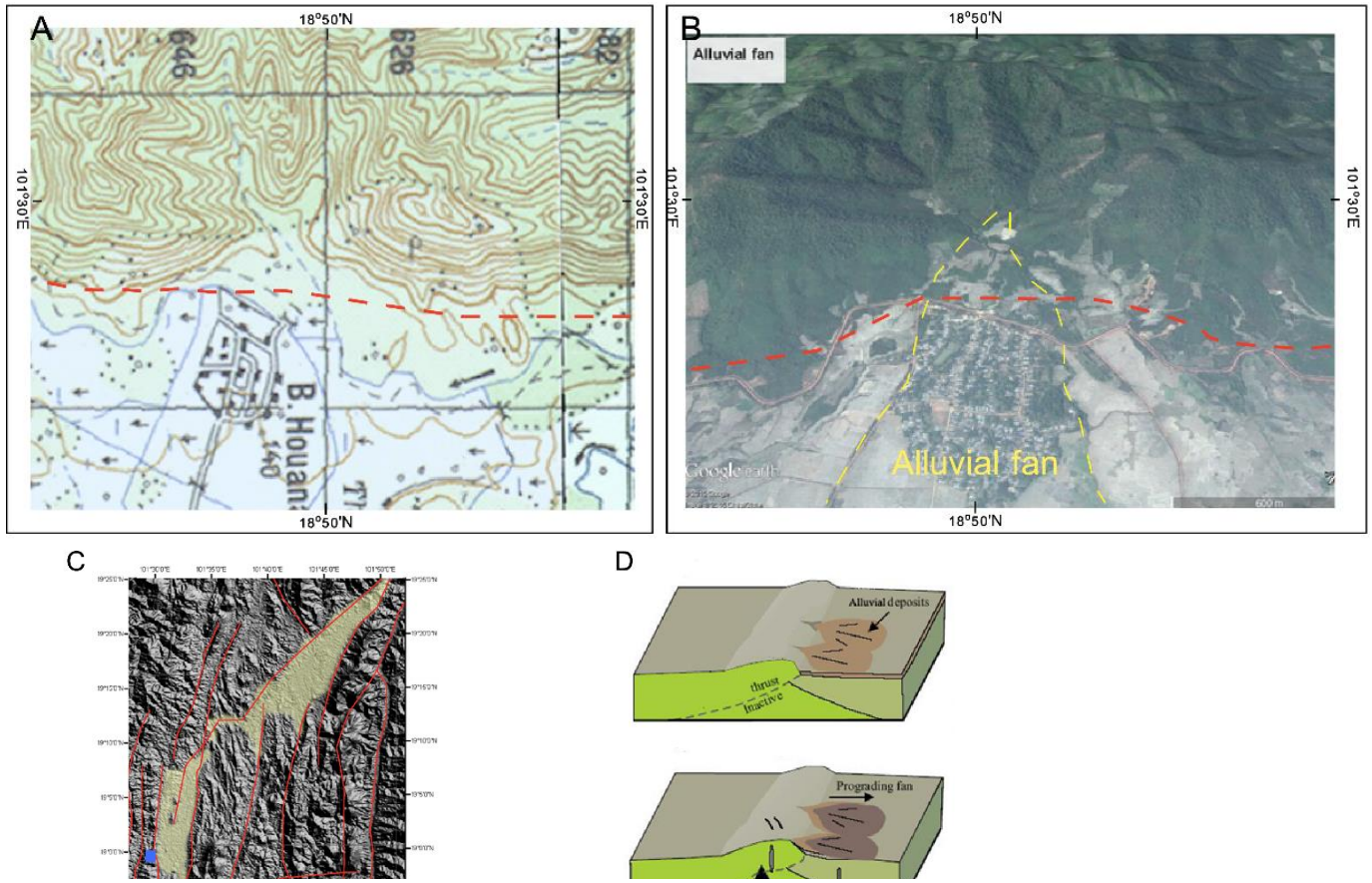

Figure 4.12 (A) topographic map, (B) Google Earth map, (C) location of the interpretation area in blue box and (D) development of propagrading fan along the fault segment in area 6 Ban Houana, Phiang basin.

4.2 Paleoseismic investigation

4.2.1 Field evidence of tectonic geomorphology

During the field survey, geological mapping at the study area and its surrounding areas was made in order to disclose the appearance of active faults. Our field survey strongly indicates the occurrence of faults not only from macroscopic evidence but also microscopic analysis (Figures 4.23-4.41). Although faults can be identified clearly in the field, but none shows good lines of evidence for the active faults. Many of the faults recognized are mainly regarded as the faults cutting the old rock strata which indicate that the faults are merely younger than those rocks. This does not mean the fault is active at present. Therefore, our mapping result can reveal only the presence of some faults but lack of good supporting evidence for their activeness. Brecciation due to strong deformation can be found in the volcaniclastic and clastic rocks near Khong River (Figures 4.39-4.41).

From thin sections under microscopic scale. Figures 4.23-4.30 display various deformation textures identified under microscope. Figures 4.31-4.32 show supporting evidence of faulting from mesoscopic scale and Figures 4.33-4.41 show similar fauting evidence found in the outcrops.

4.1.1 Area 1 Ban Nasom, Phiang Basin (Figure 4.14-4.15)

4.1.2 Area 2 Ban Sibounhuang, Phiang Basin (Figure 4.16-4.18)

4.1.3 Area 3 Ban Nakhem, Phiang Basin (Figure 4.19-4.20)

4.1.4 Area 4 Near Khong River, Xaignabouli Basin (Figure 4.21-4.22)

4.1.5 Area 5 Ban Hui Dok, Xaignabouli Basin (Figure 4.20)

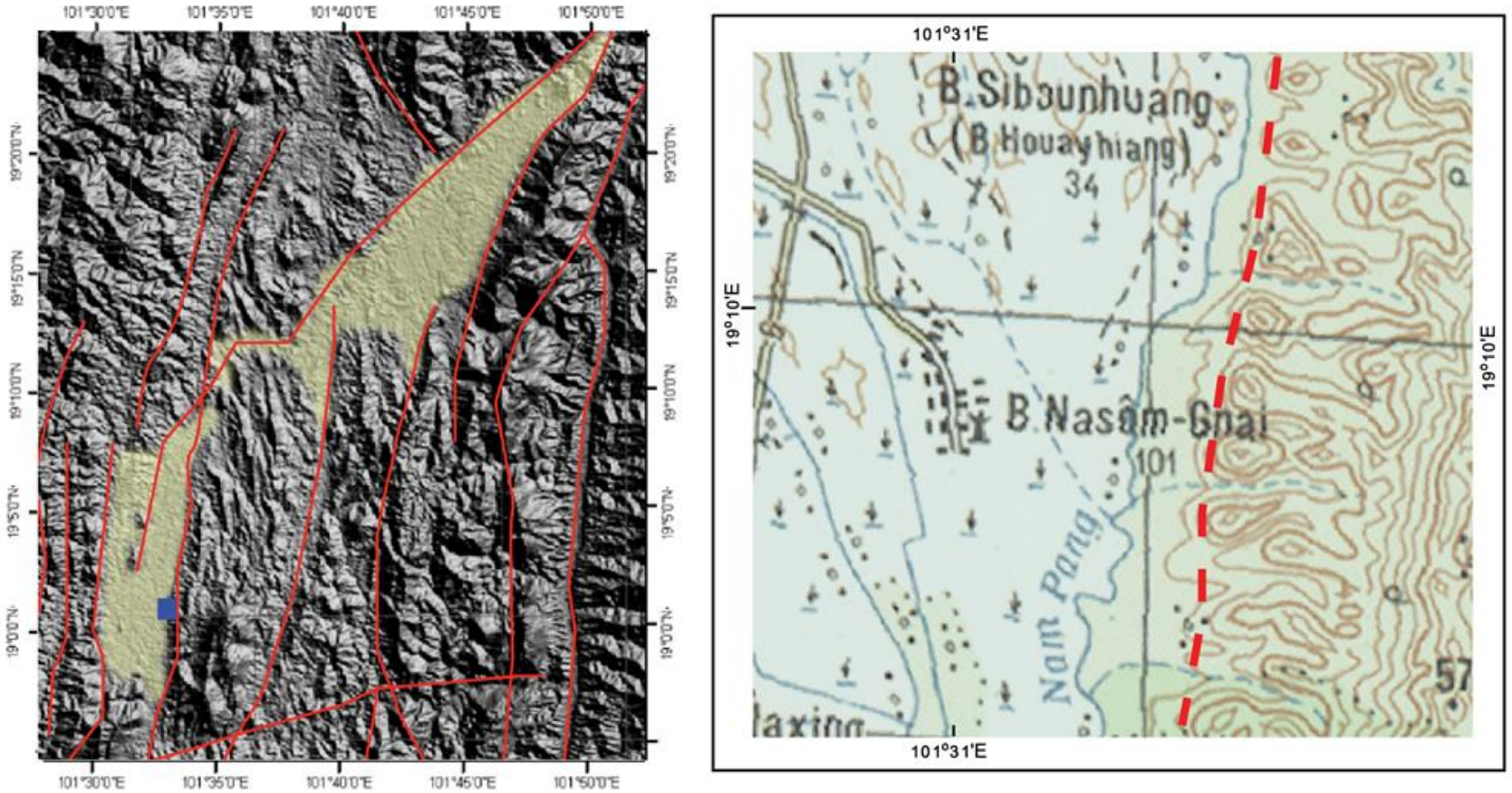

Figure 4.13 Location of the area 1 Ban Nasom in blue box (left) and topographic map (right), showing the location of triangular facet.

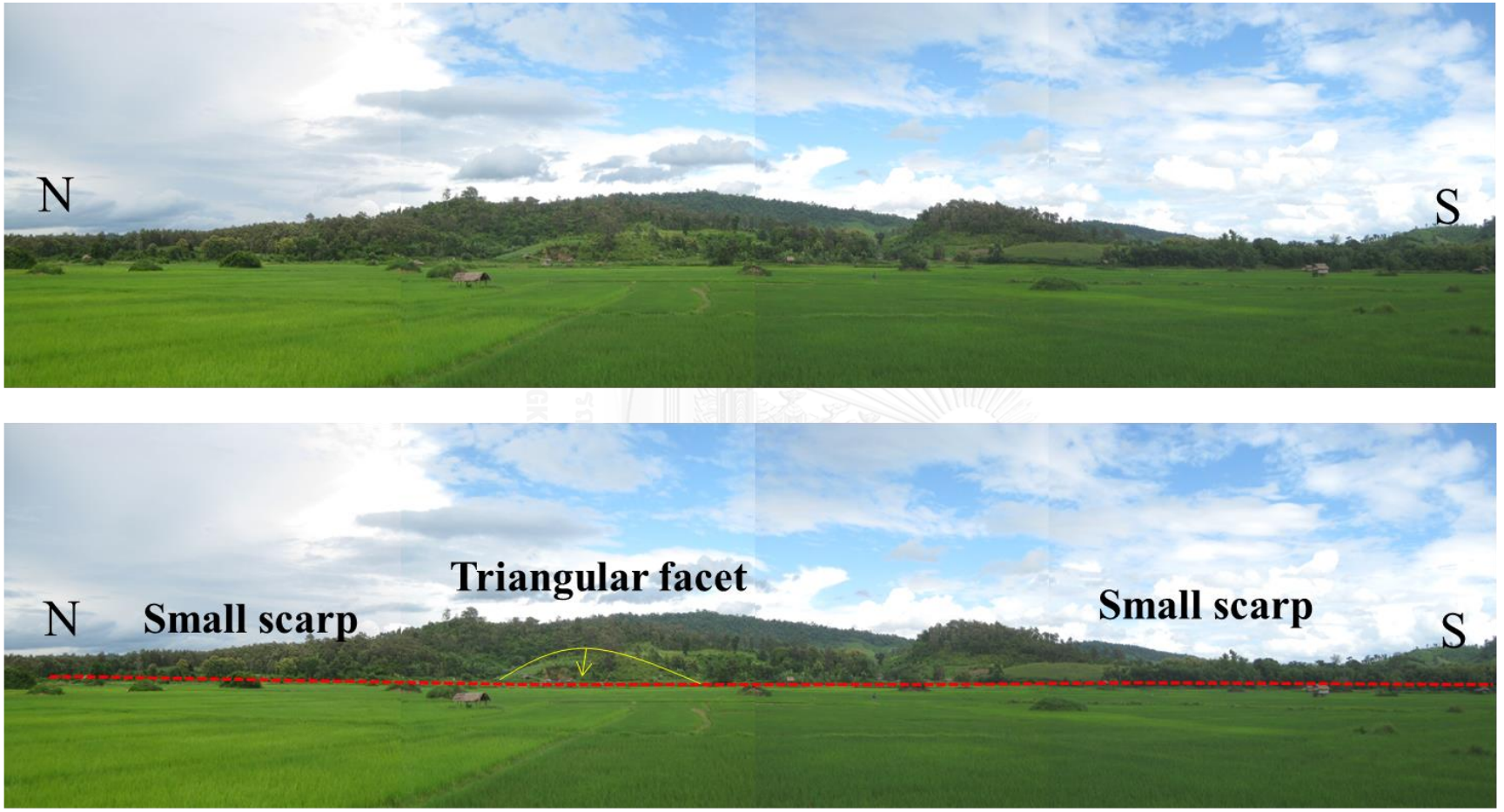

Figure 4.14 Panorama of the north-trending mountain range, Ban Nasom, eastern of Phiang Basin, showing west dipping triangular facet covered mostly by rice field (lower) interpretation photo.

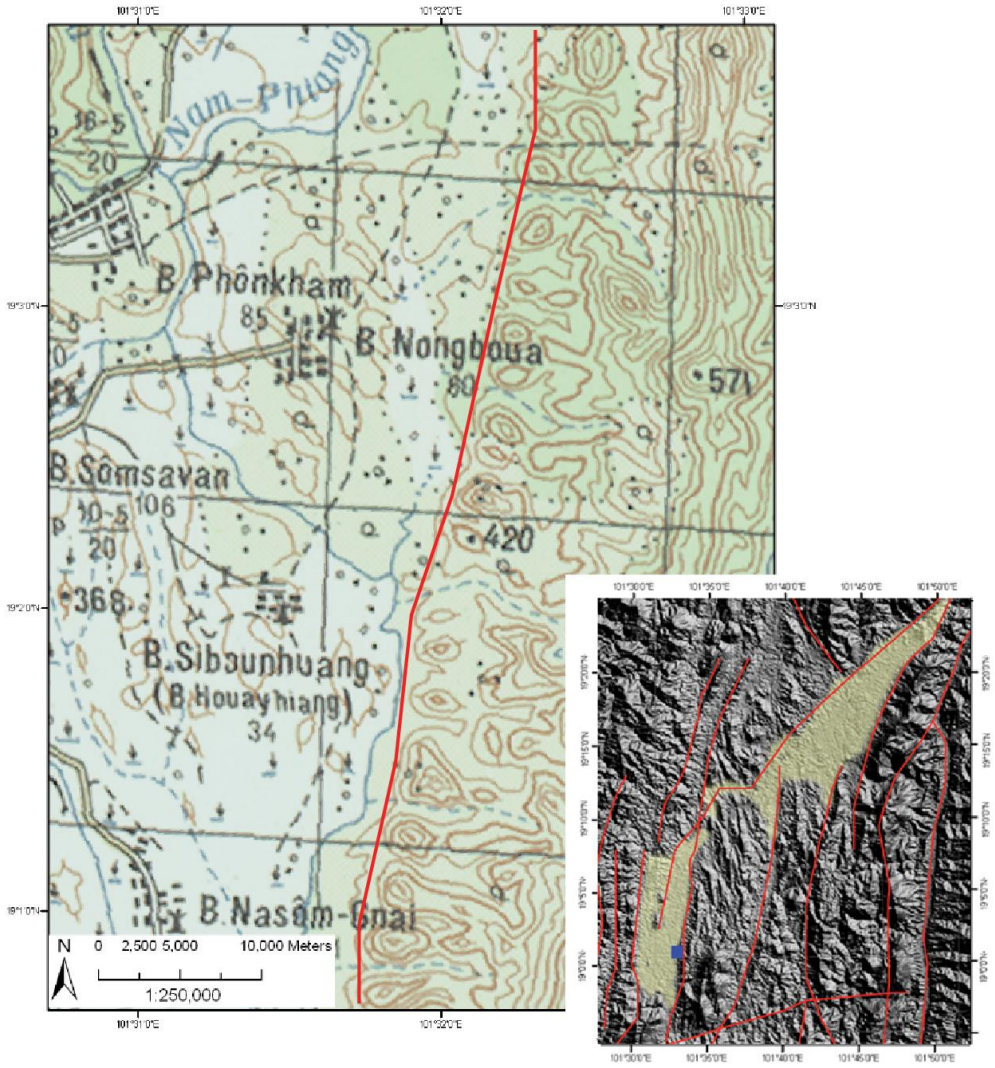

Figure 4.15 Location of the area 2 **Ban Sibounhuang** in blue box of inserted map (right) and topographic map, showing the location of triangular facet.

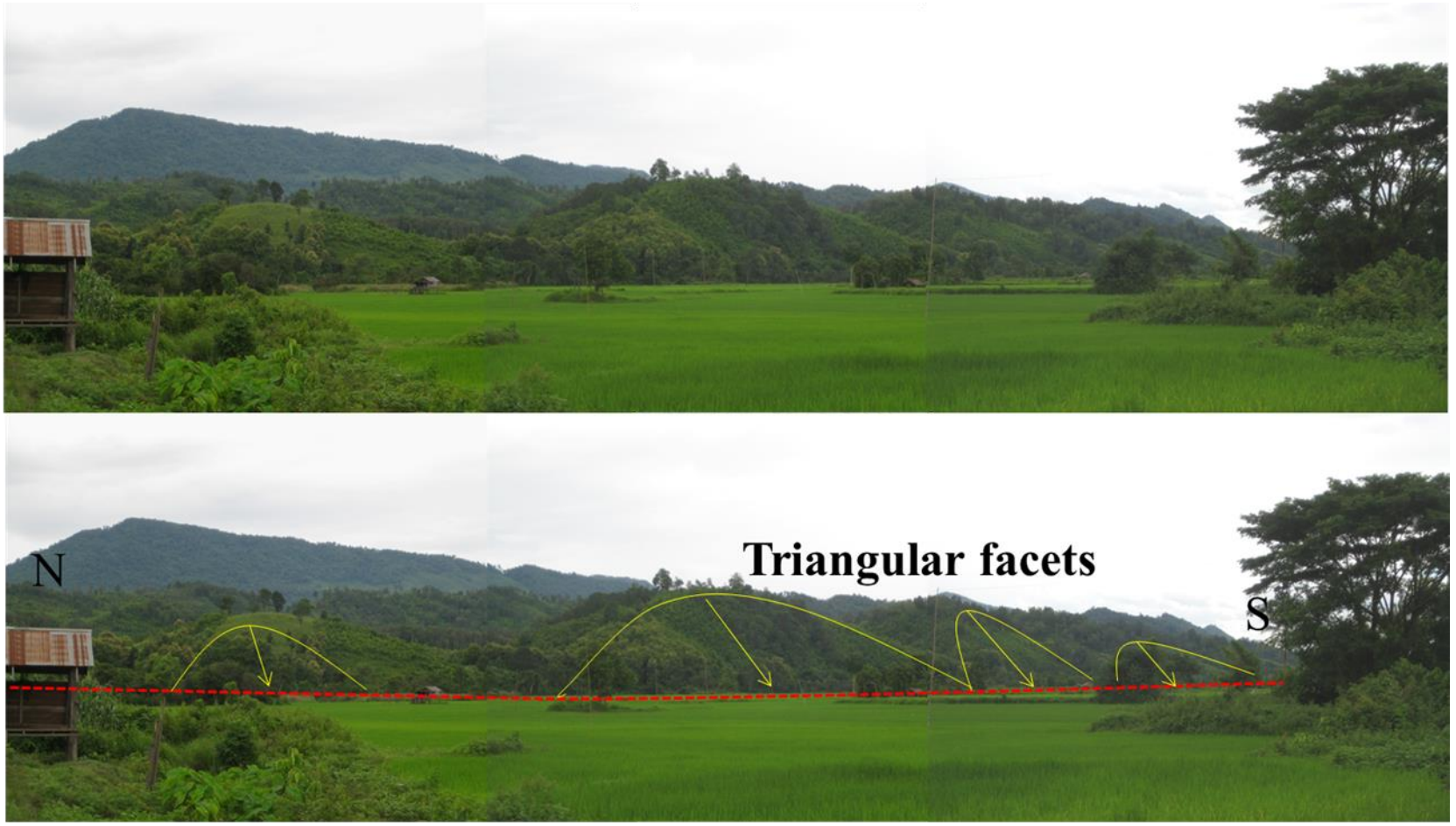

Figure 4.16 Panorama of the north-trending mountain range, Ban Sibounhuang, eastern margin of Phiang Basin, showing west dipping triangular facets covered mostly by trees (lower) interpretation photo.

Figure 4.17 Panorama of the north-trending mountain range, Ban Sibounhuang, eastern of Phiang Basin, showing west dipping triangular facets covered mostly by trees (lower) interpretation photo.

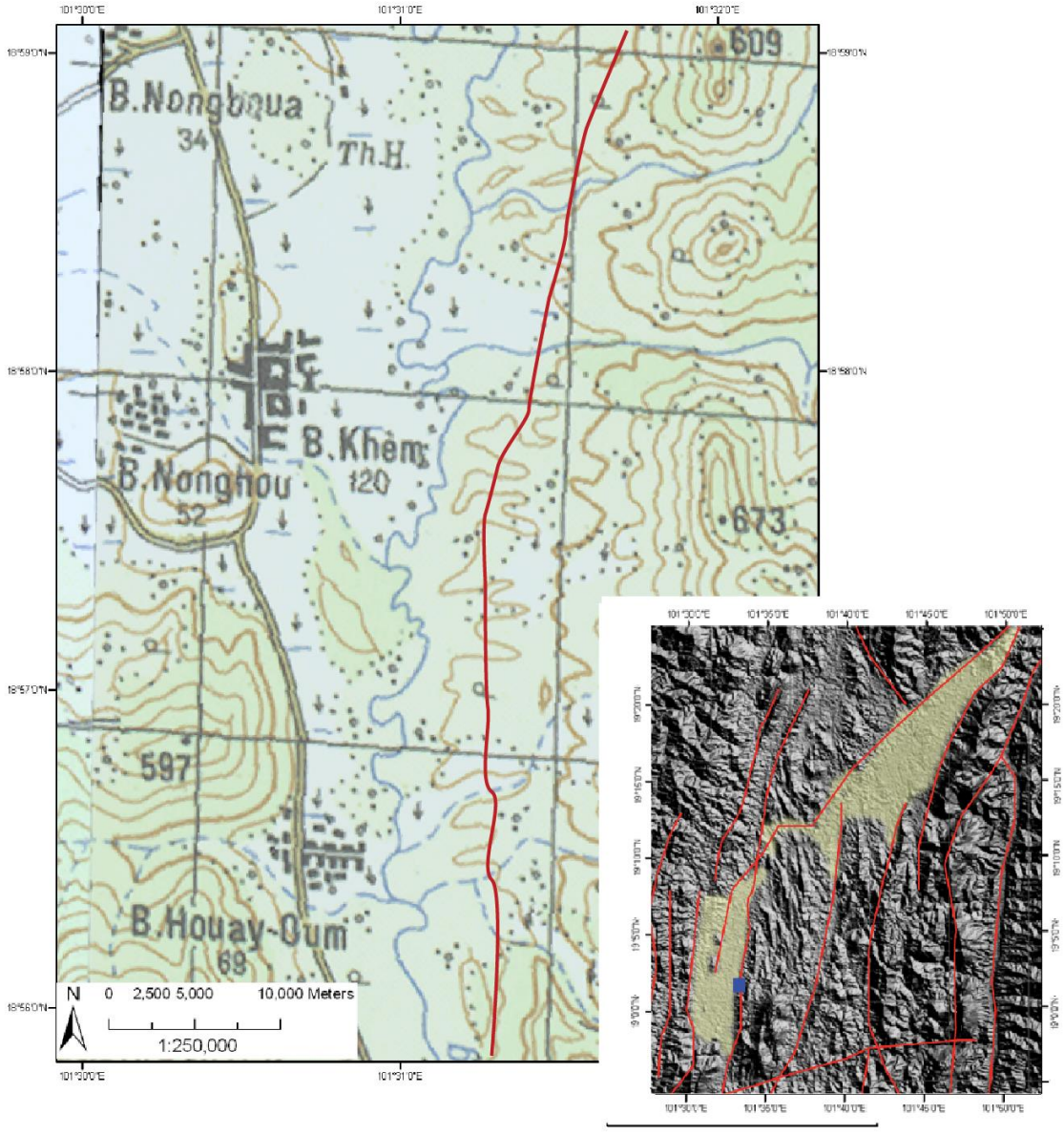

Figure 4.18 Location of the **area 3 Ban Khem** in blue box of inserted map (right) and topographic map, showing the location of offset spur and offset stream.

Figure 4.19 An offset stream of Ban Khem, eastern of Phiang Basin. Noted that red line is the fault line and the blue arrow is showing the direction of stream flowing.

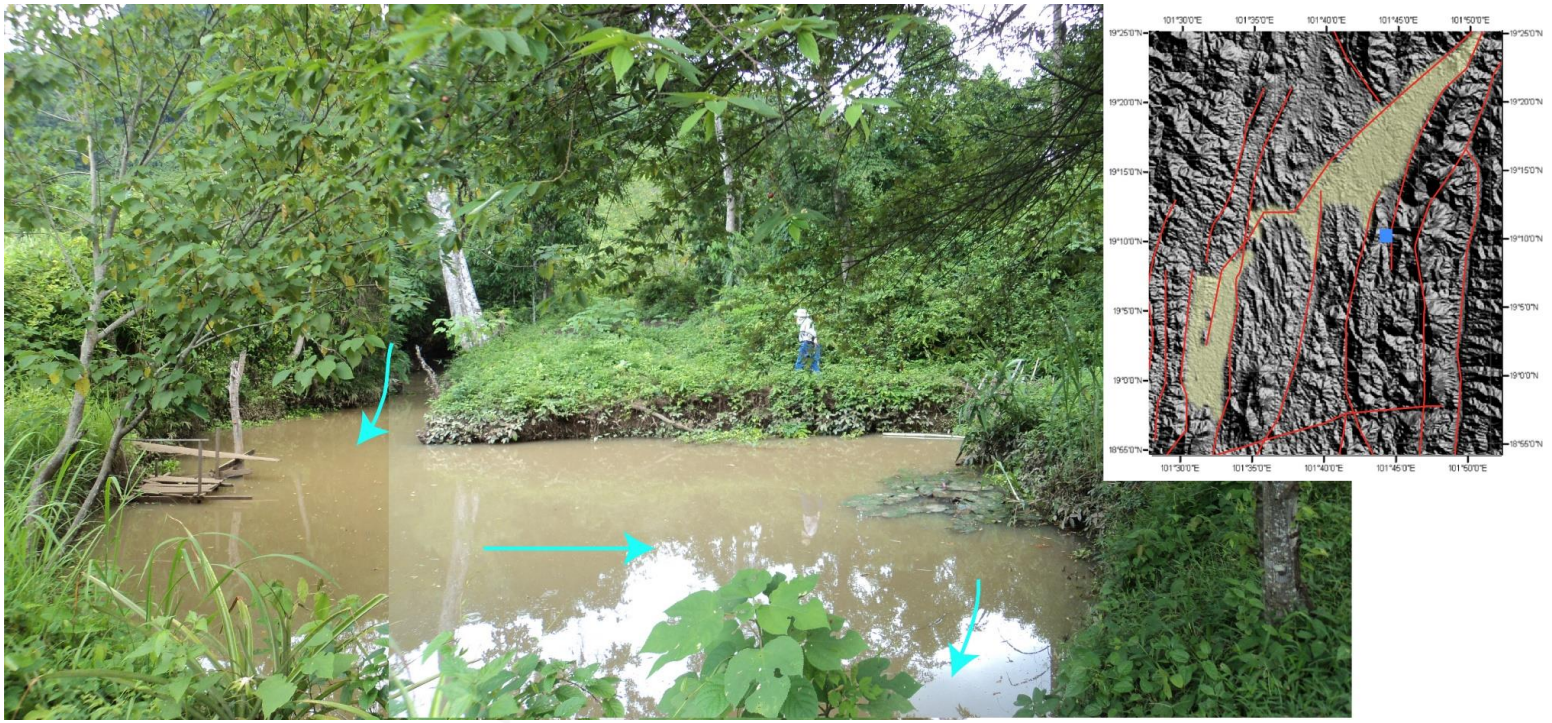

Figure 4.20 An offset stream of Ban Hui Dok (785351N, 2122748E), eastern of Xaignabouli Basin. Noted that red line is the fault line and the blue arrow is showing the direction of stream flowing.

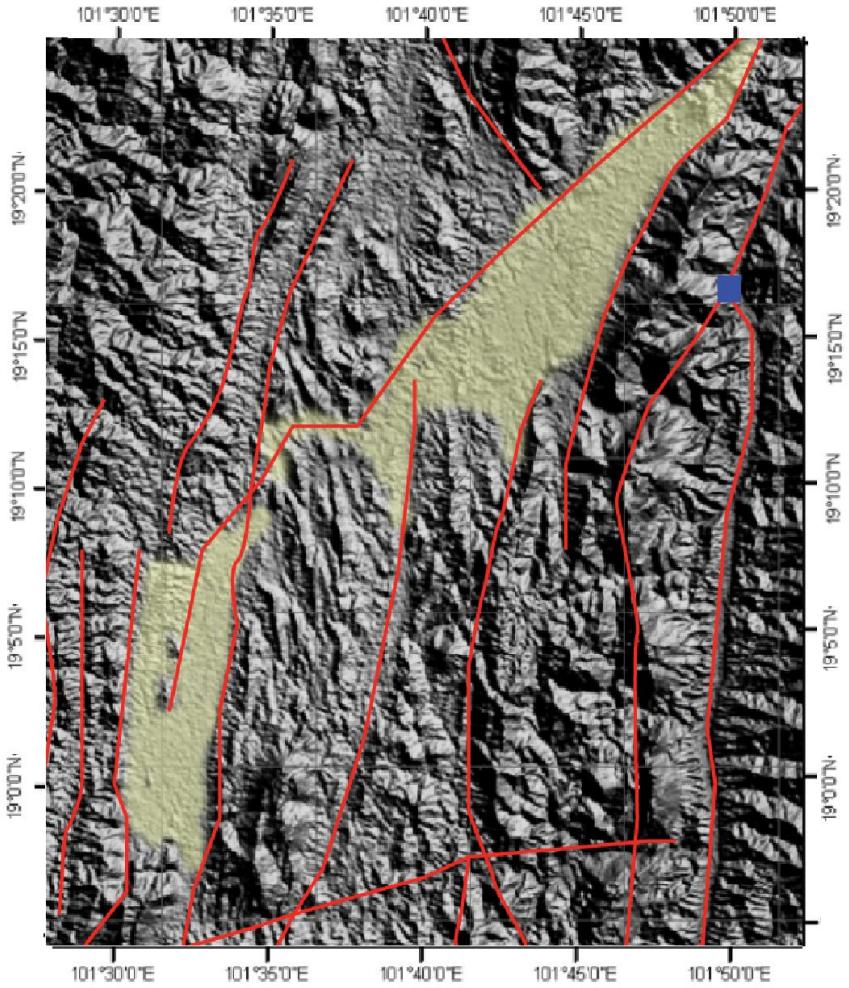

Figure 4.21 Location of the **area 4 Near Khong River, Xaignabouli Basin** in blue box of the map, showing the location of tri angular facet and fault scarp.

Figure 4.22 Fault scarp and triangular facets of area 4 Near Khong River, Xaignabouli Basin. Noted that red line is the fault line and the yellow triangular is showing the triangular facet.

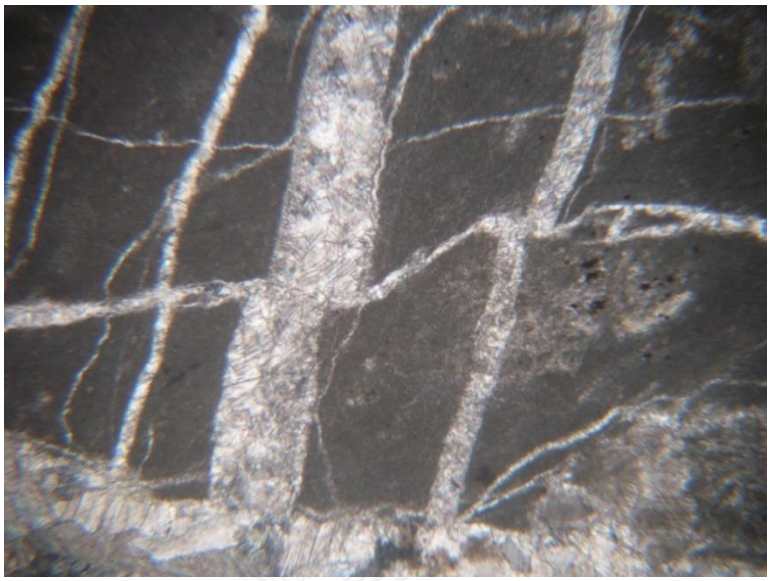

Figure 4.23 Photomicrograph of the brecciated limestone collected at the eastern bank of the area 4 site showing broken grains and offset veinlets of calcite, suggesting deformation due to faulting.

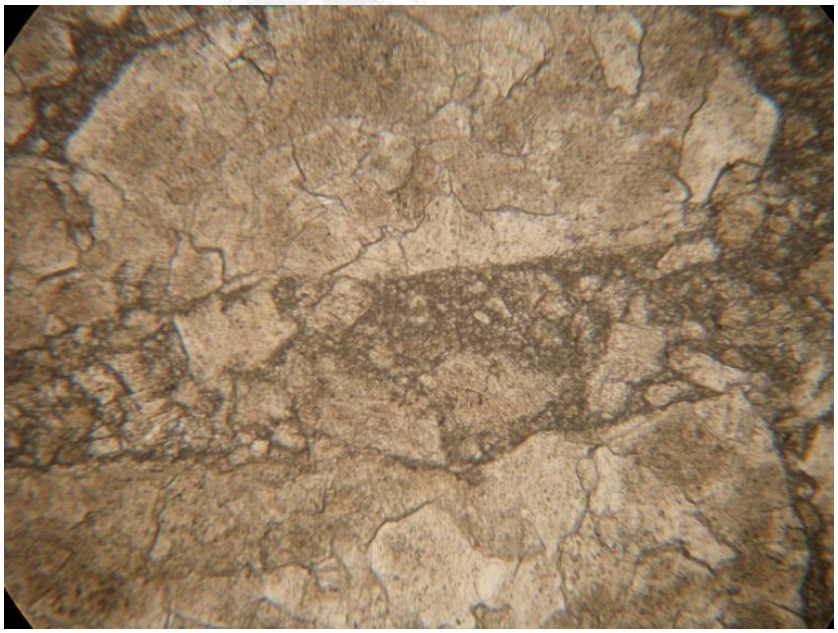

Figure 4.24 Photomicrograph of a rock slab sample collected from the western bank of the area 4 showing brecciated vein cutting crystalline limestone, suggestion some faulting event.

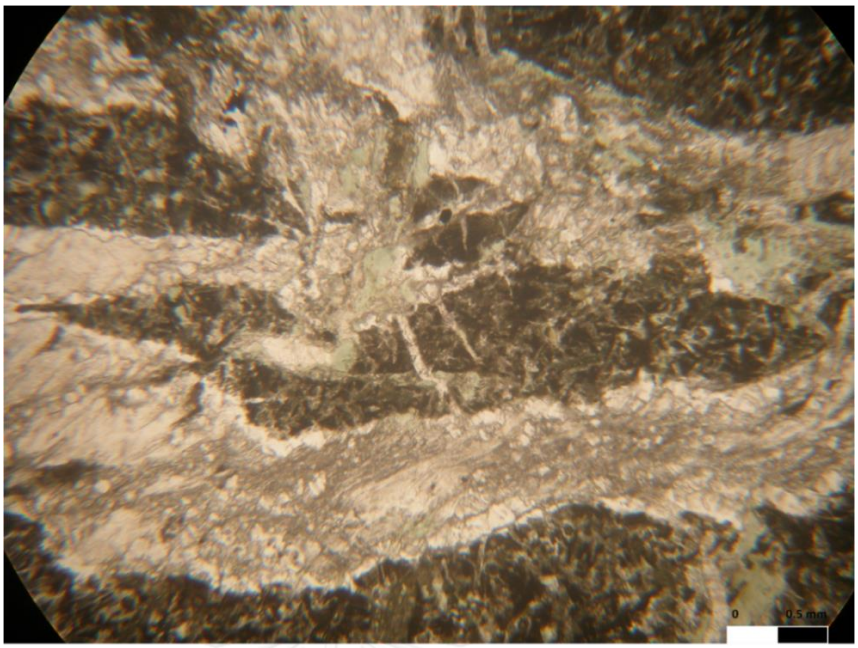

Figure 4.25 Photomicrograph of the brecciated limestone collected at the western bank of the area 4showing broken grains and distorted grains of calcite due mainly to the effect of deformation.

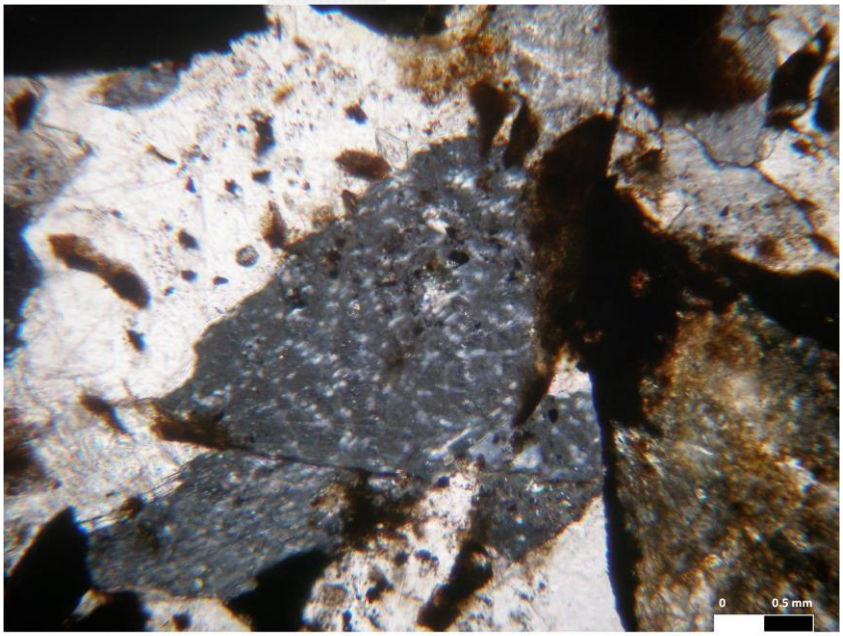

Figure 4.26 Photomicrograph of partly brecciated limestone collected at the eastern bank of the area 4 showing broken and cut grains of calcite due mainly to the effect of deformation and faulting.

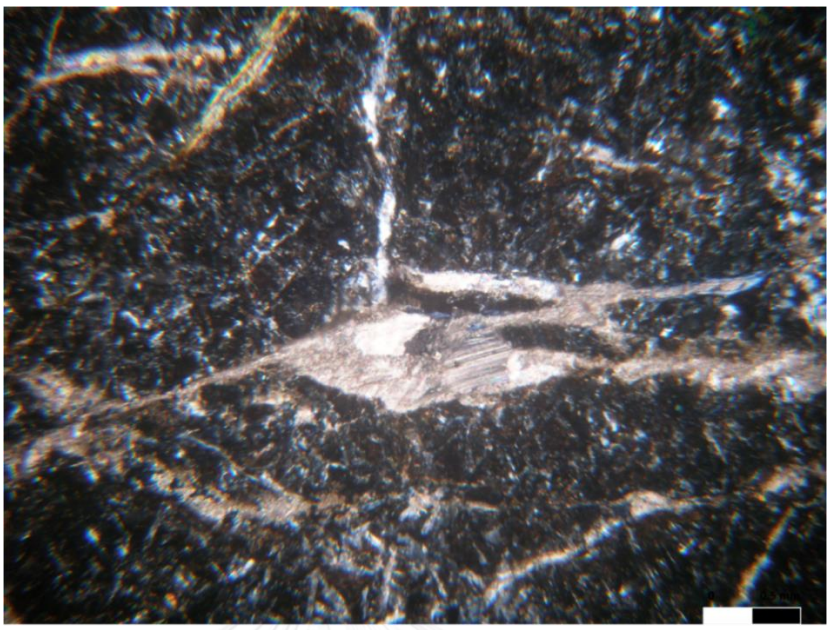

Figure 4.27 Photograph of volcanic rock near the area 4 showing a well-defined deformation of pull-apart nature as evident by the distorted of veinlet calcite.

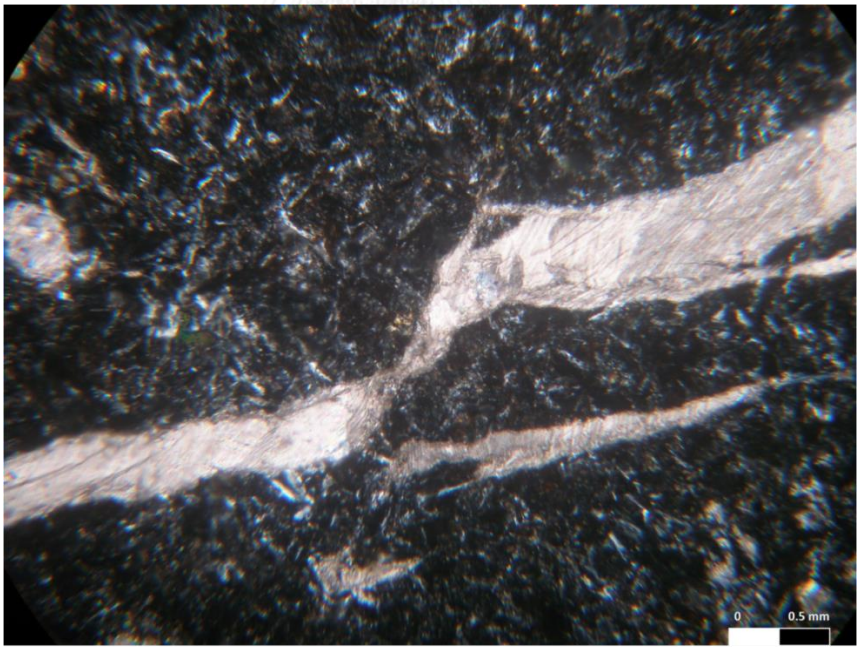

Figure 4.28 Photomicrograph of a rock slab sample collected from the western bank of the area 4 showing fault cutting the veinlets of calcite suggesting an evidence of fault.

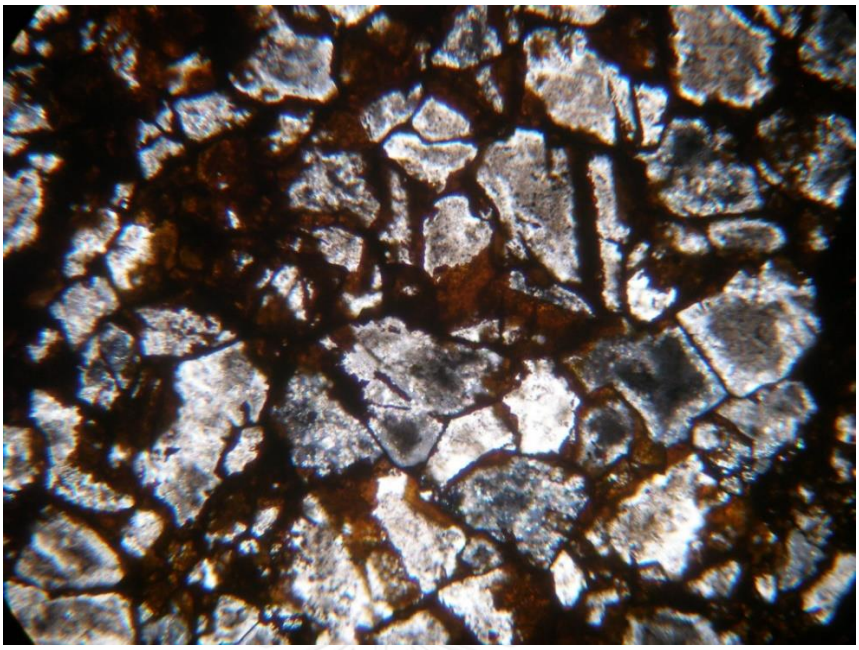

Figure 4.29 Photomicrograph of a clastic dike sample (see Figure. 4.25f) collected from the western bank of the area 4 showing rock fragments with loosely cemented iron-oxide minerals.

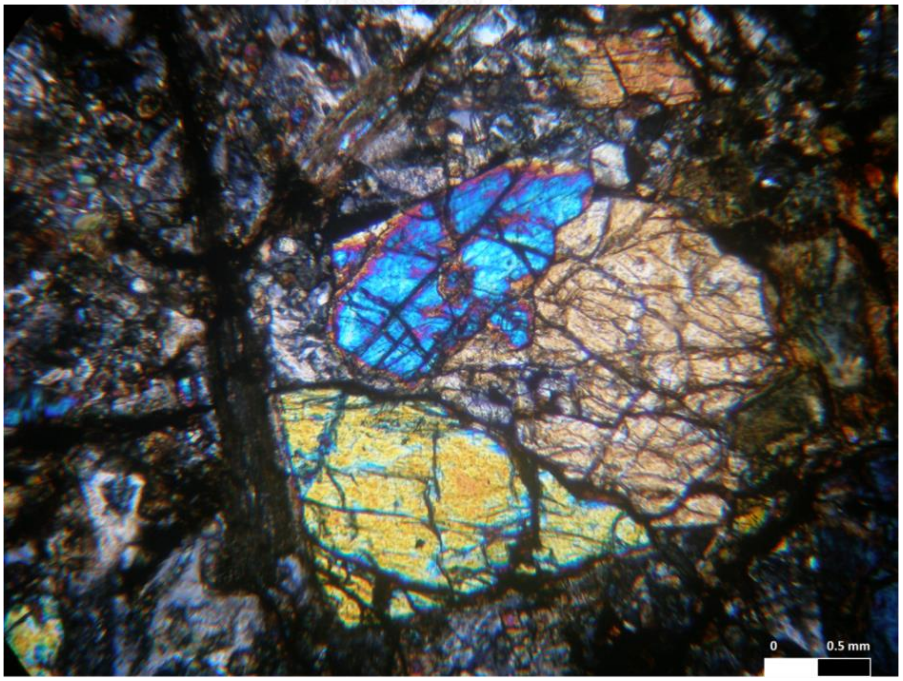

Figure 4.30 Photomicrograph of a deformed rock slab sample collected from the western bank of the barge side showing fractured clinopyroxene due to faulting.

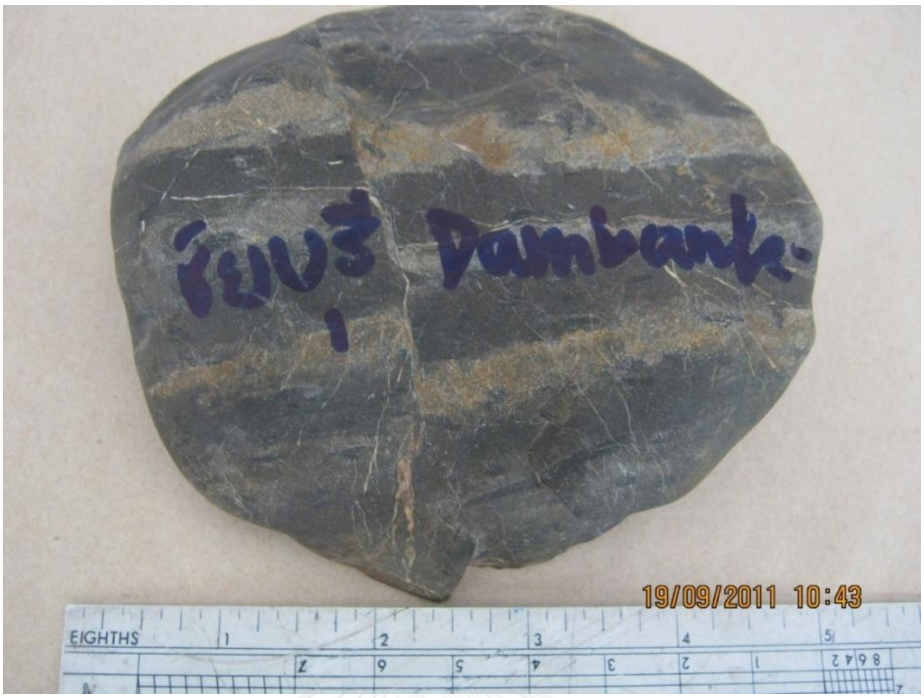

Figure 4.31 A hand slab sample of chert beds cut by fault near area 4

Figure 4.32 A rock slab of metamudstone showing fault cutting veinlets of calcite, near area 4.

Figure 4.33 A fault contact between two sedimentary sequences volcaniclastic rocks (yellowish gray) and sandstone (brownish gray) of the upper Paleozoic age.

Figure 4.34 A fault gouge found along the fault plane between two sandstone (left) and siltstone (right) of the Upper Paleozoic age, Near area 4.

Figure 4.35 A fault gouge, a good supporting evidence for faulting, recognized in the mudstone of Upper Paleozoic age, near the area 4,

Figure 4.36 A steeply – dipping slickenside showing horizontal movement, indicating a left lateral strike slip fault. Found in the Mesozoic sediments at the road cut near the area 4.

Figure 4.37 A quarry near the road near area 4 showing slickenside in the Upper Paleozoic strata, indicating a left lateral strike slip fault.

Figure 4.38 A small quarry near the road to Piang Basin, showing a clastic dike cutting brecciated strata of Mezoic age, suggesting paleoearthquake strggered in this area.

Figure 4.39 A road cut exposure showing rock brecciation in Mesozoic strata. Note that some strata were also faulted.

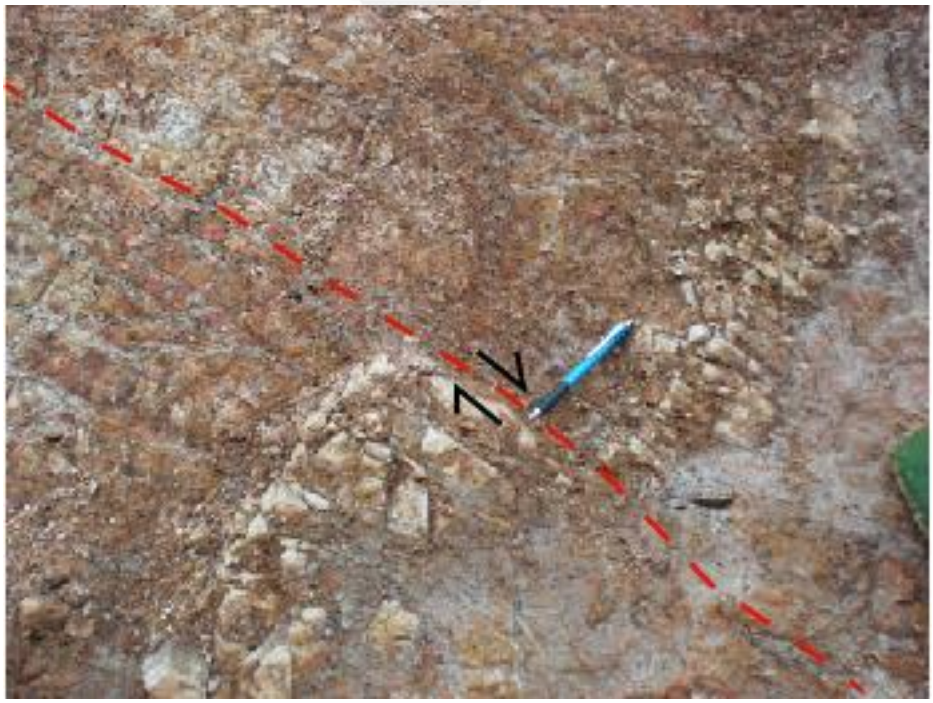

Figure 4.40 A man – made exposure near the area 4 showing a deformed (clastic?) dike cutting Mesozoic sedimentary strata,

Figure 4.41 An exposure near the area 4 showing rock brecciation which is nearby the interpreted active fault.

4.3 Trenching

4.3.1 Site selection for paleoseismic trenching

Fourteen trench sites, i.e. six trenches (T5, T6, T7, T8, T9 and T11) at Phiang basin, and eight trenches (T11, T12, T13, T14, T15, T16, T17 and T18) at Xaignabouli basin were selected. There are one potential trench and two exposures shown in Figures 4.44-4.49.

The trenches at the Khong River (T4) were completed. Faults were observed only in the bedrocks. Most of sediments overlying the bedrocks are gravel beds. Sands with some gravels were found at the trench no. T4. Six sand samples and one fault gouge samples in the bedrocks were collected from the trench no.T4 for the age-dating (Figures 4.44-4.47).

Eight selected exposures at Xaignabouli basin, seven exposures were cleaned and logged and one exposure at Ban Nahai was discarded due to the borrow area walls were collapsed. Only two exposures show evidences of tectonic activities observed in

sediments. The first exposure is the trench no. T16 at Ban Vangxoy. The gravel bed overlying the sandstone/siltstone was folded and jointed as shown in Figure 4.48. The second trench is the trench no.T18 at Ban Wang Kham. The smoky quartz dike cut into the gravel bed that overlies the highly to completely weathered siltstone as shown in Figure 4.49-4.50. Three soil samples were collected from the exposure T16 and two soil samples from the exposure T18.

4.3.2 Geochronological dating

After following all steps described in Chapter 3.3.2, the OSL dating results are shown in Table 4.2. .Apart from a total of at least 30 samples as specified in the contract, only 23 samples of the sediments at the Xaignabouli area can be selected for luminescence dating technique. This is due mainly to (1) the heavy rainfall during the course of sampling and (2) no appropriate samples are appropriate for the age dating determination using this method. No samples of organic – rich material can be observed not only in the paleoseismic trench but also from the quarry front. This is significantly caused by strong oxidation and sever weathering conditions during the survey period. So no carbon -14 dating method has been applied in this course of work.

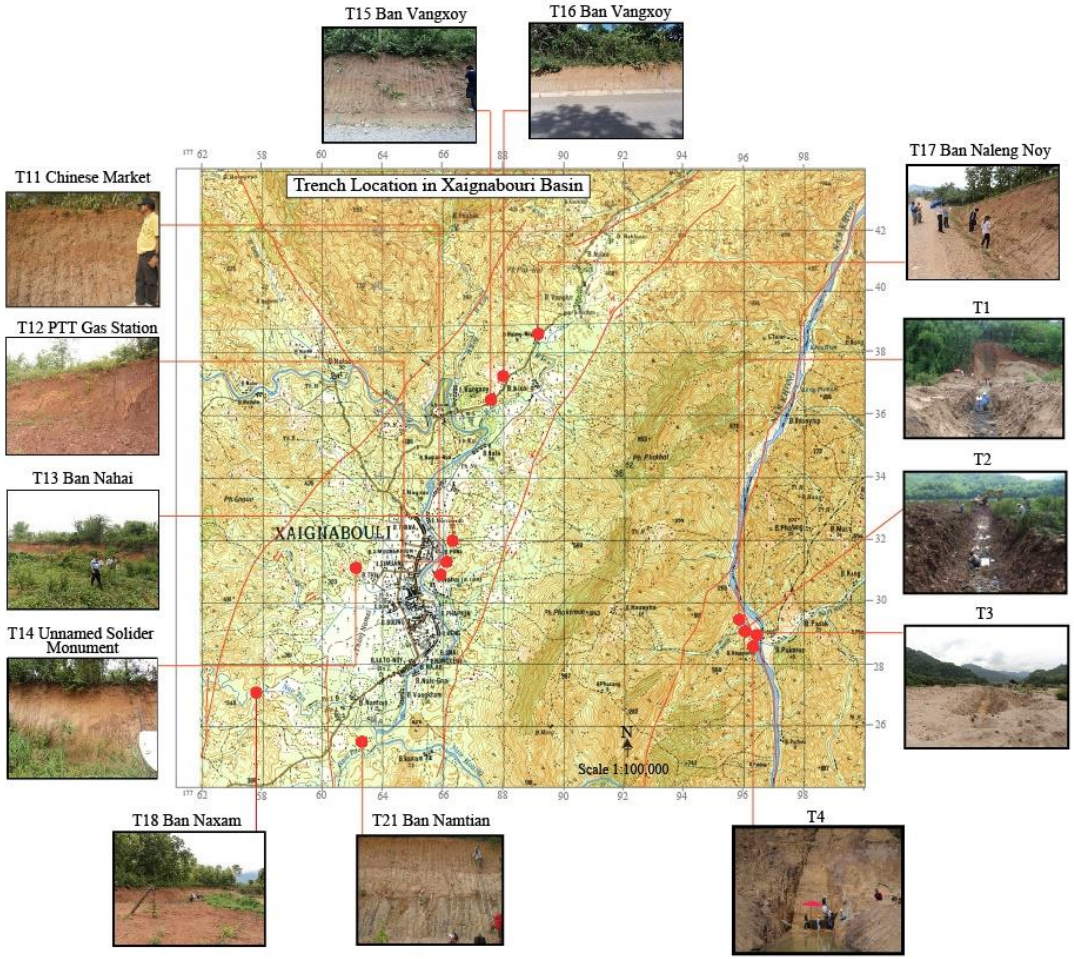

Figure 4.42 Trench/exposure locations in Xaignabouli basin.

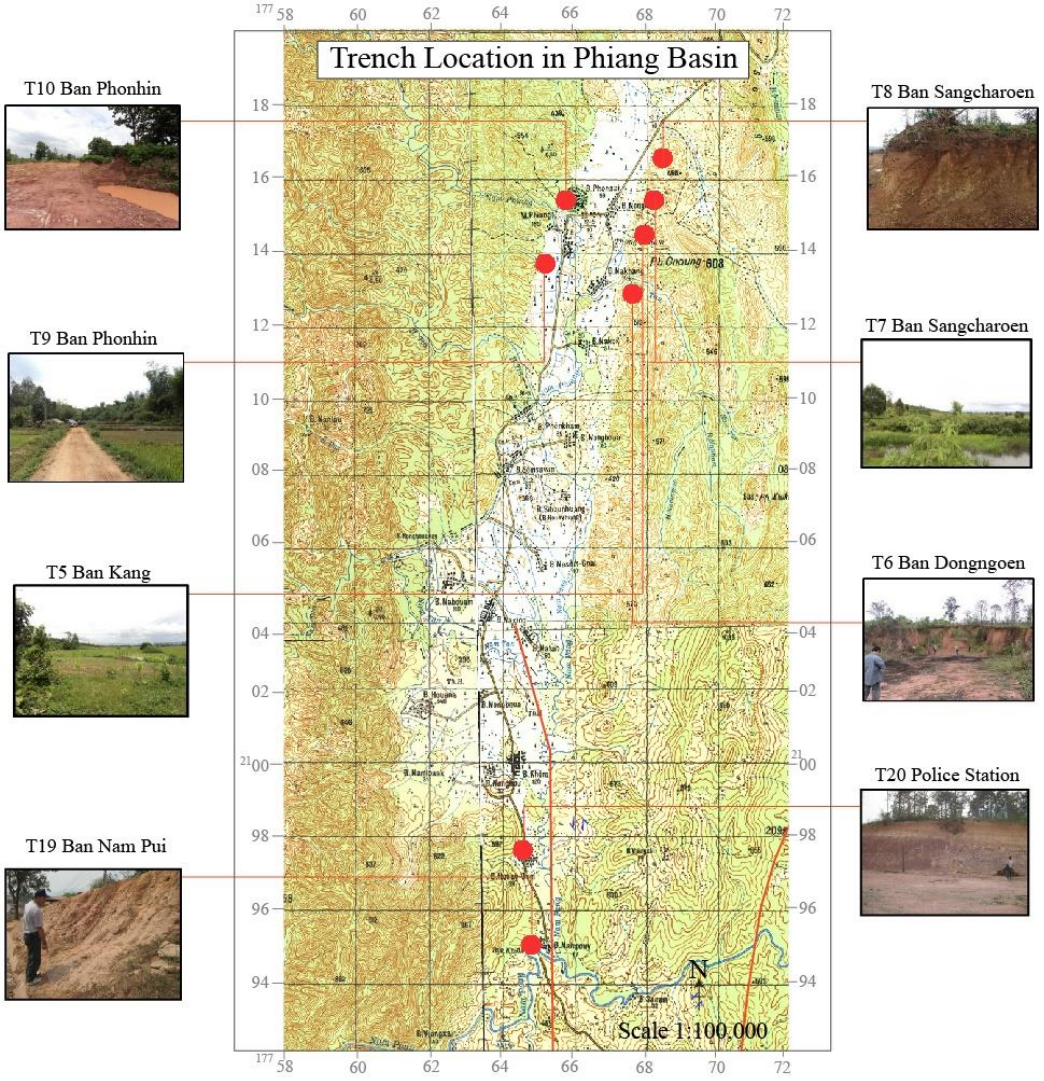

Figure 4.43 Trench/exposure locations at Phiang basin.

Table 4.2 OSL dating results of quartz-concentrate sediments for samples collected from Xaignabouli barge area, central Lao PDR.

Sample No.	U (ppm)	Th (ppm)	K (%)	W (%)	AD (Gy/ka)	ED (Gy)	Age (Yr)
NSW 1	5.52 ± 0.18	12.46 ± 1.02	1.55 ± 0.06	17.92	3.78 ± 0.76	142.85 ± 2.18	37,790 ± 870
NSW 2	1.71 ± 0.07	6.53 ± 0.39	0.78 ± 0.03	16.94	1.77 ± 0.14	142.85 ± 0.16	80,700 ± 170
NSW 3	2.11 ± 0.11	7.66 ± 0.7	0.91 ± 0.04	18.53	2.06 ± 0.29	102.24 ± 0.31	49,630 ± 210
NSW 4	1.54 ± 0.08	8.9 ± 0.55	0.8 ± 0.03	12.79	1.94 ± 0.26	192.2 ± 6.72	99,070 ± 6,660
NSW 5	1.55 ± 0.09	8.3 ± 0.57	0.81 ± 0.03	16.69	1.89 ± 0.25	105.25 ± 8.69	55,680 ± 4,840
NX 1	3.69 ± 0.11	9.59 ± 0.6	1.25 ± 0.05	24.27	2.83 ± 0.33	3.44 ± 2.98	1,210 ± 30
NX 2	1.96 ± 0.07	8 ± 0.44	0.75 ± 0.03	23.65	1.86 ± 0.18	9.69 ± 5.9	5,200 ± 300
NS 3-1	2.83 ± 0.08	11.14 ± 0.53	0.79 ± 0.03	19.64	2.32 ± 0.31	7.59 ± 10.19	3,270 ± 330
NS 3-2	2.25 ± 0.09	11.32 ± 0.64	0.97 ± 0.04	17.31	2.4 ± 0.38	7 ± 6.51	2,910 ± 180
NS 3-3	3.35 ± 0.18	14.69 ± 1.13	1.25 ± 0.06	18.03	3.14 ± 0.89	22.66 ± 3.38	7,210 ± 250
1	2.32 ± 0.07	7.95 ± 0.43	0.98 ± 0.03	19.16	2.19 ± 0.19	41.87 ± 0.79	19,110 ± 150
2	3.32 ± 0.12	12.38 ± 0.71	1.75 ± 0.05	17.86	3.48 ± 0.5	112.11 ± 1.1	32,210 ± 380

3	2.85 ± 0.1	11.76 ± 0.64	1.46 ± 0.05	21.26	3.02 ± 0.41	43.78 ± 0.78	14,490 ± 120
Sample No.	U (ppm)	Th (ppm)	K (%)	W (%)	AD (Gy/ka)	ED (Gy)	Age (Yr)
4	3.19 ± 0.14	11.31 ± 0.87	1.39 ± 0.05	16.73	3.04 ± 0.55	33.23 ± 0.29	10,930 ± 60
T4-S1	3.1 ± 0.12	13.12 ± 0.73	1.59 ± 0.05	28.24	3.22 ± 0.49	3.06 ± 6.32	950 ± 60
T4-S2	4.11 ± 0.19	18.27 ± 1.37	2.26 ± 0.09	31.18	4.38 ± 1.24	0.71 ± 8.67	160 ± 10
T4-S3	4.12 ± 0.11	24.74 ± 0.84	1.71 ± 0.04	13.15	4.53 ± 1.11	4.85 ± 5.45	1,070 ± 50
T4-S4	2.15 ± 0.15	6 ± 0.91	1.05 ± 0.06	22.58	2.07 ± 0.31	6.42 ± 5.92	3,100 ± 180
T4-N1	4.15 ± 0.18	21.74 ± 1.22	2.35 ± 0.07	34.07	4.65 ± 1.26	1.27 ± 5.38	270 ± 10
T4-N2	5.87 ± 0.16	32.52 ± 1.24	2.04 ± 0.06	36.95	5.32 ± 1.82	0.63 ± 9.65	110 ± 10
T4-N3	3.32 ± 0.12	18.17 ± 0.93	3.03 ± 0.1	10.76	5.27 ± 1.03	1.09 ± 9.23	200 ± 10
T4-F1	2.38 ± 0.09	3.99 ± 0.47	1.01 ± 0.05	29.72	1.92 ± 0.13	103.7 ± 1.27	54,010 ± 680

4.3.3 Fault Age Interpretation

Base on the chronological determination (i.e., OSL dating), the obtained dates reveal that in Xaignabouli area, clay gouge with rock fragment have a date varies from 3,100±180 to 1,070±50 yr. After that, the colluviums composed of sand and some gravels

were deposit in the age range 950±60 to 110±10 yr (Figure 4.45). As a result, we can estimate the date of faulting in the Xaignabouli barge area around 950-1,070 years ago. Fore fault gauge dating, the OSL date is 54,010±680 years. This extremely old age is according to the pressure or temperature of crushing sediment is not enough to reset the OSL signal of this fault gauge sample. Thus, the obtained fault gauge date show the geological meaningless.

For the trench no.T16, the OSL dating show the dates of and NS3-1 is 3,270±330 and NS3-2 is 2,910±180. It implies that the tectonic stress which effect sediment folding occurs around 2,910-3,270 year ago (Figure 4.48).

In Figure 4.50, there is a dike cut across the sediment. We, therefore, collected to sediment samples for OSL dating. The result confirm the date of dike cutting after 1,210 years. Because of no evidence of fault slip, the rate of fault slip cannot determine in this area. However from the OSL dating at Xaignabouli area indicate that the fault segment in the area still active with the last movement around 3,100±180 to 1,070±50 year ago.

4.3.4 Determination on slip rates

Only the estimated horizontal slip rate along the studied faults in the Xaignabouli area is reported in this study, since a vertical slip rate cannot be determined within the limit of uncertainty. This is due to the fact that observations of the vertical component of separation cannot be made presently.

The offset of stream courses range from 2.5 m (ground survey at T-16) in the Xaignabouli basin. If the maximum reliable age of faulting is ca. 3,000 years, the reliable slip rate can be estimated at ca. 0.8 mm/yr.

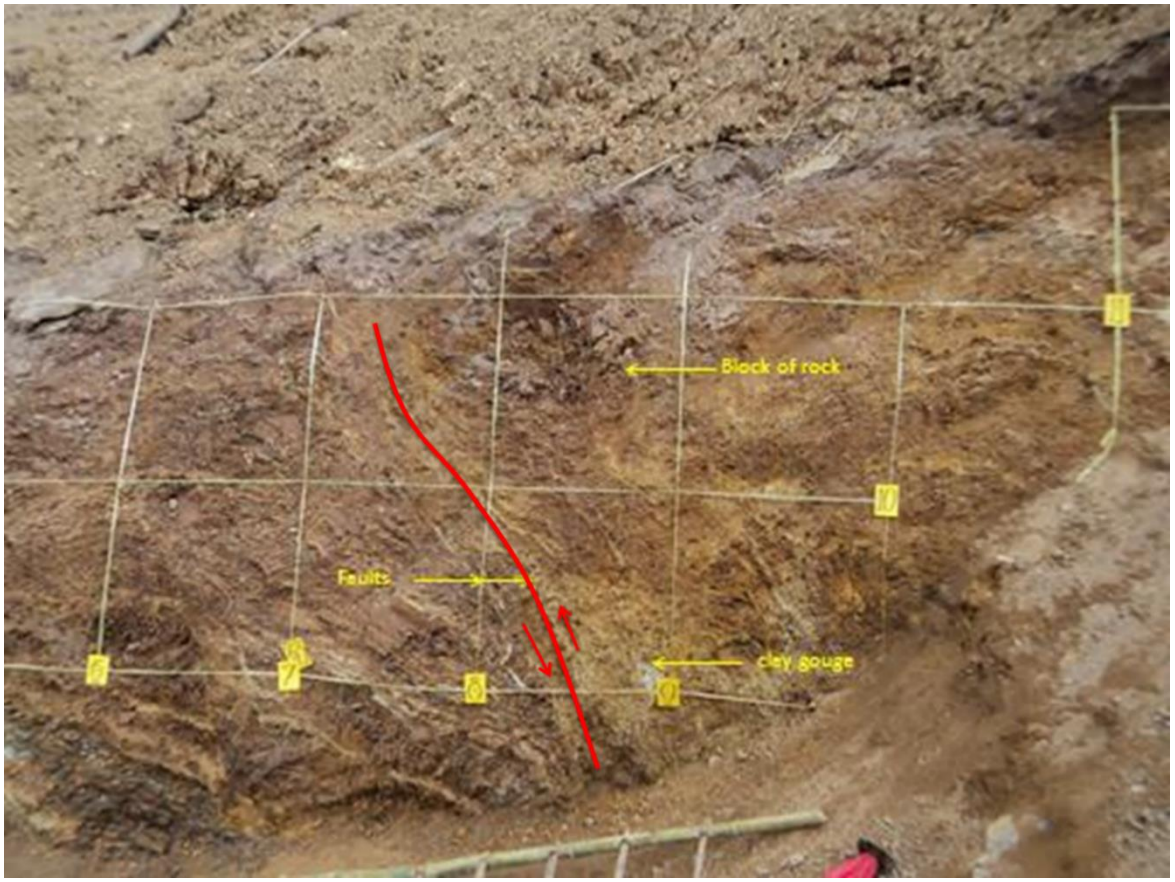

Figure 4.44 Southern wall of trench T4 , Xaignabouli, Lao PDR.

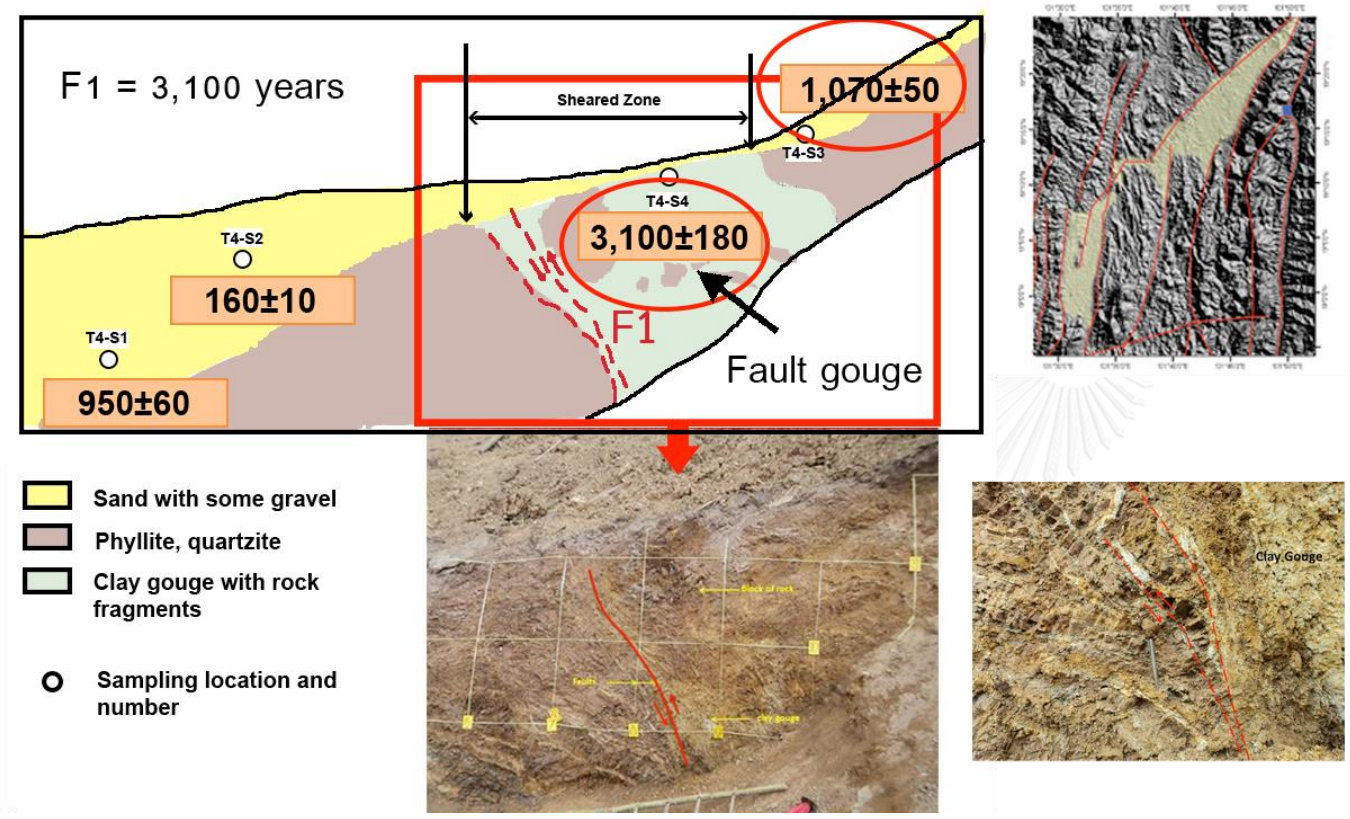

Figure 4.45 Trench log sketch and photograph of trench T4 southern wall, Xaignabouli, Lao PDR.

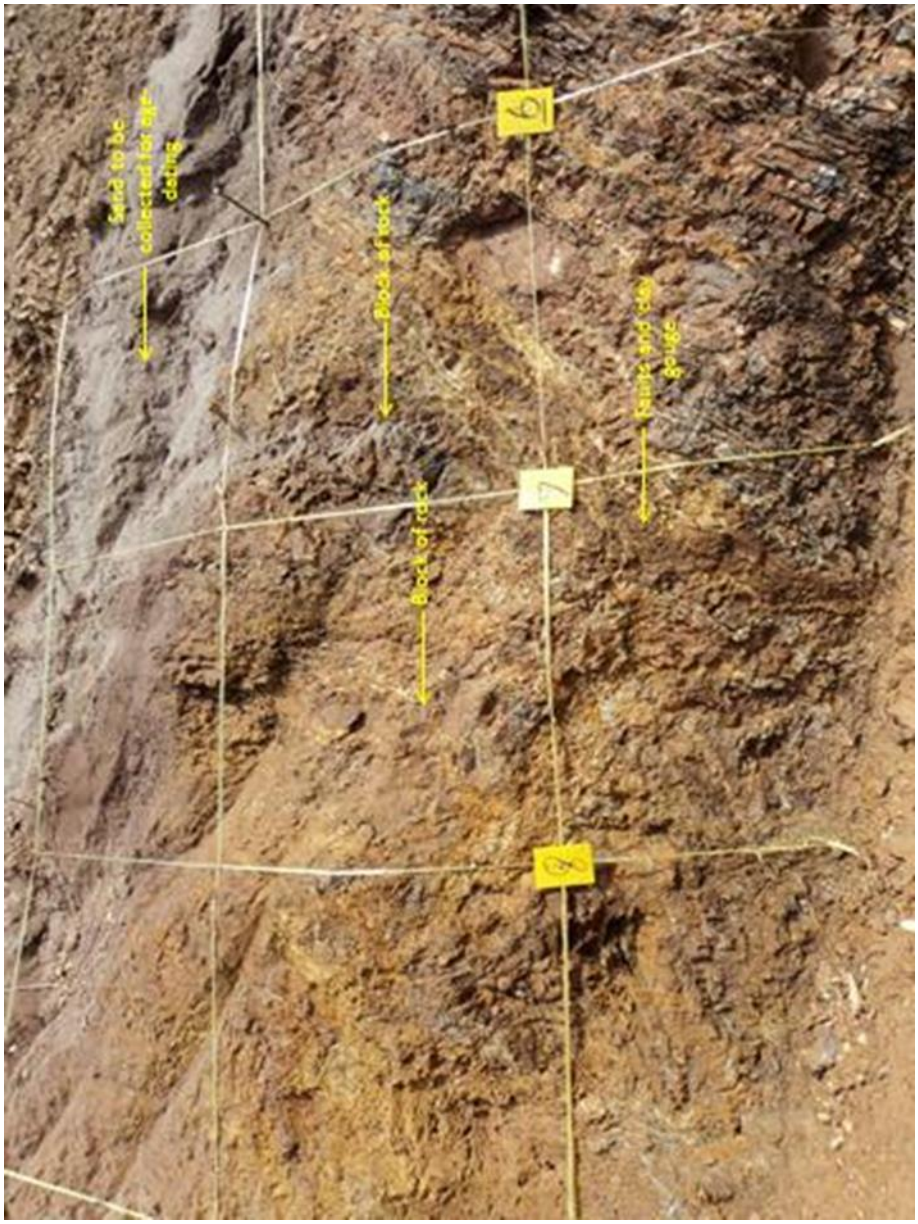

Figure 4.46 Northern wall of trench T4 , Xaignabouli, Lao PDR.

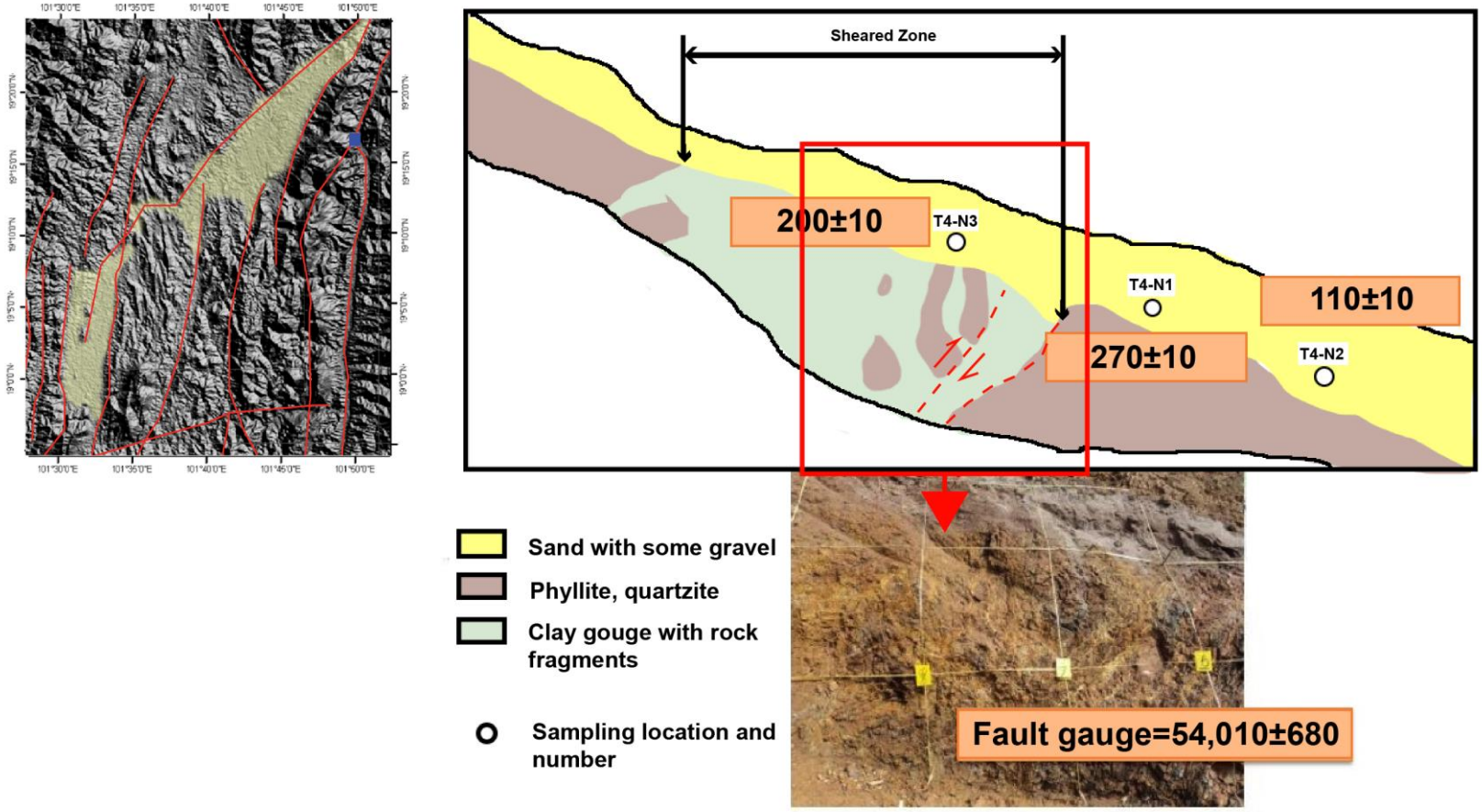

Figure 4.47 Trench log sketch and photograph of trench T4 northern wall, Xaignabouli, Lao PDR.

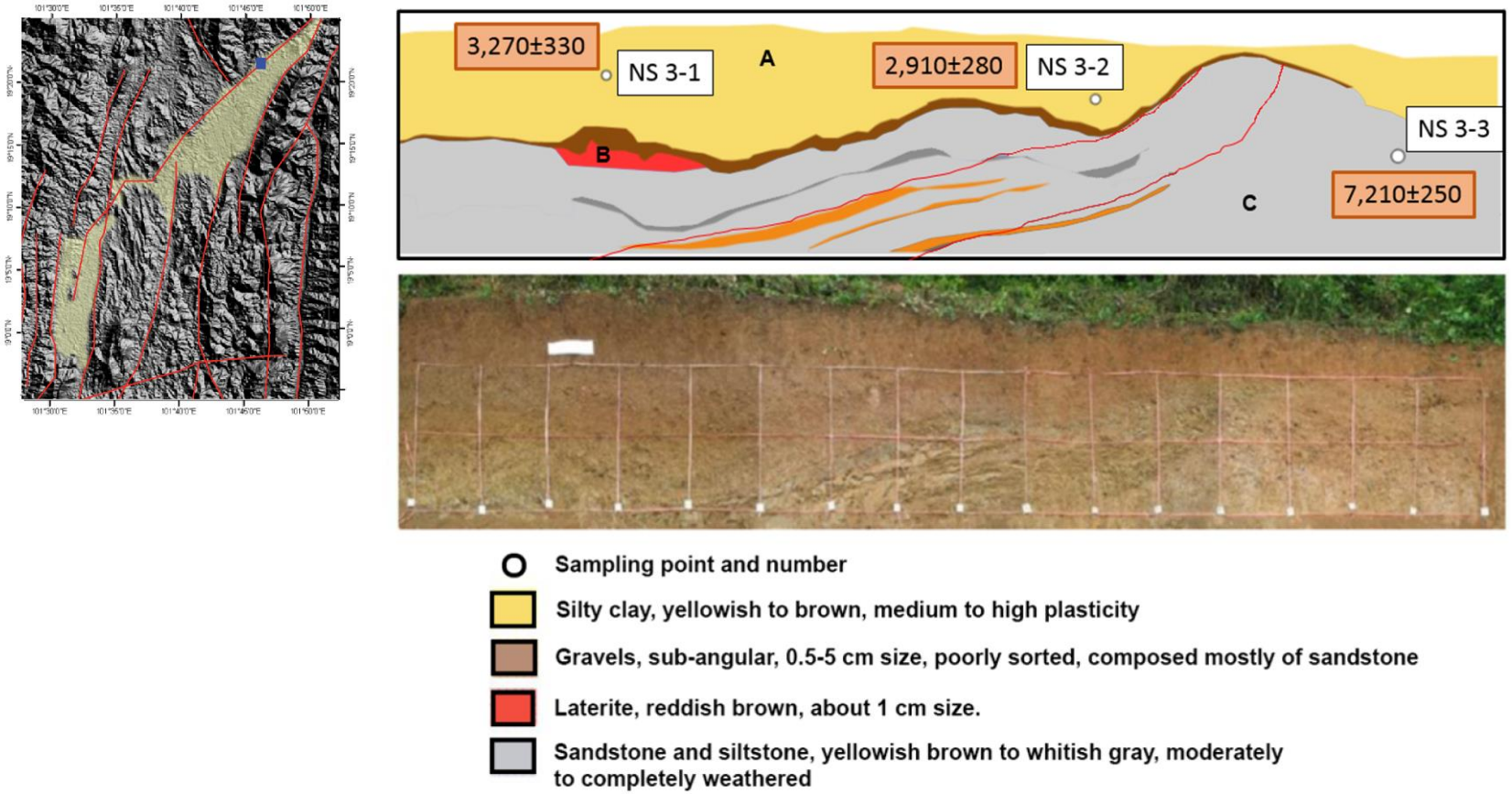

Figure 4.48 Trench log sketch map and photograph of trench no.T16 Ban Vangxoy, Xaignabouli, Lao PDR.

Figure 4.49 Trench no.T18, Ban Wang Kham, Xaignabouli district, Lao PDR.

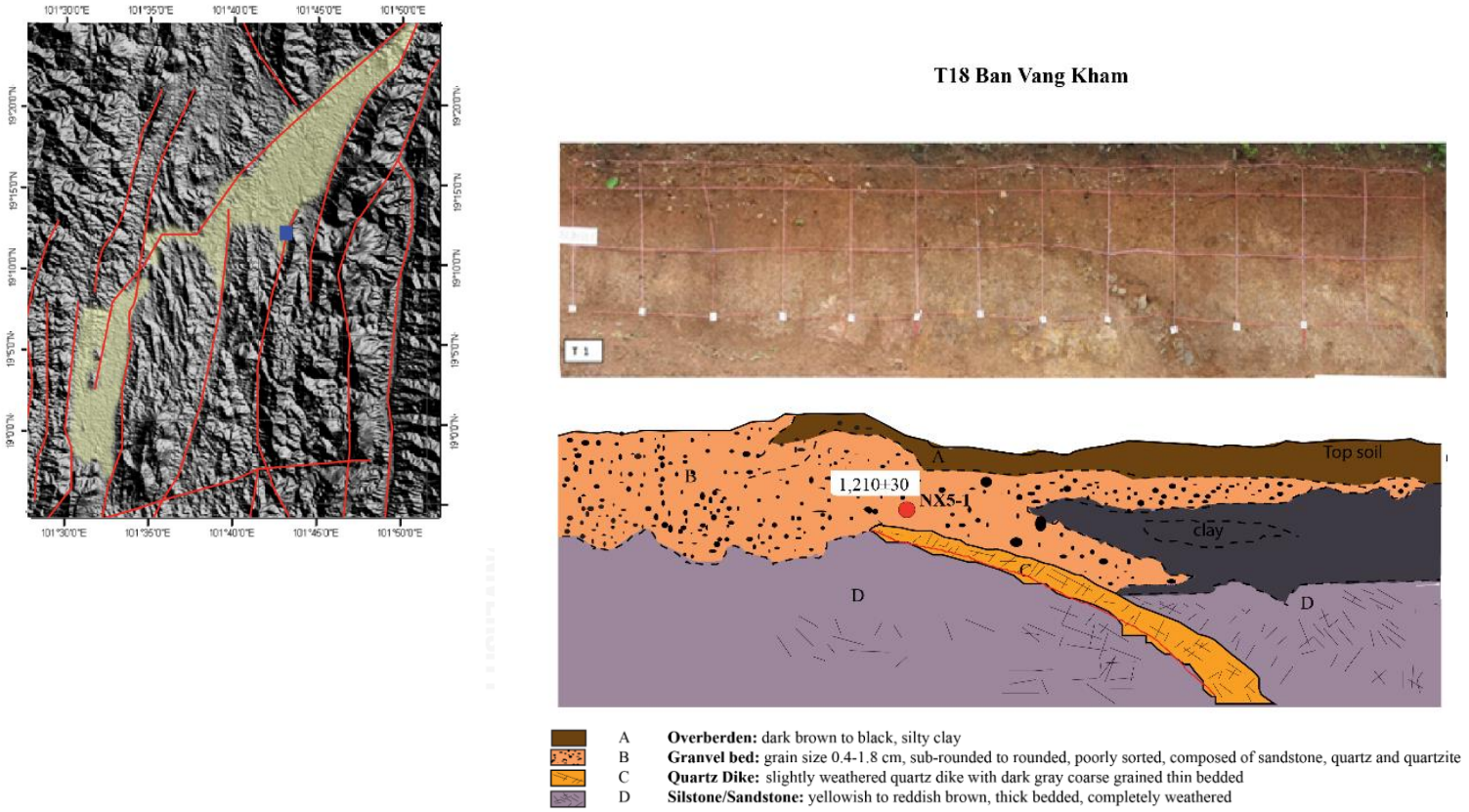

Figure 4.50 Trench log sketch map of trench no.T18, Ban Wang Kham, Xaignabouli district, Lao PDR.

4.4 Image processing

4.4.1 Results of using optical stratigraphy with trench wall images

By applying a series of image processing steps (Figure 4.51) we can autonomously determine colluvial wedges running along fault zones from trench wall images (Figure 4.52). The axes of sediment oriented in direction of wedge which we interpreted as a normal fault in exposure T11 Chinese market area.

We believe that combining the digital image processing with GPS locations and field data, will be useful in the mapping of colluvial wedges and support the process of determining seismic history and hazard of active faults. Some parameters vary depending on the digital resolution of the photo and physical distance from the trench wall. Many of the object selection parameters are experimentally determined for a certain distance and size of image. A method to calculate the parameters given a distance to the trench wall and image resolution would further improve the usefulness of the algorithm.

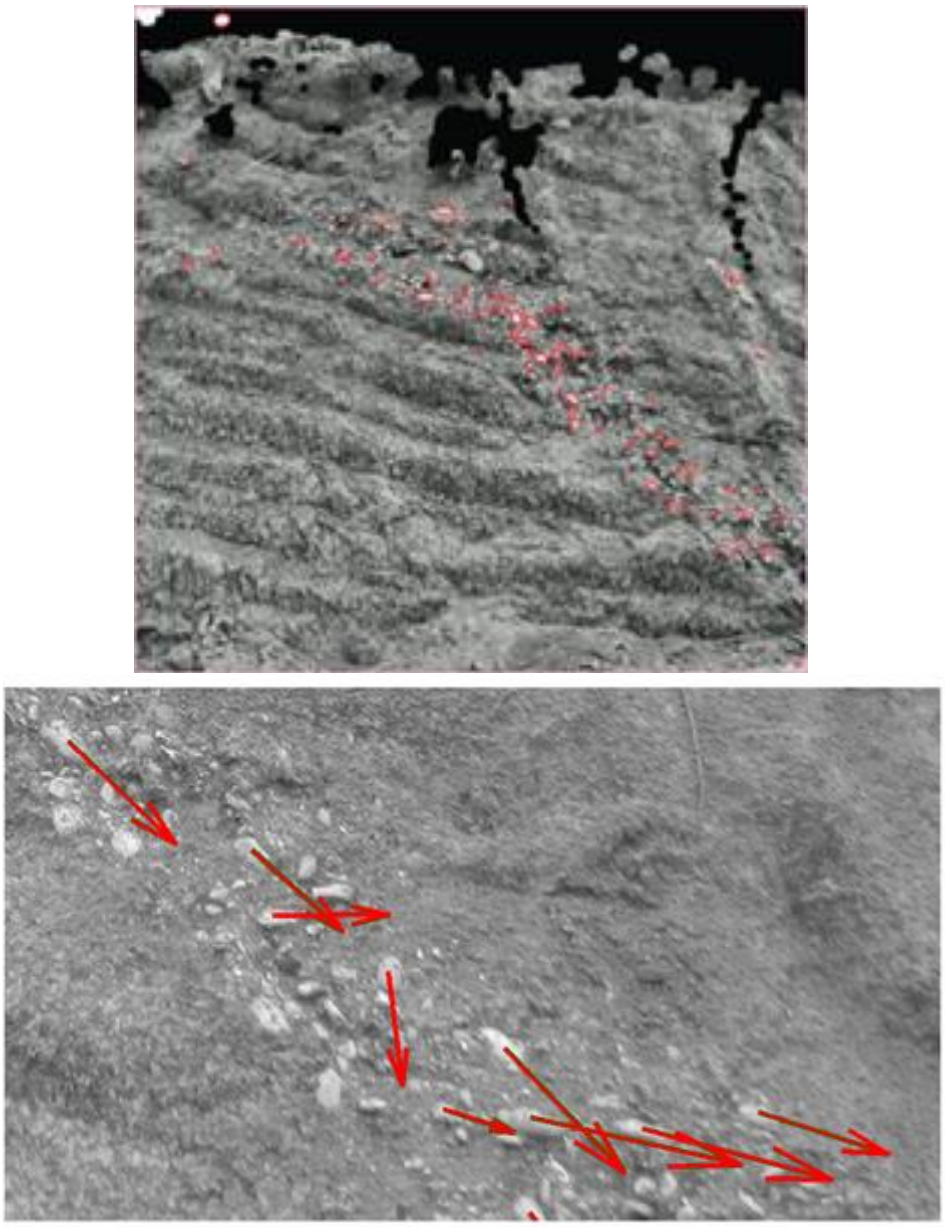

Figure 4.51 Step of determine the shape and properties of rocks via specific weighted averages known as image moments (upper) and axes give direction of rocks oriented in direction of wedge which we interpreted as a fault (lower) with trench wall images at T11.

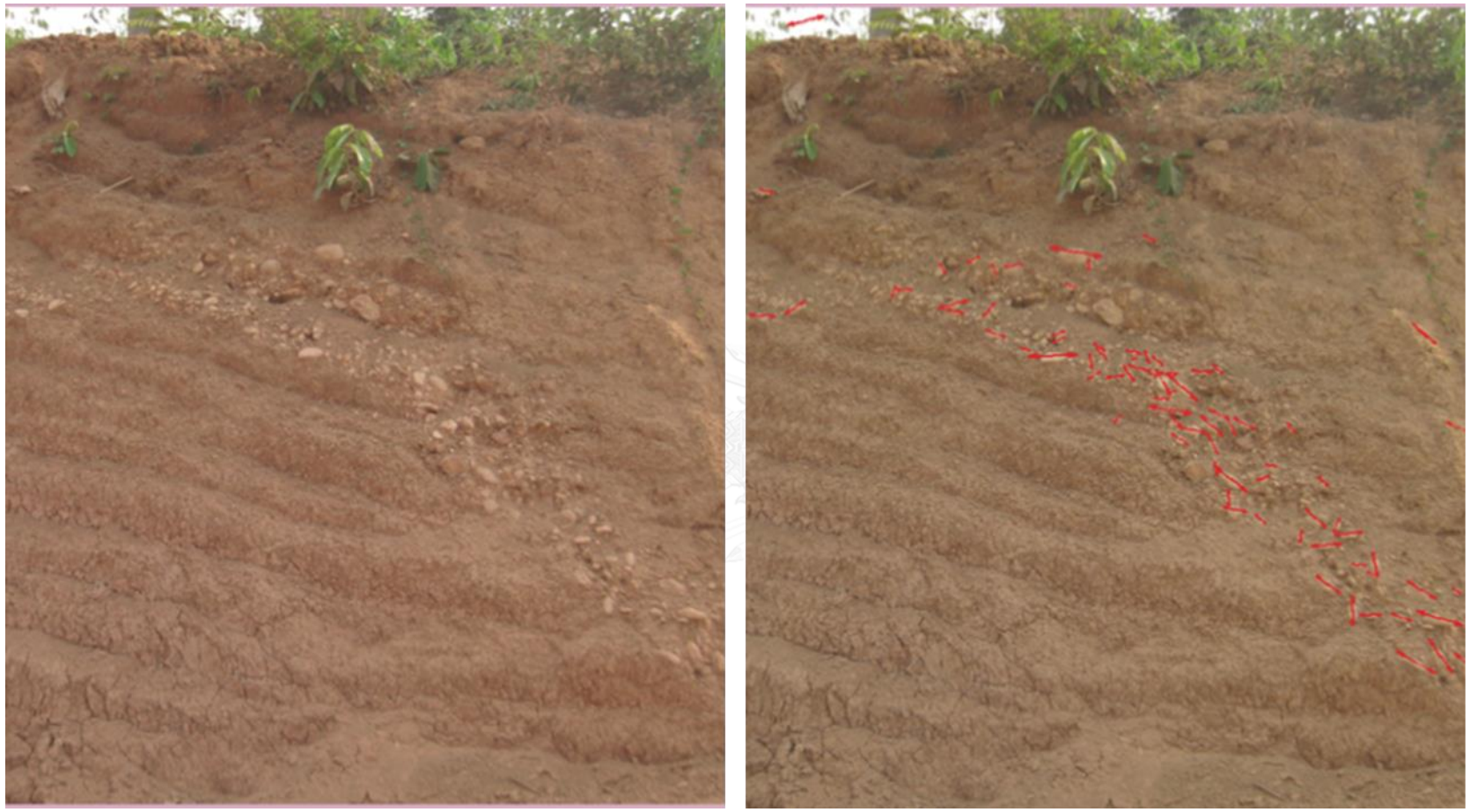

Figure 4.52 Results of using optical stratigraphy with trench wall images at T11, (left) original photo and (right) show axes give direction of rocks oriented in direction of wedge which we interpreted as a fault.

4.5 Focal mechanism

4.5.1 Inversion Results

Inversion Result show the fault type is sinistral strike-slip fault with normal fault, strike of fault plane is N30E and dip of fault plane is 31° in N60W showed in Figure 4.54.

The observed (red traces) and predicted waveforms (blue) are shown in Figure 4.55. The numbers to the left indicate the peak amplitude of each observed-predicted component, which are plotted to the same scale. Shown to the right of the predicted traces is its required time shift for maximum correlation with the corresponding observed trace, which is needed as the velocity model used in the predictions may be imperfect and as the synthetics are not computed at the exact same distance as the observed. A time shift greater than zero (shift to the right) suggests that the prediction is too fast and needs to be delayed to match the observed. A shift to the left indicates that the prediction is too slow.

Based on focal mechanism solutions of this thesis study, primary earthquake data used were provided by Thai Meteorological Department (TMD) and (IRIS) from seismic station across the world (Figure 4.53). As a result, focal mechanism diagrams from this study is shown in Figure 4.54.

According to the result of the M5.4 February 23, 2011 event, which primary data collected from 34 seismographs, it can be interpreted that seismic fault should displaces by sinistral strike-slip movement with small normal component.

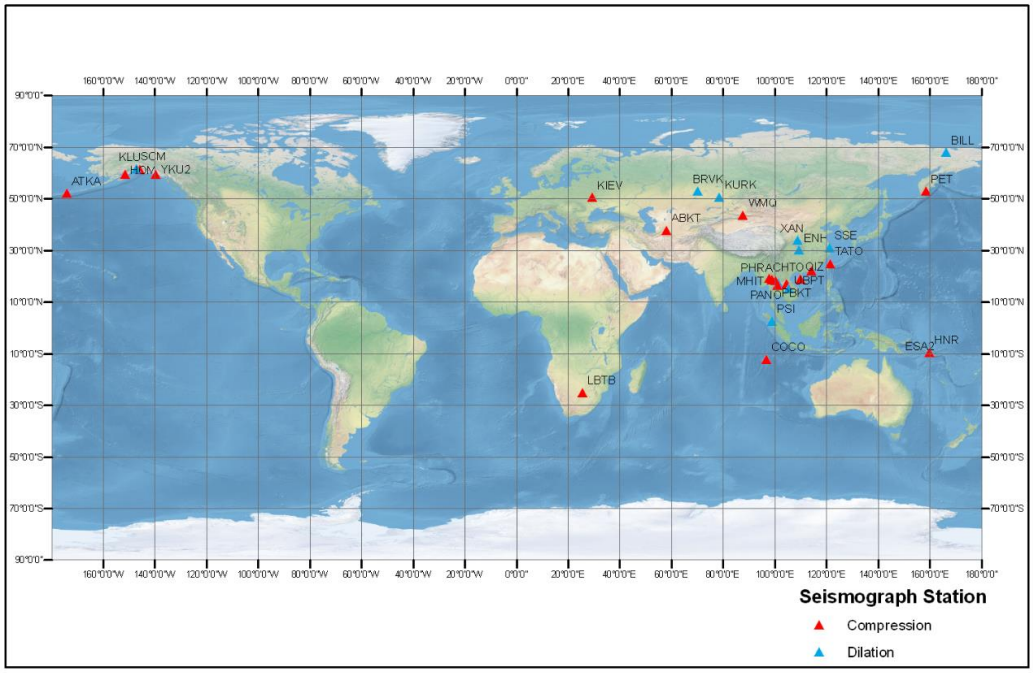

Figure 4.53 Location of 34 broadband stations around the world used for waveform inversion and location of the earthquake on 2011-02-23 @ LAO (18.82,101.74) with M5.4

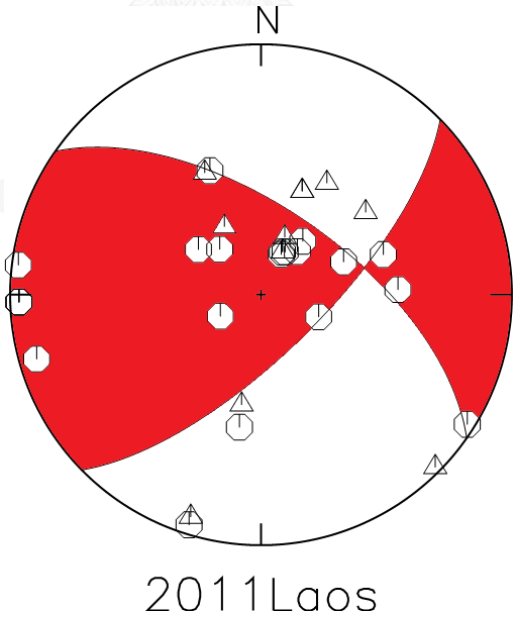

Figure 4.54 Focal mechanism solution diagram of M5.4 event on February 23, 2011 event using Focmec program for construction.

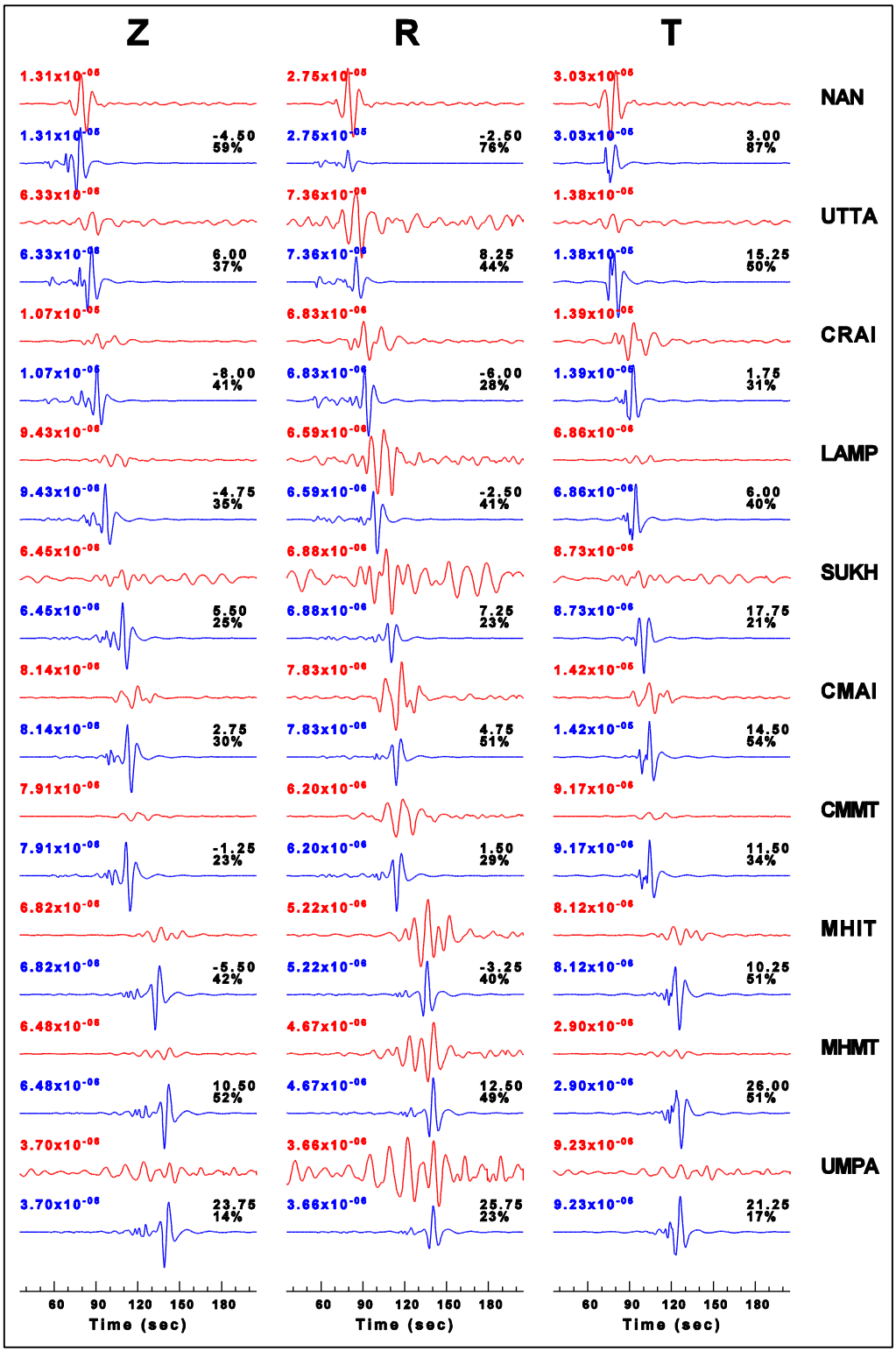

Figure 4.55 Waveform comparison Red – Data Blue – Calculated data (Z-vertical, R-radial, T-transverse)

CHAPTER V
DISCUSSION

5.1 Development of basins

5.1.1 Xaignabouli basin

As shown in the satellite image interpretation maps (Figures 3.6, 3.7, and 3.9) together with supports of our field evidence, it is likely that the Xaignabouli basin is a fault – controlled Cenozoic basin which may have formed by the development of two major sets of faults at the western and eastern rims of the basin. The faults which are mainly oblique strike slip fault and run in the NE –SW in the northern part and deviate to NNE-SSW in the southern portion. Several lines of morphotectonic evidence including many sets of offset streams and linear valleys reveal that the faults are still active till present. However, the faults in the west are less developed than those of the east as seen from the morphotectonic features. These basin-bound faults are thought herein to be the subsidiary branch of the NNE-SSW – trending Dien Bien Phu Fault.

5.1.2 Phiang basin

Faults in this basin are similar to those of the Xaignabouli Basin in that they are the oblique strike-slip fault and become the boundary faults. The faults are characterized by linear valleys, offset streams, and scarplets (see Figure 3.10). The faults are in the NE-SW direction and some sets are located in the basin. The basin is about 20 km long and its rims are controlled by two faults which merge into one fault to the northern end. It seems likely that the fault line in the east is more prominent than that in the west. We consider that the faults in the eastern side are more subsided or less uplifted than those in the west, suggesting that the vertical movement component become more prominent than that of the horizontal component.

Both of Xaignabouli and Phiang basins are pull apart basin which created by strike-slip fault (Figure 5.1).

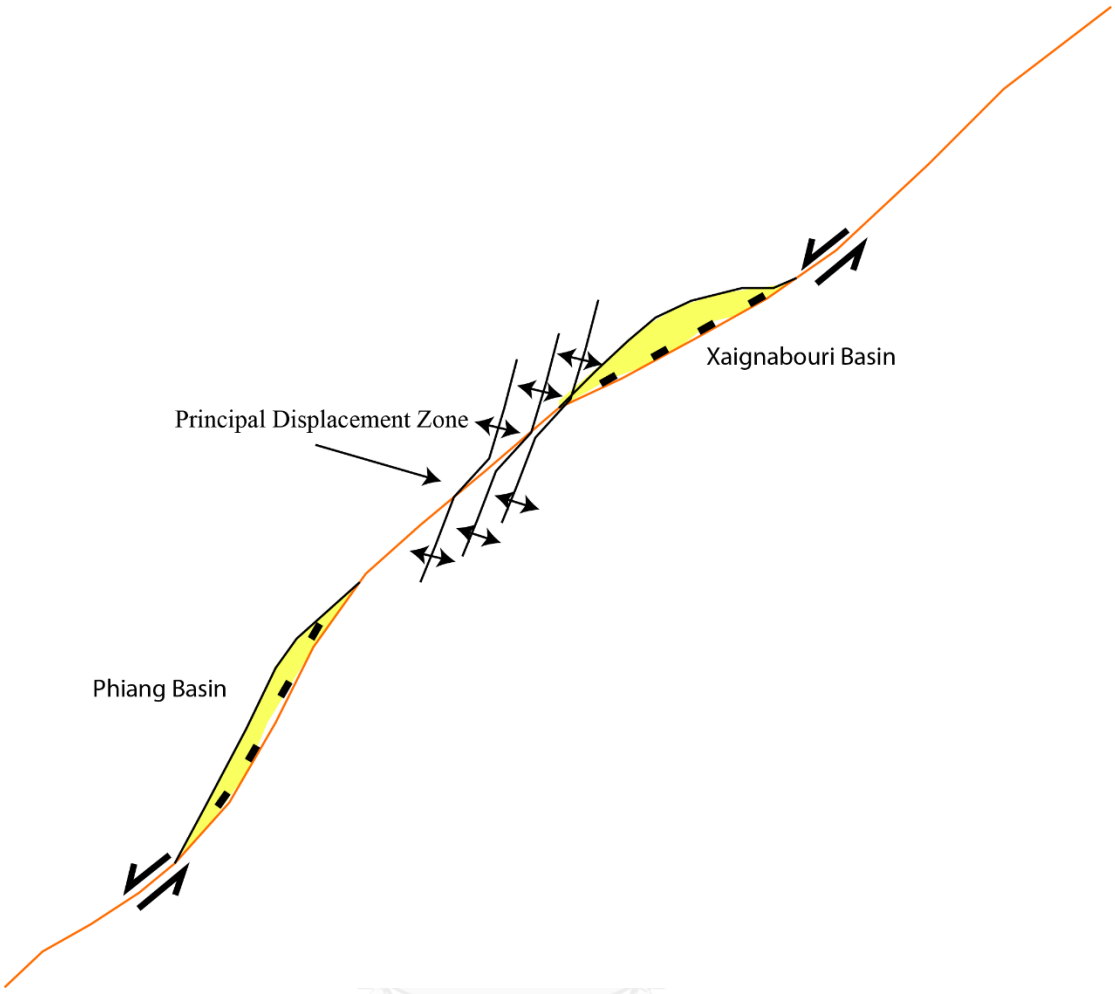

Figure 5.1 A model for development of the Xaignabouli and Phiang basins and associated structures by strike-slip tectonics (modified after Christie-Blick & Biddle, 1985; Sylvester, 1988)

5.2 Determination on slip rates

Estimation has been done for the slip rate along the studied faults in Xaignabouli area. However, a vertical slip rate cannot be made within the limit of uncertainty. This is because the vertical component of separation cannot be observed at present.

In this research only the horizontal slip rate is reported. Based on the ground truth field survey together with remote sensing interpretation results, the offset of stream courses range from 2.5 m (from ground survey at T-16) in the Xaignabouli basin. The vertical slip rate is calculated from trench T16 and T18 with a maximum reliable age of

faulting of ca. 3,000 and 2,500 yrs, respectively, giving an estimated vertical slip rate of ca. 0.5 and 0.2 mm/yr respectively.

5.3 Fault age determination

Data on luminescence age determination were taken from two alluvial samples (T4-S1 and T4-S2) and two fault gouge samples collected from the southern wall of trench no T-4 at the Xaignabouli basin. The result shows that the dates of young sediments vary approximately from 160 to 950 yrs whereas those of the fault gouge samples show two age data - one (no T4-S3) of about 1,070 yrs and the other (no T4-S4) of about 3,100 yrs. It is considered that two faulting events may have been discovered at the study area. The older faulting event occurred at ca. 3,000 yrs ago and the younger event took place at ca. 1,000 years ago.

The other age dating information is obtained from the northern wall of trench no. 4. Three samples of alluvial sedimentary samples (no. T4-N1, T4-N2 and T4-N3) and one fault gouge sample (no T4-F1) are dated. The dating result reveals that the ages of sediments vary from 110 to 270 years whereas the age of fault gouge is about ca. 54,000 yrs. The sediment ages seem to be very reliable whereas that of the gauge material seems to be obviously old. However, if this date is correct, then this date is supposed to represent the oldest movement of fault. Therefore it may be concluded that three faulting events have been encountered at the barge site.

Two samples of fine – grained alluvial sediments (no. NS 3-1) and one sample from very weathered sandstone (no. NS 3-2) were collected from the trench no T-16 at Ban Vangxoy in the Xaignabouli area. The ages of sediments range from ca. 2,900 to 3,200 years. Because the laterite layer which is intervened between colluvium and alluvium become folded, therefore the age of compressive stress associated with faulting event may have been more than 3,200 yrs. So it is consider that the faulting event may have occurred during ca. 4,000 yrs.

Two samples were collected from trench no T-18 at Ban Naxam. One sample (no NX 5-1) was taken from clayey gravel layer and the other (NX 5-2) from completely weathered siltstone. Between these two layers there exists a clastic or sand dike (paleo-

sand boil or liquidfaction) which cut across the older weathered sandstone but did not cut the overlying clayey gravel layer. The ages obtained from these two sedimentary layers are 5,200 yrs for sandstone and 1,200 yrs for clayey layer. It is interpreted that if the fault occurred associated with the sand dike or clastic dike, then the two obtained dates represent the age of faulting event. The best estimation of this faulting event would be ca. 2,000 years.

5.4 Extension of Xaignabouli fault

5.4.1 Northward extension

From detailed remote sensing investigation including those fault lines proposed by Pailoplee et al. (2009) and some lineaments from P. Charusiri et al. (2002), it is quite likely that the Dien Bien Phu Fault (DBFF) Zone, which commences from northwestern Vietnam (Witold Zuchiewicz et al., 2004) and extends to northern Lao PDR, is the nearest earthquake source. The DBFF passes through the location of the study area that may pose the earthquake hazard to the site (Figure 5.2). Thus, clarification is required for the DBFF zone.

5.4.2 Southward extension

New geological, geochemical and geochronological data from P. Charusiri et al. (2002), has resulted in new suture zones (or tectonic lines) being proposed in Thailand and Lao PDR (Figure 2.17). Nan suture zones represent the tectonic lines that border the Nakhon Thai block, which continues to the northern part through the study area in Xaignabouli. We assume that Xaignabouli fault zone in the study area merge with the Nan suture zones because have same direction of lineaments.

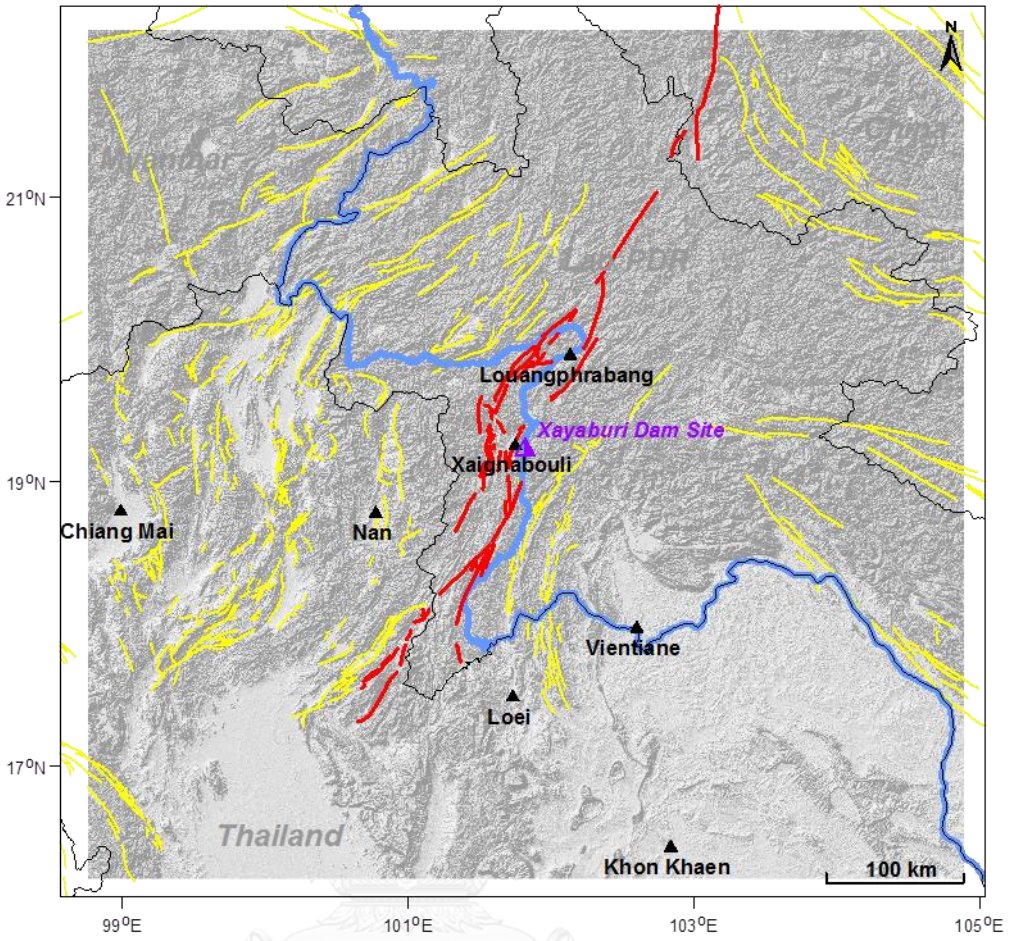

Figure 5.2 Possible active fault zones in the Xayaburi study area proposed by Pailoplee et al. (2009).

CHAPTER VI
CONCLUSION

Based on the result of remote-sensing interpretation (Landsat 7 TM, SRTM, ASTER, IKONOS and aerial photograph) integrated with ground-truth investigation, detailed topographic survey as well as those of OSL-dating of fault related sediments, and netotectonics of Xaignabouli Fault Zone in Xaignabouli and Phiand basins, western Lao PDR. The conclusions can be drawn as the followings;

1. Orientation of Fault Zone is mainly NNE-SSW with some N-S directions.
2. Morphotectonic landforms along the Xaignabouli Fault Zone in Xaignabouli basin and Phiang basin are offset streams, triangular facets, offset spur, linear valleys and fault scarps.
3. Based on trench investigation and remote sensing interpretation, the sense of movement of the Xaignabouli Fault Zone is identified as a sinistral strike-slip with normal movement and being branches of the Dien Bien Phu Fault. They are proved to be active till present.
4. Total length of the Xaignabouli Fault Zone is 218 km (with 66 geometrical fault segments), and the fault segments have a length ranging from 4-44 km.
5. Xaignabouli Fault Zone was triggered by the earthquake with a maximum paleoearthquake magnitude of ML 5.4.
6. The last movement of the Xaignabouli Fault Zone occurred 3,000 – 1,000 years ago, Recurrence interval is ~ 1,000 year, Offset stream in eastern part of Xaignabouli basin and fault age results imply the rate of horizontal fault slip being around 0.8 mm/yr.

REFERENCES

Allen, C. R., Gillespie, A. R., Yuan, H., Sieh, K. E., Buchun, Z., & Chengnan, Z. (1984). Red River and associated faults, Yunnan Province, China: Quaternary geology, slip rates, and seismic hazard. *Geological Society of America Bulletin, 95*(6), 686-700. doi: 10.1130/0016-7606(1984)95<686:rraafy>2.0.co;2

Bunopas, S. (1981). *Paleogeographic history of western Thailand and adjacent parts of South-East Asia : a plate tectonics interpretation.* (submitted for the degree of Doctor of Philosophy), Victoria University of Wellington, New Zealand. Available from http://worldcat.org

Burchfiel, B. C. (2004). New technology: new geological challenges. *GSA Today,* 4-10.

Carter, A., & Clift, P. D. (2008). Was the Indosinian orogeny a Triassic mountain building or a thermotectonic reactivation event? *Comptes Rendus Geoscience, 340*(2–3), 83-93. doi: http://dx.doi.org/10.1016/j.crte.2007.08.011

Carter, A., Roques, D., Bristow, C., & Kinny, P. (2001). Understanding Mesozoic accretion in Southeast Asia: Significance of Triassic thermotectonism (Indosinian orogeny) in Vietnam. *Geology, 29*(3), 211-214. doi: 10.1130/0091-7613(2001)029<0211:umaisa>2.0.co;2

Chapman, M., Powell, C., Vlahovic, G., & Sibol, M. (1997). A statistical analysis of earthquake focal mechanisms and epicenter locations in the eastern Tennessee seismic zone. *Bulletin of the Seismological Society of America, 87*(6), 1522-1536.

Charusiri, P., Buenkhuntod, P., Won-In, K., Thayakupt, M., & Niampan, J. (2003). Characteristics of The Chantaburi Thermal Spring, Eastern Thailand. *Journal of Scientific Research Chulalongkorn University, 28*, 71-95.

Charusiri, P., Kosuwan, K., Daorerk, V., Vajbunthoeng, B., & Khutaranon, S. (2000). Final Report on Earthquake in Thailand and Southeast Asia (pp. 171): Thailand Research Fund (TRF).

Charusiri, P., V., D., Archibald, D., Hisada, K., & Ampaiwan, T. (2002). Geotectonic evolution of Thailand: a new synthesis. *Journal of the Geological Society of Thailand*(1), 1-20.

Christie-Blick, N., & Biddle, K. T. (1985). Deformation and basin formation along strike-slip faults. *Strike-Slip Deformation, Basin Formation, and Sedimentation, 37*, 1-34.

Clark, M. K., Schoenbohm, L. M., Royden, L. H., Whipple, K. X., Burchfiel, B. C., Zhang, X., . . . Chen, L. (2004). Surface uplift, tectonics, and erosion of eastern Tibet from large-scale drainage patterns. *Tectonics, 23*, 20. doi: 10.1029/2002TC001402

Cung, T. C., Dorobek, S., Richter, C., Flower, M., Kikawa, E., Nguyen, Y. T., & McCabe, R. (1998). Paleomagnetism of Late Neogene Basalts in Vietnam and Thailand: Implications for the Post-Miocene Tectonic History of Indochina. In M. Flower (Ed.), *Mantle Dynamics and Plate Interactions in East Asia* (pp. 289-299): American Geophysical Union.

Ducrocq, S., Buffetaut, E., Buffetaut-Tong, H., Jaeger, J.-J., Yongkanjanasoontorn, Y., & Suteethorn, V. (1992). First fossil flying lemur: a dermopteran from the late Eocene of Thailand. *Palaeontology, 35*(Part 2), 373-380.

Duong, C., Yun, H.-S., & Cho, J.-M. (2002). GPS measurements of horizontal deformation across the Lai Chau-Dien Bien (Dien Bien Phu) fault. *Northwest of Vietnam, 2004*, 523-528.

Dy, N., Tu, D., Thuan, D., & Tan, M. (1999). Relationship between Quaternary sedimentation and landslide-mudflow formation in NW Vietnam. *Journal of Geology, Series B, 13*(14), 256-261.

Fenton, C. H., Charusiri, P., & Wood, S. C. (2003). Recent paleoseismic investigations in Northern and Western Thailand. *Annals of Geophysics*.

Flusser, J. (2006). *Moment invariants in image analysis.* Paper presented at the proceedings of world academy of science, engineering and technology.

Fontaine, H., & Workman, D. R. (1997). Encyclopedia of European and Asian regional geology. In E. M. Moores, Fairbridge, Rh.W. (Ed.), *Encyclopedia of Earth Sciences Series* (pp. 774–782). London: Chapman & Hall.

Hoang, N., Flower, M. F., & Carlson, R. W. (1996). Major, trace element, and isotopic compositions of Vietnamese basalts: Interaction of hydrous EM1-rich asthenosphere with thinned Eurasian lithosphere. *Geochimica et Cosmochimica Acta, 60*(22), 4329-4351.

Hùng, N. V., & Vinh, H. Q. (2001). Moving characteristics of the Lai Châu-Điện Biên fault zone during Cenozoic. *Journal of Geology, Series B, 17*(18), 65-77.

Hutchinson, C. S. (1975). Ophiolite in Southeast Asia. *Geological Society of America Bulletin, 86*(6), 797-806. doi: 10.1130/0016-7606(1975)86<797:oisa>2.0.co;2

Hutchison, C. S. (1989). Geological evolution of South-east Asia (pp. 368): Clarendon Press.

Kiem, D., Quy, H., Tuyet, D., & Van, T. (1999). Some tectonic-structural characteristics of NW Vietnam. *Journal of Geology, Series B, 13*(14), 96-106.

Lee, J.-C., Angelier, J., Chu, H.-T., Yu, S.-B., & Hu, J.-C. (1998). Plate-boundary strain partitioning along the sinistral collision suture of the Philippine and Eurasian plates: Analysis of geodetic data geological observation in southeastern Taiwan. *Tectonics, 17*(6), 859-871.

Leloup, P. H., Lacassin, R., Tapponnier, P., Schärer, U., Zhong, D., Liu, X., . . . Trinh, P. T. (1995). The Ailao Shan-Red River shear zone (Yunnan, China), Tertiary transform boundary of Indochina. *Tectonophysics, 251*(1–4), 3-84. doi: http://dx.doi.org/10.1016/0040-1951(95)00070-4

Lepvrier, C., Maluski, H., Van Tich, V., Leyreloup, A., Truong Thi, P., & Van Vuong, N. (2004). The Early Triassic Indosinian orogeny in Vietnam (Truong Son Belt and Kontum Massif); implications for the geodynamic evolution of Indochina. *Tectonophysics, 393*(1–4), 87-118. doi: http://dx.doi.org/10.1016/j.tecto.2004.07.030

Lepvrier, C., Maluski, H., Van Vuong, N., Roques, D., Axente, V., & Rangin, C. (1997). Indosinian NW-trending shear zones within the Truong Son belt (Vietnam) 40Ar□39Ar Triassic ages and Cretaceous to Cenozoic overprints. *Tectonophysics, 283*(1–4), 105-127. doi: http://dx.doi.org/10.1016/S0040-1951(97)00151-0

Lin, T.-H., Lo, C.-H., Chung, S.-L., Wang, P.-L., Yeh, M.-W., Lee, T.-Y., . . . Anh, T. T. (2009). Jurassic Dextral Movement along the Dien Bien Phu Fault, NW Vietnam: Constraints from 40Ar/39ArAr40/Ar39 Geochronology. *The Journal of Geology, 117*(2), 192-199.

Lorenzetti, E., Brennan, P., & Hook, S. (1994). Structural styles in rift basins: interpretation methodology and examples from Southeast Asia. *AAPG Bulletin (American Association of Petroleum Geologists);(United States), 78*(CONF-940803--).

McCaffrey, R. (1996). Estimates of modern arc-parallel strain rates in fore arcs. *Geology, 24*(1), 27-30.

McCalpin, J. (1996). *Paleoseismology*: Academic Press.

Michel, G. W., Yu, Y. Q., Zhu, S. Y., Reigber, C., Becker, M., Reinhart, E., . . . Matheussen, S. (2001). Crustal motion and block behaviour in SE-Asia from GPS measurements. *Earth and Planetary Science Letters, 187*(3–4), 239-244. doi: http://dx.doi.org/10.1016/S0012-821X(01)00298-9

Molnar, P., & Qidong, D. (1984). Faulting associated with large earthquakes and the average rate of deformation in central and eastern Asia. *Journal of Geophysical Research: Solid Earth, 89*(B7), 6203-6227. doi: 10.1029/JB089iB07p06203

Morley, C. (2007). Variations in late Cenozoic–Recent strike-slip and oblique-extensional geometries, within Indochina: The influence of pre-existing fabrics. *Journal of Structural Geology, 29*(1), 36-58.

My, B. P., Ky, P. V., Hoanh, N. V., Tuyet, T. D., & My, B. P. (Cartographer). (1978). Geological map of the Socialist Republic of Vietnam.

Nutalaya, P., Sodsri, S., & Arnold, E. P. (1985). Series on Seismology - Volume II - Thailand. In E. P. Arnold (Ed.), *Southeast Asia Association of Seismology and Earthquake Engineering* (pp. 403). Thailand.

O'Leary, J., & Hill, G. (1989). *Tertiary basin development in the southern central plains, Thailand.* Paper presented at the Proceeding of the International Conference on Geology and Mineral Resources of Thailand, Bangkok.

Packham, G. H. (1993). Plate tectonics and the development of sedimentary basins of the dextral regime in western Southeast Asia. *Journal of Southeast Asian Earth Sciences, 8*(1), 497-511.

Pailoplee, S., Channarong, P., & Chutakositkanon, V. (2013). Earthquake Activities in the Thailand-Laos-Myanmar Border Region: A Statistical Approach. *Terr. Atmos. Ocean. Sci., 24*(4), 721-730. doi: 10.3319/TAO.2013.04.26.01(T)

Pailoplee, S., Sugiyama, Y., & Charusiri, P. (2009). Deterministic and probabilistic seismic hazard analyses in Thailand and adjacent areas using active fault data. *Earth, Planets and Space, 61*(12), 1313-1325. doi: 10.1186/BF03352984

Pécskay, Z., Balogh, K., & Tóth, E. (2002). Radiometric age determinations of magmatic rocks from Vietnam. *Institute of Nuclear Research, Hungarian Academy of Sciences, Debrecen, 9*.

Peltzer, G., & Tapponnier, P. (1988). Formation and evolution of strike-slip faults, rifts, and basins during the India-Asia Collision: An experimental approach. *Journal of Geophysical Research: Solid Earth, 93*(B12), 15085-15117. doi: 10.1029/JB093iB12p15085

Polachan, S., Pradidtan, S., Tongtaow, C., Janmaha, S., Intrawijitr, K., & Sangsuwan, C. (1991). Development of Cenozoic basins in Thailand. *Marine and Petroleum Geology, 8*, 84-97.

Snoke, J., Munsey, J., Teague, A. G., & Bollinger, G. (1984). A program for focal mechanism determination by combined use of polarity and SV-P amplitude ratio data. *Earthquake notes, 55*(3), 15.

Son, L. (2000). Focal mechanism of Ta Khoa, Lai Chau and Muong Luan earthquakes in North-West of Vietnam. *Journal of Earth Science (Hanoi), 22*, 355-360.

Srisuwon, P. (2002). *Structural and sedimentological evolution of the Phare Basin, Northern Thailand.* Royal Holloway, University of London.

Stokes, R. B., Lovatt Smith, P. F., & Soumphonphakdy, K. (1996). Timing of the Shan-Thai-Indochina collision: new evidence from the Pak Lay Foldbelt of the Lao PDR. *Geological Society, London, Special Publications, 106*(1), 225-232. doi: 10.1144/gsl.sp.1996.106.01.14

Sylvester, A. G. (1988). Strike-slip faults. *Geological Society of America Bulletin, 100*(11), 1666-1703.

Takashima, Isao, & Watanabe, K. (1994). Thermoluminescence age determination of lava flows/domes and collapsed materials at Unzen volcano, SW Japan. *Bull. Volcanol. Soc. Japan, 39*(1), 1-12.

Tapponnier, P., Peltzer, G., & Armijo, R. (1986). On the mechanics of the collision between India and Asia. *Geological Society, London, Special Publications, 19*(1), 113-157.

Tapponnier, P., Peltzer, G., Le Dain, A. Y., Armijo, R., & Cobbold, P. (1982). Propagating extrusion tectonics in Asia: New insights from simple experiments with plasticine. *Geology, 10*(12), 611-616. doi: 10.1130/0091-7613(1982)10<611:petian>2.0.co;2

Thanh, T.-D., Janvier, P., & Phuong, T. H. (1996). Fish suggests continental connections between the Indochina and South China blocks in Middle Devonian time. *Geology, 24*(6), 571-574.

Tien, P. C., & Nguyen, V. C. (Cartographer). (1991). Geological map of Cambodia, Laos and Vietnam.

Trieu, C. (2001). The Thin Toc Ms 5.3 earthquake in the 19 February 2001. *Geology A (Hanoi), 264*(5-6), 1-14.

Trieu, C., Xuan, N. T., Thang, N., Dung, L., & Tuyen, N. (1999). Seismic hazard assessment in Tay Bac region, Vietnam. *Journal of Geology, Series B, 13*(14), 163-173.

Trinh, P. T., Lacassin, R., Tapponnier, P., Leloup, P., & Yem, N. (1993). Evidence for active strike-slip movements in Northwestern Vietnam *Terra Abstracts, Abstract Suppl. No. 1 to Terra Nova 5* (pp. 265).

Trinh, P. T., Van Tri, T., Can, N., Van Bat, D., Tien, P. H., Chuong, V. D., . . . Hue, T. T. (1999). Active tectonics and seismic hazards in Sonla hydropower dam (North Vietnam). *Journal of Geology, Series B*(13-14), 19-32.

Trung, N. M., Tsujimori, T., & Itaya, T. (2006). Honvang serpentinite body of the Song Ma fault zone, Northern Vietnam: A remnant of oceanic lithosphere within the Indochina–South China suture. *Gondwana Research, 9*(1), 225-230.

Tuyet, T. D., Hoi, N. V., Hung, N. B., & Thong, A. V. (Cartographer). (1978). Geological map of the Socialist Republic of Vietnam.

Vedder, J. G., & Wallace, R. E. (1970). *Map showing recently active breaks along the San Andreas and related faults between Cholame Valley and Tejon Pass, California*.

Wang, E., Burchfiel, B. C., Royden, L. H., Chen, L., Chen, J., Li, W., & Chen, Z. (1998). Late Cenozoic Xianshuihe-Xiaojiang, Red River, and Dali Fault Systems of Southwestern Sichuan and Central Yunnan, China. *Geological Society of America Special Papers, 327*, 1-108. doi: 10.1130/0-8137-2327-2.1

Warnitchai, P. (2004). *Development of seismic design requirements for buildings in Bangkok against the effects of distant large earthquakes.* Paper presented at the Proceedings of the 13th world conference on earthquake Engineering (13WCEE), Vancouver.

Warnitchai, P. (2011). *Probabilistic seismic hazard assessment for Xayaburi Hydroelectric Power Project*. Unpublished internal report. Ch. Karnchang Public Co., Ltd.

Wells, D. L., & Coppersmith, K. J. (1994). New empirical relationships among magnitude, rupture length, rupture width, rupture area, and surface displacement. *Bulletin of the Seismological Society of America, 84*(4), 974-1002.

Wemmer, K., Sievers, H., Thang, T. T., & Trinh, P. T. (1999). New hints for nappe tectonics in northern Vietnam by K/Ar dating of very low grade sediments. *Journal of Geology, Series B, 13*(14), 107-109.

Wongsomsak, & Charusiri, P. (Cartographer). (2000). Geological Map of Laos.

Xuyen, C., & Dy, N. (1994). Urban geology investigation of Dien Bien–Son La area *Urban geology program of Vietnam (in Vietnamese with English abstract).* (pp. 69). Hanoi: Ministry of Heavy Industry, Ministry of Construction, Geol. Survey of Vietnam, Hydrogeological Division.

Zhang, P.-Z., Shen, Z., Wang, M., Gan, W., Bürgmann, R., Molnar, P., . . . Wu, J. (2004). Continuous deformation of the Tibetan Plateau from global positioning system data. *Geology, 32*(9), 809-812.

Zuchiewicz, W., & Cuong, N. (2002). *Morphotectonic and seismic properties of the Dien Bien Phu fault in Vietnam.* Paper presented at the Program with Abstracts, IGCP 430 2nd Annual Meeting 'Mantle Responses to Tethyan Closure.

Zuchiewicz, W., Cuong, N. Q., Bluszcz, A., & Michalik, M. (2004). Quaternary sediments in the Dien Bien Phu fault zone, NW Vietnam: a record of young tectonic processes in the light of OSL-SAR dating results. *Geomorphology, 60*(3–4), 269-302. doi: http://dx.doi.org/10.1016/j.geomorph.2003.08.004

APPENDIX

Results of OSL dating

NSW 1

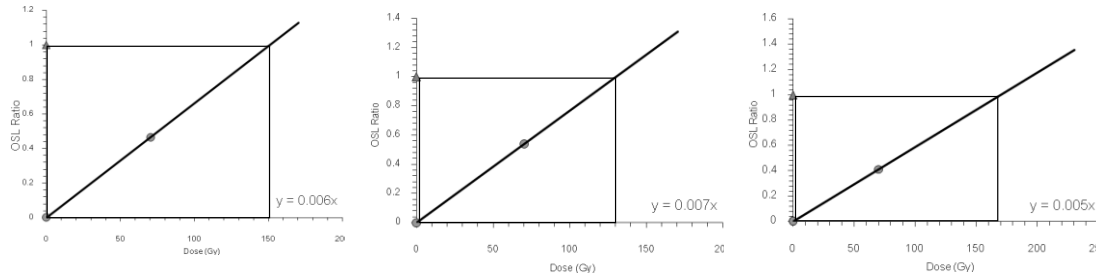

NSW 2

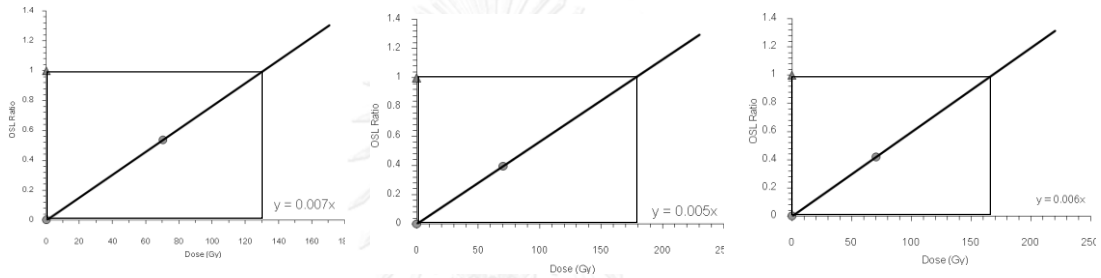

NSW 3

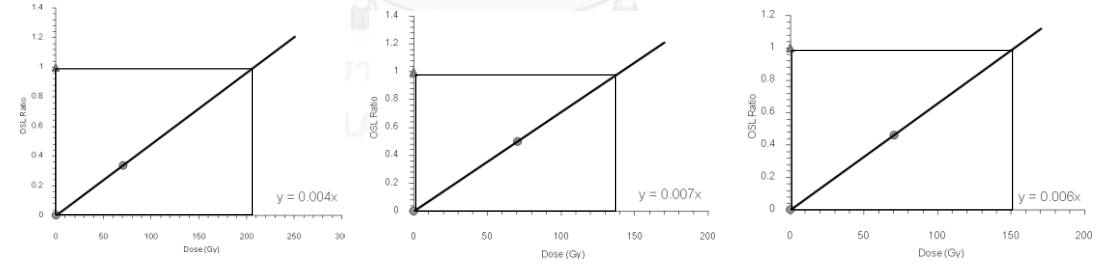

NSW 4

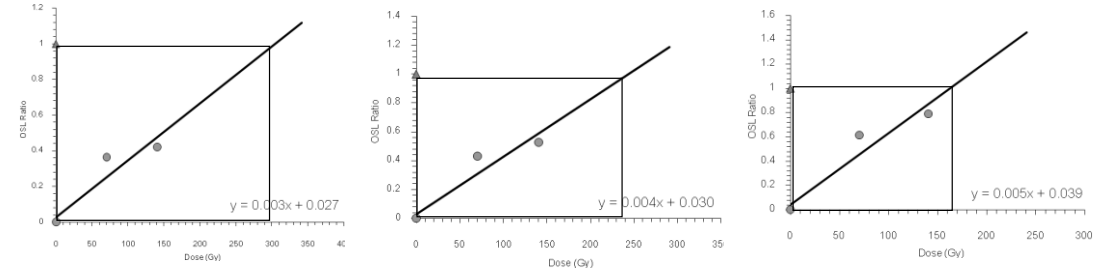

NSW 5

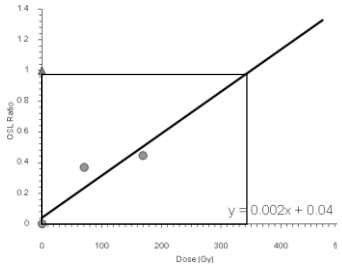

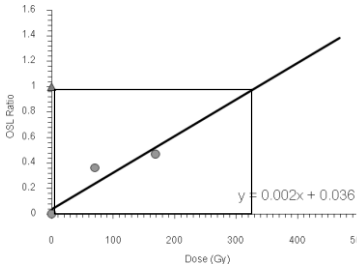

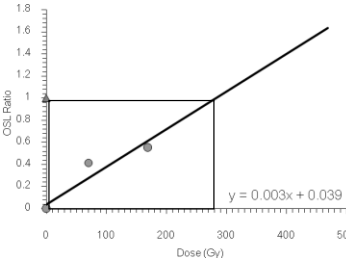

NX 1

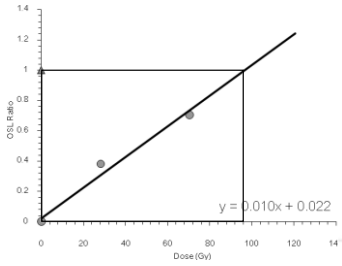

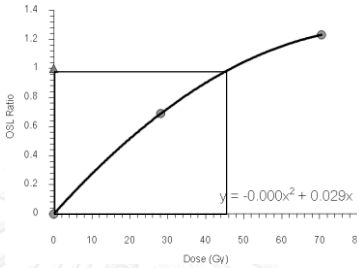

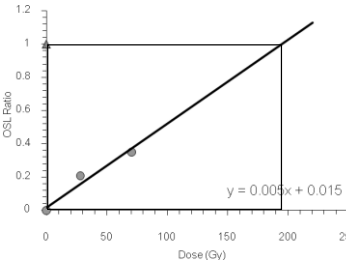

NX 2

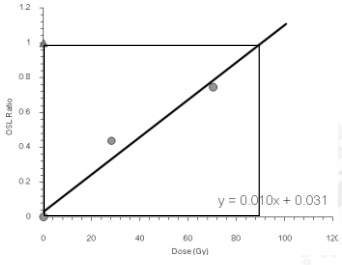

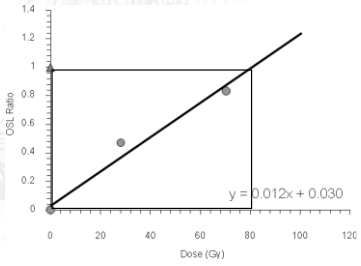

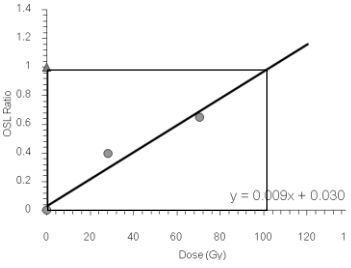

NS 3-1

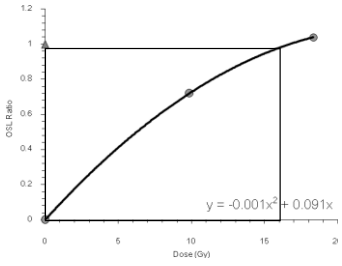

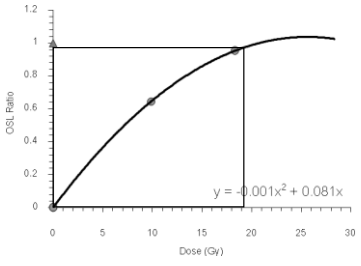

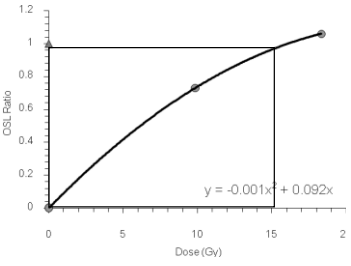

NS 3-2

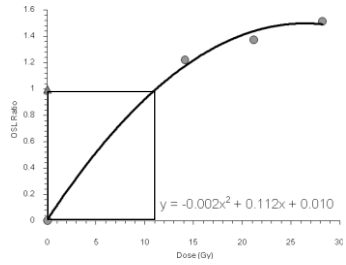

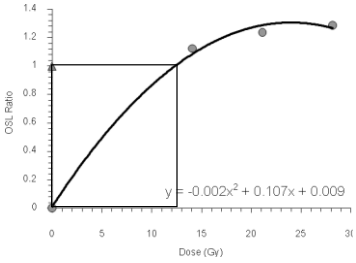

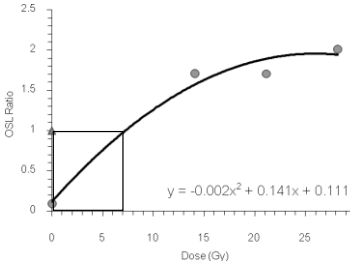

NS 3-3

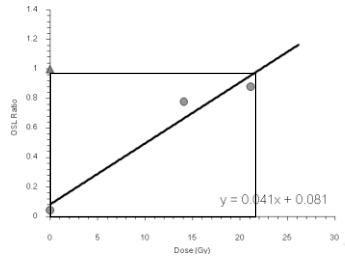

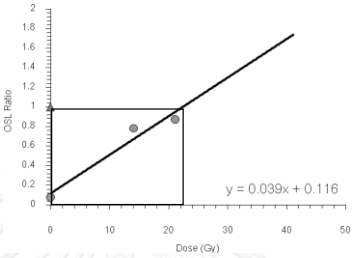

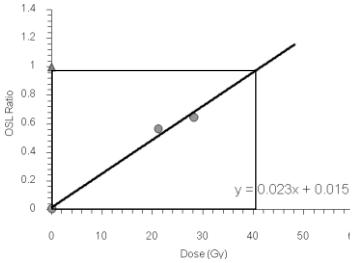

1

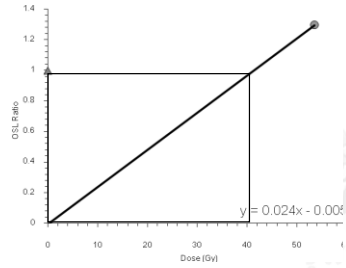

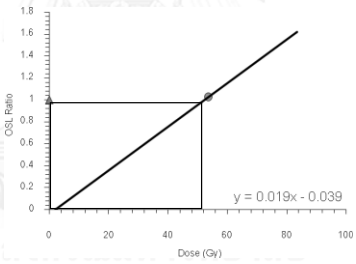

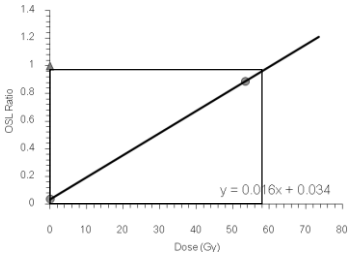

2

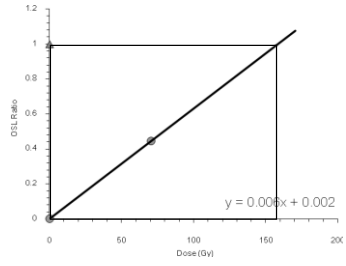

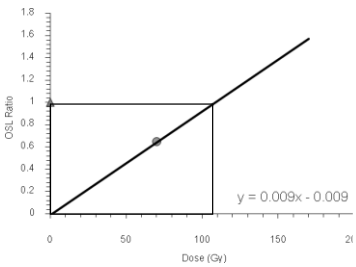

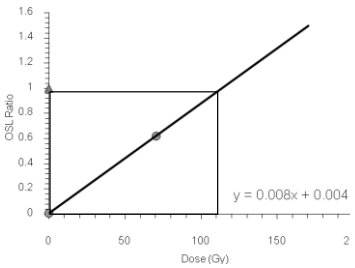

3

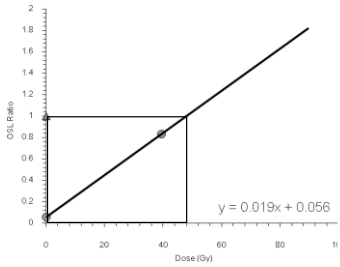
y = 0.019x + 0.056
OSL Ratio
Dose (Gy)

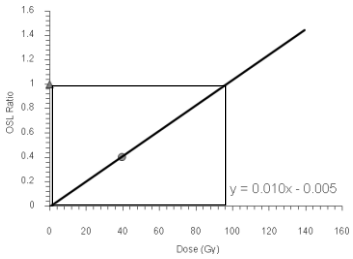
y = 0.010x - 0.005
OSL Ratio
Dose (Gy)

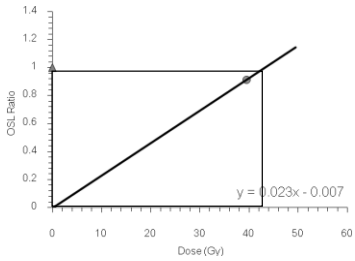
y = 0.023x - 0.007
OSL Ratio
Dose (Gy)

4

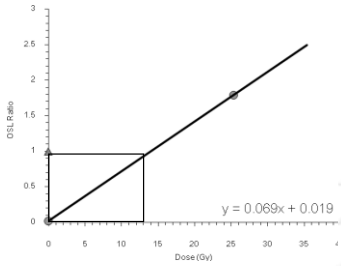
y = 0.069x + 0.019
OSL Ratio
Dose (Gy)

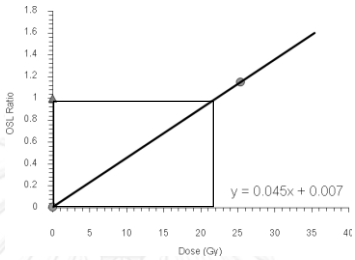
y = 0.045x + 0.007
OSL Ratio
Dose (Gy)

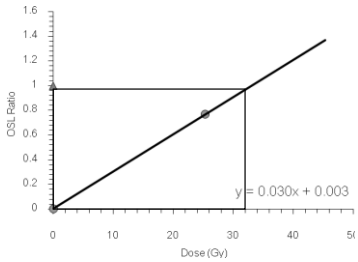
y = 0.030x + 0.003
OSL Ratio
Dose (Gy)

T4-S1

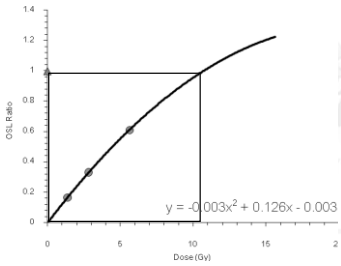
y = -0.003x² + 0.126x - 0.003
OSL Ratio
Dose (Gy)

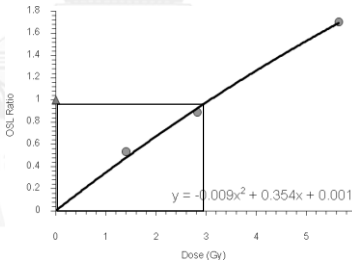
y = -0.009x² + 0.354x + 0.001
OSL Ratio
Dose (Gy)

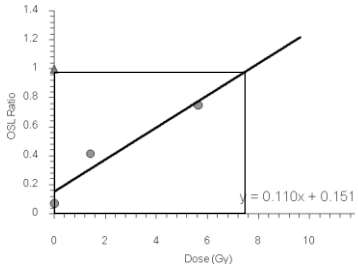
y = 0.110x + 0.151
OSL Ratio
Dose (Gy)

T4-S2

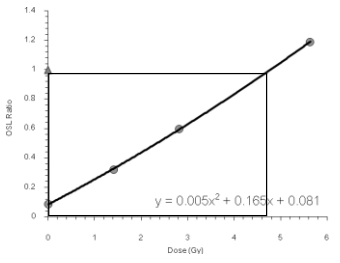
y = 0.005x² + 0.165x + 0.081
OSL Ratio
Dose (Gy)

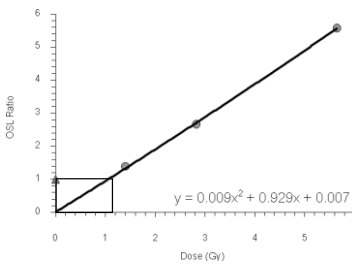
y = 0.009x² + 0.929x + 0.007
OSL Ratio
Dose (Gy)

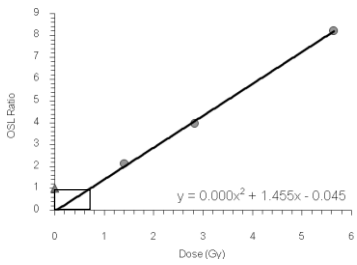
y = 0.000x² + 1.455x - 0.045
OSL Ratio
Dose (Gy)

T4-S3

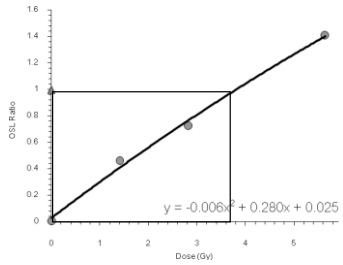

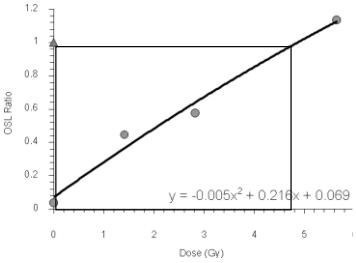

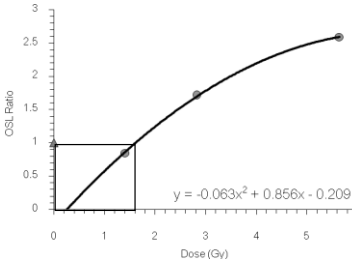

T4-S4

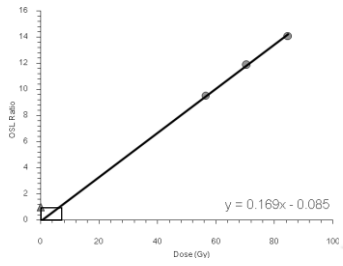

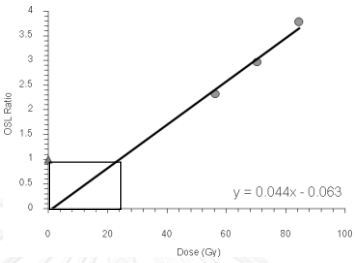

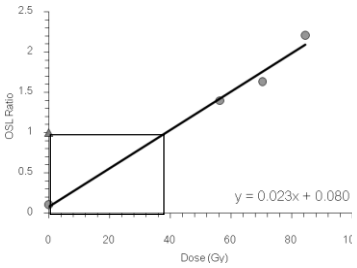

T4-N1

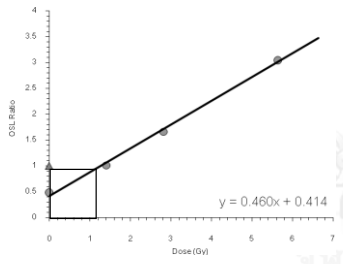

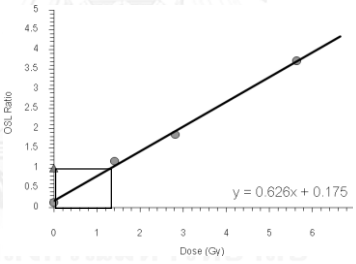

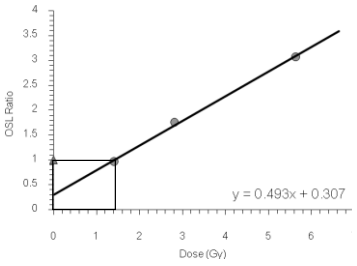

T4-N2

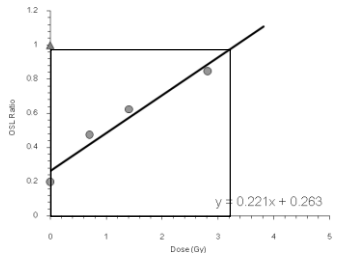

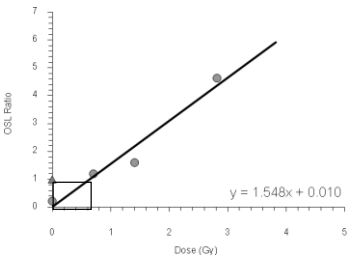

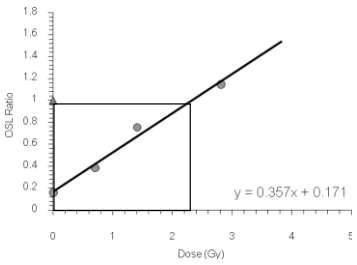

T4-N3

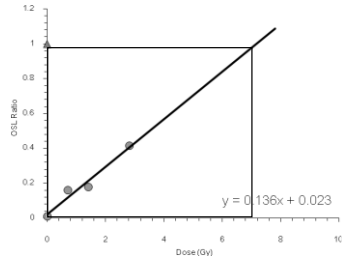

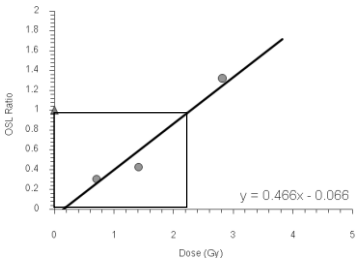

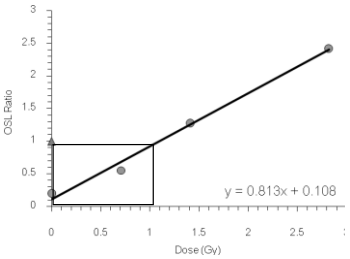

T4-F1

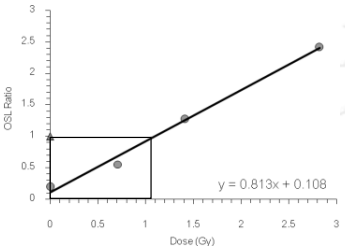

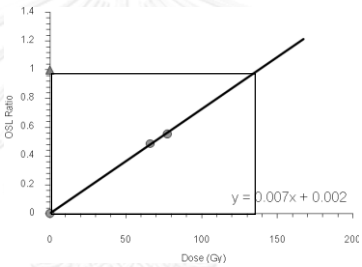

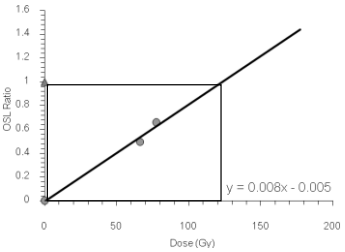

VITA

Miss Patchawee Nualkhao was born on October 3, 1985 in Bangkok, Thailand. She graduated at high school level from Sri Ayudhya School, Bangkok, in 2004. In 2008, she received a B.Sc. degree in Geoscience program from the Department of Physics, Faculty of Sciences, Mahidol University, Kanchanaburi, Thailand. In 2012, she enrolled as a graduate student for M.Sc. program of Geology programme at Graduate School, Chulalongkorn University, Bangkok, Thailand. Her research on “PALEOEARTHQUAKES ALONG XAIGNABOULI FAULT ZONE IN WESTERN LAO PDR” has been published in the Bulletin of Earth Sciences of Thailand (BEST) journal volume 7 number 1, August 2015.